

1-1-2012

A Complex-Lamellar Description Of Boundary Layer Transition

Maureen L. Kolla
Ryerson University

Follow this and additional works at: <http://digitalcommons.ryerson.ca/dissertations>

 Part of the [Aerospace Engineering Commons](#)

Recommended Citation

Kolla, Maureen L., "A Complex-Lamellar Description Of Boundary Layer Transition" (2012). *Theses and dissertations*. Paper 1548.

This Dissertation is brought to you for free and open access by Digital Commons @ Ryerson. It has been accepted for inclusion in Theses and dissertations by an authorized administrator of Digital Commons @ Ryerson. For more information, please contact bcameron@ryerson.ca.

**A COMPLEX-LAMELLAR DESCRIPTION OF BOUNDARY LAYER
TRANSITION**

by

Maureen Louise Kolla

Master of Science in Mechanical Engineering

Ryerson University, October 2006

Bachelor of Science in Mechanical Engineering

University of Alberta, June 2002

A dissertation presented to Ryerson University in partial fulfillment of the requirements for the degree of Doctor of Philosophy in the Program of Aerospace Engineering.

Toronto, Ontario, Canada, 2012

©Maureen Louise Kolla 2012

AUTHOR'S DECLARATION FOR ELECTRONIC SUBMISSION OF A DISSERTATION

I hereby declare that I am the sole author of this dissertation. This is a true copy of the dissertation, including any required final revisions, as accepted by my examiners.

I authorize Ryerson University to lend this dissertation to other institutions or individuals for the purpose of scholarly research.

I further authorize Ryerson University to reproduce this dissertation by photocopying or by other means, in total or in part, at the request of other institutions or individuals for the propose of scholarly research.

I understand that my dissertation may be electronically available to the public.

ABSTRACT

A COMPLEX-LAMELLAR DESCRIPTION OF BOUNDARY LAYER TRANSITION

Doctor of Philosophy, Aerospace Engineering

Ryerson University, 2012

Maureen Louise Kolla

Flow transition is important, in both practical and phenomenological terms. However, there is currently no method for identifying the spatial locations associated with transition, such as the start and end of intermittency. The concept of flow stability and experimental correlations have been used, however, flow stability only identifies the location where disturbances begin to grow in the laminar flow and experimental correlations can only give approximations as measuring the start and end of intermittency is difficult. Therefore, the focus of this work is to construct a method to identify the start and end of intermittency, for a natural boundary layer transition and a separated flow transition. We obtain these locations by deriving a complex-lamellar description of the velocity field that exists between a fully laminar and fully turbulent boundary condition. Mathematically, this complex-lamellar decomposition, which is constructed from the classical Darwin-Lighthill-Hawthorne drift function and the transport of enstrophy, describes the flow that exists between the fully laminar Pohlhausen equations and Prandtl's fully turbulent one seventh power law. We approximate the difference in enstrophy density between the boundary conditions using a power series. The slope of the power series is scaled by using the shape of the universal intermittency distribution within the intermittency region. We solve the complex-lamellar decomposition of the

velocity field along with the slope of the difference in enstrophy density function to determine the location of the laminar and turbulent boundary conditions. Then from the difference in enstrophy density function we calculate the start and end of intermittency. We perform this calculation on a natural boundary layer transition over a flat plate for zero pressure gradient flow and for separated shear flow over a separation bubble. We compare these results to existing experimental results and verify the accuracy of our transition model.

ACKNOWLEDGEMENTS

I would like to thank my supervisor, Dr. Jeff Yokota, for all his guidance and unending belief in me. He has taught me a lot about fluid dynamics and an even more about life. The biggest lesson I will take with me is that to succeed means having to fail, over and over again. Failing shows us what we do not yet understand or know and is an opportunity to continue learning. There have been a number of set backs over the years however with each one our research became stronger and more interesting. Thank you for giving me the opportunity to work with you, it has been an honour.

To my parents, Don and Kathleen, thank you for teaching me that anything is possible as long as you are willing to work hard and not give up when things get tough. I feel honoured to have had your constant support and belief in me. To my sister, Stephanie, thank you for all the life coaching conversations. You are my best friend. To my brother and sister-in-law, Derreck and Aimee, thank you for all the photos and videos that always helped to cheer me up and cheer me on. To my little brother, Timothy, thank you for unending belief that would succeed, you never doubted it even when I might have. To Cathy, thank you for opening up your home to me and for your constant generosity. You made it easier to spend the last few months in Toronto. To Danielle, thank you for all the dinners and the chats. I will always look back on this last summer and be so thankful that you were here and that I could call on you whenever I needed a friend. To Michelle, your guidance and friendship over the last year was been invaluable. Our runs and chats helped me recognize that it was time to step up and get it finished. Finally, to all my friends and extended family, thank you for all your support and encouragement, you were always there whenever I needed something, whether it was a sympathetic ear, a yoga class, a run or a dinner with family. Without you all, I would not have had the perseverance to finish.

My biggest thanks, must go to my husband, David. He has stood by me through all the ups and downs, the successes and failures, the break throughs and the break downs. He has become the person I depend on to help me through the toughest times and the first person I want to share my successes with. His constant belief and pride in me has meant so much over the years. He has consistently supported me in so many ways and has never asked for anything in return. I guess now perhaps that can change. Merci David, je t'aime!

Finally, I would like to thank the Government of Ontario for the financial support that I received throughout the course of this degree.

I dedicate this to Jeff. Never fear failure.

Table of Contents

Author's Declaration	ii
Abstract	iv
Acknowledgements	v
Dedication	vi
Table of Contents	vii
List of Tables	x
List of Figures	xi
Nomenclature	xii
1 Introduction	1
1.1 Motivation	1
1.1.1 What is Transition?	1
1.1.2 Why is Transition Important?	2
1.2 Literature Review	3
1.2.1 Modes of transition	4
1.2.2 Start of transition prediction	5
1.2.3 Transition models	6
1.2.4 Examples where complex-lamellar decompositions have been used . .	8
1.3 Research Objectives	9

2	Complex-lamellar derivation	10
2.1	Governing Equations	10
2.2	General complex-lamellar description	11
2.3	Transitioning complex-lamellar decomposition	13
2.4	Transitioning complex-lamellar decomposition based on enstrophy density . .	15
2.5	Transitioning complex-lamellar equation boundary conditions	18
2.5.1	Drift function	19
2.5.2	Difference in enstrophy across transition	21
3	Boundary layer transition: Region modelling	24
3.1	Fully laminar boundary condition	32
3.2	Fully turbulent boundary condition	34
3.3	Modelling the slope of the difference in enstrophy density function	35
3.4	Expanded complex-lamellar velocity condition	39
3.5	Boundary layer transition model equations	40
3.5.1	Numerical method	42
4	Natural boundary layer transition	43
4.1	Effective leading edge of turbulent boundary layer	44
4.2	Length of intermittency correlation	46
5	Natural boundary layer transition results	47
5.1	Boundary layer transition equations evaluated at $Re_{\theta} _{x_1}$	49
5.1.1	Comparison of Reynolds numbers based on x with experimental data	53
5.1.2	Comparison of the length of the intermittency region with experimen- tal correlation	54
5.1.3	Comparison of the length of breakdown with experimental observation	55
5.1.4	Conclusions	56
5.2	Boundary layer transition equations evaluated at $Re_{\theta} _{x_2}$	57
6	Separated flow transition over a separation bubble	60
6.1	Effective leading edge of turbulent boundary layer	62
6.2	Length of intermittency region	63
7	Separated flow transition: Results	65
7.1	Short separation bubble	67
7.1.1	Comparison of Reynolds number based on x with experimental data .	70
7.1.2	Comparison of the start of intermittency with experimental observation	71
7.1.3	Mayle [1] correlations for short separation bubbles	73
7.1.4	Conclusions for short separation bubble	74
7.2	Long separation bubble	75

7.2.1	Comparison with Mayle [1] experimental correlations for long separation bubble	78
7.2.2	Conclusions regarding the long separation bubble	80
7.2.3	Conclusions regarding the comparison of short and long bubbles . . .	80
8	Conclusions	82
8.1	Conclusions	82
8.2	Future work	84
A	Matlab code	86
	References	127

List of Tables

5.1	Start and end of intermittency location comparison between calculated results and the experimental data of Schubauer and Klebanoff [2] for natural boundary layer transition.	53
5.2	Comparison of the length of the intermittency region between the experimental correlation of Narasimha [3] and our analysis for a natural boundary layer transition.	55
5.3	Comparison of the results obtained at a cross-flow location $Re_{\theta _{x_1}}$ and $Re_{\theta _{x_2}}$	57
5.4	Comparison of start and end of intermittency locations obtained at a cross-flow location $Re_{\theta _{x_1}}$ and $Re_{\theta _{x_2}}$	58
7.1	Comparison between calculated results and Gaster's [4] experimental data for a short separation bubble at $Re_{\theta _s} = 394$	70
7.2	Short bubble length comparison between calculated lengths and Mayle's [1] experimental correlations	74
7.3	Long bubble lengths calculated from our results comparison with Mayle's [1] experimental correlations	79

List of Figures

3.1	Boundary layer model 1	25
3.2	Boundary layer model 1	26
3.3	Figure recreated from Narasimha and Dey [5] representing the stages from laminar to turbulent flow along a flat plate.	28
3.4	Boundary layer model 2	29
3.5	Boundary layer model 3	30
3.6	Flow around a separation bubble recreated from Mayle [1]	31
3.7	Boundary layer model 4	32
5.1	Difference in enstrophy density versus Reynolds number based on x for natural boundary layer transition	50
5.2	Natural transition boundary layer	52
7.1	Difference in enstrophy density between Re_{x_A} and Re_{x_B} for short separation bubble	68
7.2	Short separation bubble	69
7.3	Pressure distribution for short bubble reproduced from Gaster's [4] experimental data.	72
7.4	Difference in enstrophy density between Re_{x_A} and Re_{x_B} for long separation bubble	76
7.5	Long separation bubble	77

Nomenclature

LATIN SYMBOLS

p	Fluid pressure
\vec{c}	Arbitrary vector field
f, g, h	Scalar functions
x, y, z	Cartesian coordinate components
u, v, w	Cartesian velocity components
\vec{u}_{lam}	Velocity vector of the baseline laminar flow
\vec{u}_{turb}	Velocity vector of the mean turbulent flow
$\nabla^2 \vec{u}$	Flexion vector
C_n	Power series coefficients
E	Enstrophy, the integral of the square of vorticity, $E = \int \omega^2 dV$
E_{lam}	Baseline laminar enstrophy, $E_{lam} = \int \omega_{lam}^2 dV$
\tilde{E}	Difference in enstrophy, $\tilde{E} = \int (\omega^2 - \omega_{lam}^2) dV$
\vec{n}	Unit normal vector
R	Transition length ratio of Re_{x_B} to Re_{x_A}
R_L	Transition length ratio of Re_{x_t} to Re_{x_A}
Re_x	Reynolds number based on x

$Re_{x_{cr}}$	x Reynolds number at the critical stability location
Re_{x_s}	x Reynolds number at separation
Re_{x_r}	x Reynolds number at reattachment
Re_{x_t}	x Reynolds number at the effective leading edge of the turbulent boundary layer
Re_{x_A}	x Reynolds number at fully laminar boundary condition
Re_{x_B}	x Reynolds number at fully turbulent boundary condition
Re_{x_0}	x Reynolds number at the start of intermittency
Re_{x_T}	x Reynolds number at the end of intermittency
$Re_{x_{Tp}}$	x Reynolds number at the end of constant pressure region on the pressure distribution curve
$Re_{x _{\gamma=0.25}}$	x Reynolds number where the intermittency is 0.25
$Re_{x _{\gamma=0.75}}$	x Reynolds number where the intermittency is 0.5
Re_{θ}	Momentum thickness Reynolds number
$Re_{\theta _x}$	Momentum thickness Reynolds number at x
$Re_{\theta _s}$	Momentum thickness Reynolds number at separation
$Re_{\theta _{x_1}}$	Momentum thickness Reynolds number at the location where the surface velocity gradient begins to increase
$Re_{\theta _{x_2}}$	Momentum thickness Reynolds number at the location where the surface velocity gradient becomes zero
\vec{t}	Unit tangent vector
Tu	Free-stream turbulence level
$T(t)$	Function dependent only in time
U_{∞}	Free-stream velocity
x_{cr}	Critical stability location
x_s	Separation location
x_r	Reattachment location
x_t	Location of the effective leading edge of the turbulent boundary layer
x_A	Location where the fully laminar boundary condition is imposed

x_B	Location where the fully turbulent boundary condition is imposed
x_0	Start of intermittency
x_T	End of intermittency
x_{Tp}	End of constant pressure region on pressure distribution curve
x_1	Location where the surface velocity gradient begins to increase
x_2	Location where the surface velocity gradient becomes zero
$x _{\gamma=0.25}$	Location of x at an intermittency of 0.25
$x _{\gamma=0.75}$	Location of x at an intermittency of 0.75

GREEK SYMBOLS

δ_{lam}	Laminar boundary layer thickness
δ_{turb}	Turbulent boundary layer thickness
η	Difference in enstrophy density function
γ	Intermittency
λ	Pohlhausen pressure gradient term
μ	Kinematic viscosity
θ_{lam}	Laminar momentum thickness
θ_{turb}	Turbulent momentum thickness
θ_x	Momentum thickness at x
$\omega_x, \omega_y, \omega_z$	Cartesian vorticity components
$\vec{\omega}_{lam}$	Vorticity vector of the baseline laminar vorticity
$\vec{\omega}_{turb}$	Vorticity vector of the mean turbulent vorticity
ω^2	Enstrophy density
ρ	Fluid density
τ	Drift function
Γ	Circulation
Φ	Craig's circulation-preserving flexion potential

Ψ Source term

SYNTAX

$|_{x_B}$ The value preceding this symbol will be evaluated at x_B

CHAPTER 1

Introduction

1.1 Motivation

1.1.1 What is Transition?

Transition, as the name implies, is the passage from one state to another. In fluid flows, a transitional flow occurs between laminar and turbulent flows. Laminar flow is considered the simplest type of flow and forms orderly, roughly parallel streamlines. Between these streamlines, the fluid parameters, such as velocity, pressure and temperature, will vary smoothly from one streamline to the next. Turbulent flow is more complex. There are many physical descriptions of turbulent flow however the most widely accepted is that of Hinze [6], who described it as “an irregular condition of flow in which various quantities show a random variation with time and space coordinates, so that statistically distinct average values can be discerned.” Turbulent flows are sensitive to small changes in initial or boundary conditions.

1.1 Motivation

What is known about turbulence comes from experiments and heuristic modelling, not from first principle solutions [7]. Turbulent flow has the following characteristics: it is basically a random, unsteady process; it has a general swirling nature with indistinct lumps of fluid called eddies; the instantaneous boundary between the turbulent region and the outer inviscid flow is distinct; turbulence is always three-dimensional, even when the background flow is two-dimensional [8].

Transitional flow is not an instantaneous occurrence and cannot be described as a single type of flow. It is a process that results from a sequence of events that depend on many parameters such as Reynolds number, pressure gradients, surface roughness, and environmental disturbances. This means that each transition process is unique and there are several paths the flow can take to reach a fully turbulent state [9].

1.1.2 Why is Transition Important?

In nature, most flows will become turbulent and as such will have gone through a transitional stage. It is at the transitional stage where an increase in losses begins and the performance or safety is affected. For example, in commercial aircraft design, drag reduction is an important factor for increasing fuel efficiency. An increase in drag is directly related to an increase in the skin friction coefficient, which has been experimentally shown to begin near transition onset. By accurately predicting transition, the possibility of extending the laminar boundary layer and maintaining a lower skin friction coefficient is plausible. In another example, the thickness of the thermal protection layer on a reentry spacecraft, is determined by the altitude at which transition is predicted to begin. Due to the fact that a turbulent boundary layer has significantly greater heating rates than a laminar boundary layer, an accurate prediction of the transitional altitude is critical for astronaut safety. In both examples, a designer may assume fully turbulent conditions to achieve satisfactory, if not optimal, results provided that the laminar and transitional boundary layer region is significantly smaller than the

fully turbulent region. An example where predicting transition is essential is in designing turbomachinery blades. It is crucial to accurately predict where transition occurs and for how long it will last. Failure to do so results in a significant increase in drag and a reduction in efficiency.

The need to understand and predict transition is not limited to the aircraft industry. Race cars need to be aerodynamic in order to reduce drag and to increase speed. Within the sporting world, road bike companies, cyclists, and alpine ski racing suit designers all use wind tunnel testing to improve design or alignment to generate the least amount of drag. Trial and error is often used in this testing because there is no concrete understanding of the transition process. A final example of where transition is important is in predicting cerebral vascular accident, otherwise known as a stroke. Researchers at the University of Chicago [10] hypothesize that certain flow patterns may predispose plaque in arteries to progress and build up while other flow patterns may predispose the plaque to break down. The flow through healthy arteries is laminar. As the plaque builds up on the walls, the arteries narrow, the flow speeds up and transition to turbulent flow begins. With the increase in flow speed, comes an increase in force and this can cause the plaque to break free and potentially block a vital artery leading to a stroke. By predicting the flow patterns, doctors can predict which patients may need blood thinners, surgery or no treatment at all.

Overall, the limiting factor in our ability to accurately predict aerodynamic flows is the current inability to reliably predict laminar-turbulent transition [11].

1.2 Literature Review

The focus of this review will be on 2D, incompressible boundary layer flow. We will begin this review by first identifying the different modes of transition, since the location of where transition begins and the length over which it occurs depend on the manner in which transition occurs. We will then discuss how the start of transition has been predicted, followed

1.2 Literature Review

by highlights of some of the different transition models. Our goal is to generate a transition model that bounds the region between a laminar flow and a turbulent flow and describe this region mathematically using a complex-lamellar decomposition of the flow field. It will become evident within this review that this has not been attempted before and therefore, we will finish off the literature review with a discussion of types of flow problems that have made use of complex-lamellar decomposition with the intent of illustrating that this type of decomposition is well established.

1.2.1 Modes of transition

Natural transition occurs in a boundary layer when the environmental disturbances are small so that wave-like oscillations develop downstream of a critical point. The transition process has been described by many researchers [12, 13, 14, 15, 16, 5, 17, 18, 19] and can be summarized as follows. In two-dimensional flows, these oscillations, called Tollmien-Schlichting (TS) waves, at first exhibit exponential growth and can be computed using linear stability theory. Further downstream, the TS waves reach a finite amplitude and three-dimensional and nonlinear disturbances begin to appear and grow. This is followed by a ‘breakdown’ zone in which vortices are continuously broken down into smaller vortices until turbulent spots appear. The turbulent spots develop intermittently until finally fully developed turbulent flow is reached. This is the benchmark mode of transition that has been studied extensively.

Bypass transition occurs when large environmental disturbances, caused by high free stream turbulence or large roughness elements, affect the laminar flow. These disturbances result in the transitional flow bypassing the TS wave development and are immediately influenced by three-dimensional and nonlinear disturbances. Like natural transition, the flow will reach a breakdown zone, followed by turbulent spots and finally fully developed turbulent flow [17, 1]. For this mode of transition linear stability theory has been shown to be irrelevant

[20].

Separated flow transition can occur behind boundary layer trip wires or when the laminar boundary layer flow is subjected to a large adverse pressure gradient [1, 21]. In this type of transition, the laminar boundary layer separates and transition occurs in the free shear layer flow near the surface. If the flow reattaches downstream a separation bubble is formed. These bubbles are typically present close to the leading edge of thin airfoils and on gas turbine blades [22, 1]. The bubble length depends on the transition process within the free shear layer and this process may involve all the stages associated with natural transition [1]. Separation bubbles are described as being either short or long. Experiments, with low free-stream turbulence, have been performed on long bubbles and TS instabilities have been detected [4]. As well, studies have been conducted to determine the dynamics of separation bubbles [22]. Studying this model of transition is important as short separation bubbles are an effective way to force transition to control performance [1, 22].

There also exists wake-induced transition and reverse transition or relaminarization. These modes typically apply for flow in gas turbines and are beyond the scope of this research. Detailed descriptions can be found in Mayle [1], and Langtry et. al. [23].

1.2.2 Start of transition prediction

A method used to predict where transition occurs was developed by Jaffe et. al. [24] as an extension of the hydrodynamic stability theory. This model is termed the e^n model. Through the stability analysis and the solving of the Orr-Sommerfeld equation, a neutral stability point is determined to be where the two-dimensional disturbances have an amplification rate of zero. Beyond this point, the amplification rate grows rapidly until three-dimensional disturbances begin to form and then eventually turbulence. This model tracks the amplification rate from the neutral stability point to the position downstream where the integrated amplification rate with respect to surface distance reaches a factor e^n , indicative of transition.

1.2 Literature Review

The n factor is determined from experimental data and varies for different types of flows. Typically, it is set between 8-10. A downside to this method is that it only deals with the linear region of the flow and two-dimensional disturbances and as such is not very rigorous. However, Arnal [17] determined that for flat plate conditions, the linear region covers up to approximately 85% of the distance between the leading edge and the beginning of transition. This explains why most practical transition prediction methods are based on linear stability only.

The other method for predicting the start of transition is by using experimental correlations. These correlations are determined from experimental data and typically relate the free-stream turbulence intensity to the momentum thickness Reynolds number at transition. The most well know correlation by Abu-Ghannam and Shaw [25] relates both the free-stream turbulence intensity and the effect of pressure gradients to the momentum thickness Reynolds number. These correlations are popular because they provide sufficiently accurate results, however, to determine the momentum thickness Reynolds number and free-stream conditions involves non-local operations, thus making this method more difficult to implement within modern computational fluid dynamics (CFD) codes [23].

1.2.3 Transition models

In 1951, Emmons [26] published an article on the formation of turbulent spots that he discovered while performing a water table experiment. He observed that these turbulent spots would begin to form within the laminar flow at a point downstream of the leading edge. These spots would then begin to grow as the flow moved downstream until the flow became fully turbulent. As the turbulent spots appeared intermittently within the laminar flow, he termed this region intermittent and defined intermittency as the fraction of time that the flow is turbulent at a specific location.

In 1955, Schubauer and Klebanoff [2] performed an experimental wind tunnel investigation

of a boundary layer over a flat plate, and using hot-wire probes they measured velocity fluctuations within the boundary layer from laminar to turbulent flow. When they observed the output from the hot-wire probes on the oscilloscope, they were able to distinguish between laminar flow and bursts of turbulent flow. Ultimately they were able to determine the fraction of time the flow was turbulent at any point. In essence they discovered a way to obtain a measure of intermittency. They were the first to note that for different conditions leading to transition, the length of the intermittency region changed. However, the shape of the distributions were similar. Then, in 1957, Narasimha [27] determined a universal intermittency distribution from which intermittency transition models have been obtained. As many different models currently exist, researchers [28, 29, 5] have divided them into three categories; linear-combination models, algebraic models and differential models.

Linear combination models assume the mean flow during transition can be modelled as a linear combination of the laminar and turbulent flow. The proportion of laminar to turbulent flow within the transition region is obtained using the intermittency distribution and is proportional to $(1 - \gamma) : \gamma$ for laminar and turbulent flow respectively. These models require the calculation of the laminar boundary layer, an estimate of the mean flow parameters in the fully turbulent boundary layer, prediction of the start of transition, and an intermittency distribution [5]. The most popular linear combination model is the original one developed by Dhawan and Narasimha [30] who utilize the universal intermittency distribution developed by Narasimha [27]. Since then, there have been many models developed with the distinguishing features being the intermittency distribution and the prediction of the start of transition. Narasimha and Dey [5] have an excellent review of some of the different models.

Algebraic and differential transition models both require solving the Reynolds-averaged equations of motion. The algebraic intermittency model is implemented by multiplying eddy viscosity of a turbulence model by the value of intermittency. So like the linear combination method the eddy viscosity has a proportion of $(1 - \gamma) : \gamma$. When the boundary layer is laminar the eddy viscosity is zero and then once transition begins, the intermittency is

1.2 Literature Review

slowly ramped up from zero to one until the fully turbulent boundary layer is achieved. This model also requires the start of transition to be determined from a different model, typically experimental correlations. Like the linear combination, many algebraic models exist .

Differential models model the intermittency through the use of transport equations that mimic the behaviour of some of the other algebraic intermittency models. These models do not require specific definitions of the start and end of transition. However, they do need some initial disturbance to trigger transition.

As will be shown within this dissertation, our proposed model of transition does not fall into any of these categories. As stated at the beginning of this review, we are attempting to model transition by bounding the intermittency region between laminar and turbulent boundary conditions. We then solve a complex-lamellar decomposition of the velocity field across these boundary conditions to obtain the location of the start and end of intermittency.

1.2.4 Examples where complex-lamellar decompositions have been used

Complex-lamellar decompositions have been used by Panton [31] for studying turbulent flows, since this decomposition can be used to separate the flow into an irrotational component and a rotational component. Yokota [32], has used this decomposition for studying stratified flow. Finnigan [33] used complex-lamellar decomposition in defining a streamwise coordinate system for studying turbulence. In Rapid Distortion Theory, this decomposition is used to calculate the distortion of large scale turbulence [34, 35]. Yokota [36] developed complex-lamellar decompositions for a variety of flows, including inviscid flows, circulating-preserving viscous flows, and general viscous flows.

A reason that this decomposition is not readily used is because it does not generate a unique solution and requires the governing equations to be linked to a particular flow phenomena of interest. The decomposition is also time-dependent as it is a solution to the transport equations.

1.3 Research Objectives

The objectives for this research are

- We will derive a complex-lamellar decomposition of the velocity field across transition and between a fully laminar and fully turbulent boundary condition.
- We will construct a boundary layer transition model between a fully laminar and fully turbulent boundary condition to determine the location of the intermittency region.
- We will identify the breakdown region and the start and end of intermittency for natural transition and separated flow transition over a separation bubble.
- We will identify the separation and reattachment locations for short and long separation bubbles.
- We will compare the results we obtain for the locations and lengths associated with transition with various sources of experimental data.

CHAPTER 2

Complex-lamellar derivation

2.1 Governing Equations

We will consider a viscous, incompressible flow in the Cartesian coordinate system, (x, y, z) . The conservation of mass and linear momentum equations along with the transport of vorticity equation are written as

$$\nabla \cdot \vec{u} = 0 \tag{2.1}$$

$$\frac{D\vec{u}}{Dt} = -\frac{1}{\rho}\nabla p + \frac{\mu}{\rho}\nabla^2\vec{u} \tag{2.2}$$

$$\frac{D\vec{\omega}}{Dt} = (\vec{\omega} \cdot \nabla)\vec{u} + \frac{\mu}{\rho}\nabla^2\vec{\omega} \tag{2.3}$$

where $\vec{u} = (u, v, w)$ are the Cartesian velocity components, $\vec{\omega} = (\omega_x, \omega_y, \omega_z)$ are the Cartesian vorticity components, ρ is the fluid density, p is the fluid pressure, μ is the kinematic viscosity.

and the material derivative is written as

$$\frac{D}{Dt} = \frac{\partial}{\partial t} + (\vec{u} \cdot \nabla) \quad (2.4)$$

2.2 General complex-lamellar description

Any continuously differentiable vector field, \vec{c} , may be represented locally as a superposition of an irrotational component and a rotational component,

$$\vec{c} = \nabla h + f \nabla g \quad (2.5)$$

where f, g, h are scalar functions. If we take the curl of \vec{c} , using vector calculus we obtain

$$\nabla \times \vec{c} = \nabla \times \nabla h + \nabla \times f \nabla g \quad (2.6)$$

$$= \nabla f \times \nabla g + f \nabla \times \nabla g \quad (2.7)$$

$$= \nabla f \times \nabla g \quad (2.8)$$

The first term, in Eq.(2.6), $\nabla \times \nabla h = 0$ so ∇h is the irrotational component. The second term, $\nabla \times f \nabla g$ does not go to zero and is therefore, the rotational component.

When the vector $f \nabla g$ is perpendicular to its own curl,

$$f \nabla g \cdot (\nabla \times f \nabla g) = 0 \quad (2.9)$$

the vector $f \nabla g$ is complex-lamellar [37, 38, 39].

We want to decompose the velocity vector in order to describe a viscous flow. The necessary and sufficient condition for the existence of a velocity potential, $\nabla \phi$, is that the flow be irrotational, therefore, $\nabla h = \nabla \phi$. Then we can write the velocity vector, \vec{u} , in potential/complex-lamellar form

2.2 General complex-lamellar description

$$\vec{u} = \nabla\phi + f\nabla g \quad (2.10)$$

We will define the scalar functions, f and g , in Section 2.4 and demonstrate that the complex-lamellar condition, Eq.(2.9) is satisfied.

The curl of vector is defined as the vorticity, $\vec{\omega}$,

$$\nabla \times \vec{u} = \vec{\omega} = \nabla f \times \nabla g \quad (2.11)$$

Physically, vorticity can be interpreted in a few different ways. The most common interpretation is that vorticity is a measure of the solid-bodylike rotation of a material point, P' about the neighbouring primary material point, P [39]. Another interpretation connects circulation and vorticity. Circulation is the integral of the velocity field along a path,

$$\Gamma = \oint_C \vec{t} \cdot \vec{u} dl \quad (2.12)$$

where \vec{t} is a tangent unit vector and dl is the line element along the circuit, C . Physically, we can interpret circulation as the total ‘push’ the velocity field gives along the path. From Stokes theorem, we can write

$$\Gamma = \int_S \vec{n} \cdot \vec{\omega} d\sigma \quad (2.13)$$

where S is any surface having C as its boundary, \vec{n} is the unit normal vector and $d\sigma$ is the area element. Then we can interpret vorticity as the circulation per unit area for an elemental surface perpendicular to the vorticity vector:

$$\vec{n} \cdot \vec{\omega} = \frac{d\Gamma}{dS} \quad (2.14)$$

This interpretation gives the physical meaning of vorticity as the amount of pushing, twisting, or turning force when the path is shrunk down to a single point, with its direction being

normal to the surface.

2.3 Transitioning complex-lamellar decomposition

Dhawan and Narasimha [30] showed that transitional flow can be modelled as a flow in which, at each point, the boundary layer alternates between a laminar and a turbulent layer, with the laminar layer originating from the leading edge of the plate and the turbulent layer at a location further downstream. The amount of time that the flow is turbulent, at each point, is represented by the intermittency distribution, γ . Although this is an unsteady process, it has been modelled as a linear combination such that the transitional velocity can be determined as

$$\vec{u} = (1 - \gamma)\vec{u}_{laminar} + \gamma\vec{u}_{turbulent} \quad (2.15)$$

where $\vec{u}_{laminar}$ is the laminar velocity and $\vec{u}_{turbulent}$ is the turbulent velocity with γ varying from 0 to 1. The laminar and turbulent velocity profiles are calculated, each at its appropriate Reynolds number, from theoretical equations. Therefore, in this model $\vec{u}_{laminar}$ is the laminar velocity that begins from the leading edge and $\vec{u}_{turbulent}$ is the turbulent velocity that begins at a location downstream of the leading edge.

Similarly, we can generate a model that decomposes a transitioning velocity field into a baseline laminar flow and potential/complex-lamellar components.

$$\vec{u} = \vec{u}_{lam} + \nabla\phi + f\nabla g \quad (2.16)$$

where \vec{u}_{lam} is the baseline laminar velocity that would exist if a laminar boundary layer did not transition. Note that \vec{u}_{lam} in our model is not necessarily the same as $\vec{u}_{laminar}$ from Dhawan and Narasimha's model. This will be discussed further in Chapter 3.

Then the vorticity becomes

$$\vec{\omega} = \vec{\omega}_{lam} + \nabla f \times \nabla g \quad (2.17)$$

2.3 Transitioning complex-lamellar decomposition

This decomposition is governed by the equations of motion and as such, the material derivative of this velocity field may be written as

$$\frac{D\vec{u}}{Dt} = \nabla \left(\frac{D\phi}{Dt} - \frac{\vec{u} \cdot \vec{u}}{2} \right) + \frac{Df}{Dt} \nabla g + f \nabla \left(\frac{Dg}{Dt} \right) \quad (2.18)$$

with the material derivative of the vorticity being

$$\frac{D\vec{\omega}}{Dt} = (\vec{\omega} \cdot \nabla) \vec{u} + \nabla \left(\frac{Df}{Dt} \right) \times \nabla g + \nabla f \times \nabla \left(\frac{Dg}{Dt} \right) \quad (2.19)$$

Then when we substitute the material derivatives for the velocity and vorticity into the linear momentum and vorticity transport equations, Eqs. (2.2) and (2.3), respectively, we get the following transport conditions

$$\nabla \left(\frac{D\phi}{Dt} + \frac{p}{\rho} - \frac{\vec{u} \cdot \vec{u}}{2} \right) + \frac{Df}{Dt} \nabla g + f \nabla \left(\frac{Dg}{Dt} \right) = \frac{\mu}{\rho} \nabla^2 \vec{u} \quad (2.20)$$

and

$$\nabla \left(\frac{Df}{Dt} \right) \times \nabla g + \nabla f \times \nabla \left(\frac{Dg}{Dt} \right) = \frac{\mu}{\rho} \nabla^2 \vec{\omega} \quad (2.21)$$

Since this decomposition is not unique, these transport conditions must be made physically meaningful by linking the governing equations to a particular flow phenomenon. Yokota [36] illustrated this for inviscid, circulation preserving and viscous motions using the convection of vorticity as the flow phenomena of interest. We will make use of the concepts outlined in Yokota's [36] paper to determine a solution to the transport conditions, Eqs. (2.20) and (2.21) with the convection of enstrophy being our flow phenomenon of interest. We will discuss the boundary conditions associated with Eq.(2.16) in Section 2.5.

2.4 Transitioning complex-lamellar decomposition based on enstrophy density

We may write a transitioning velocity field in a complex-lamellar form that depends on the difference in enstrophy, \tilde{E} ,

$$\vec{u} = \vec{u}_{lam} + \nabla\phi + \tilde{E}\nabla\tau \quad (2.22)$$

where $\tilde{E} = E - E_{lam}$, the difference between the enstrophy present in the transitional region, E , and that present in baseline laminar flow, E_{lam} . ϕ is a velocity potential that represents the irrotational component of the velocity field and τ is the classic drift function [40, 41, 42].

To verify that $\tilde{E}\nabla\tau$ is complex-lamellar, consider the required condition, Eq.(2.9), and apply to obtain

$$\begin{aligned} \tilde{E}\nabla\tau \cdot (\nabla\tilde{E} \times \nabla\tau) &= \tilde{E}\nabla\tau \cdot \left[\left(\frac{\partial\tilde{E}}{\partial y} \frac{\partial\tau}{\partial z} - \frac{\partial\tilde{E}}{\partial z} \frac{\partial\tau}{\partial y} \right) \hat{i} - \left(\frac{\partial\tilde{E}}{\partial x} \frac{\partial\tau}{\partial z} - \frac{\partial\tilde{E}}{\partial z} \frac{\partial\tau}{\partial x} \right) \hat{j} \right. \\ &\quad \left. + \left(\frac{\partial\tilde{E}}{\partial x} \frac{\partial\tau}{\partial y} - \frac{\partial\tilde{E}}{\partial y} \frac{\partial\tau}{\partial x} \right) \hat{k} \right] \\ &= \tilde{E} \frac{\partial\tau}{\partial x} \left(\frac{\partial\tilde{E}}{\partial y} \frac{\partial\tau}{\partial z} - \frac{\partial\tilde{E}}{\partial z} \frac{\partial\tau}{\partial y} \right) - \tilde{E} \frac{\partial\tau}{\partial y} \left(\frac{\partial\tilde{E}}{\partial x} \frac{\partial\tau}{\partial z} - \frac{\partial\tilde{E}}{\partial z} \frac{\partial\tau}{\partial x} \right) \\ &\quad + \tilde{E} \frac{\partial\tau}{\partial z} \left(\frac{\partial\tilde{E}}{\partial x} \frac{\partial\tau}{\partial y} - \frac{\partial\tilde{E}}{\partial y} \frac{\partial\tau}{\partial x} \right) \end{aligned} \quad (2.23)$$

Then for a 2D flow, $\tilde{E}\nabla\tau \cdot (\nabla\tilde{E} \times \nabla\tau) = 0$ and therefore, $\tilde{E}\nabla\tau$ is complex-lamellar.

Enstrophy is the area integral of the magnitude of vorticity squared,

$$E = \int (\vec{\omega} \cdot \vec{\omega}) d\sigma = \int (\omega^2) d\sigma \quad (2.24)$$

where $d\sigma$ is a surface element and enstrophy density is ω^2 . We can obtain enstrophy density,

2.4 Transitioning complex-lamellar decomposition based on enstrophy density

by taking the scalar multiplication of the vorticity transport equation, Eq.(2.3), to obtain

$$\frac{D\omega_i\omega_i}{Dt} = 2\omega_i\omega_j\frac{\partial u_i}{\partial x_j} + \nu\frac{\partial^2\omega_i\omega_i}{\partial x_j\partial x_j} - 2\nu\frac{\partial\omega_i}{\partial x_j}\frac{\partial\omega_i}{\partial x_j} \quad (2.25)$$

where

$\omega_i\omega_j\frac{\partial u_i}{\partial x_j}$ - is the production of vorticity by stretching

$\nu\frac{\partial(\omega_i\omega_i)}{\partial x_j\partial x_j}$ - is the viscous diffusion of $\omega_i\omega_i$

$\nu\frac{\partial\omega_i}{\partial x_j}\frac{\partial\omega_i}{\partial x_j}$ - is the viscous dissipation $\omega_i\omega_i$

Physically, we can interpret enstrophy density as a measure of the viscous dissipation of the kinetic energy component of the flow.

Lighthill [40] defined the drift function, τ , as the time a fluid particle takes to reach any given point. This particle is moving along a streamline and is measured from some fixed position. This requires the solution of

$$d\tau = \frac{dx}{u} = \frac{dy}{v} = \frac{dz}{w} \quad (2.26)$$

If we take the derivative with respect to time we obtain

$$\frac{D\tau}{Dt} = 1 \quad (2.27)$$

Then to satisfy the transport conditions, Eqs. (2.20) and (2.21), we may write the flexion vector [37], $\nabla^2\vec{u}$, in potential/complex-lamellar form using Monge potentials

$$\nabla^2\vec{u} = \nabla\Phi + \Psi\nabla\tau \quad (2.28)$$

where the first term can represent Craig's [43] circulation preserving flexion potential and

the second represents the diffusion of vorticity. Then we can substitute the flexion vector into the transport conditions to obtain the transport of the velocity potential, ϕ

$$\frac{D\phi}{Dt} = - \left(\frac{p - \mu\Phi}{\rho} \right) + \frac{\vec{u} \cdot \vec{u}}{2} \quad (2.29)$$

which defines the irrotational component of the velocity field. Then for dimensional consistency, the transport of the difference in enstrophy is

$$\frac{D\tilde{E}}{Dt} = \frac{\mu}{\rho} \Psi \quad (2.30)$$

where Ψ is a source term that either creates or destroys enstrophy along a particle path. Given a closed curve c around a material surface s , with surface elements $d\sigma$, the transport of the enstrophy, E , must satisfy the following equation

$$\frac{DE}{Dt} = \frac{\mu}{\rho} \int_V \nabla^2 (\vec{\omega} \cdot \vec{\omega}) d\sigma \quad (2.31)$$

which, assuming all variables are single-valued, we can re-cast as

$$\frac{DE}{Dt} = \frac{\mu}{\rho} \int_V \nabla^2 [\nabla E \times \nabla \tau]^2 d\sigma \quad (2.32)$$

Then from our definition of the difference in enstrophy, the corresponding transport equation becomes

$$\frac{D\tilde{E}}{Dt} = \frac{\mu}{\rho} \int_V \nabla^2 [\nabla \tilde{E} \times \nabla \tau]^2 d\sigma \quad (2.33)$$

which then allows us to identify the source term, Ψ , as

$$\Psi = \int_V \nabla^2 [\nabla \tilde{E} \times \nabla \tau]^2 d\sigma \quad (2.34)$$

2.5 Transitioning complex-lamellar equation boundary conditions

As the complex-lamellar description of velocity, Eq. (2.22), is only valid locally, we will define our region of interest around a 2D transitioning boundary layer flow field. We will use the end of the fully laminar region, x_A , and the start of the fully turbulent region, x_B , to define our region of interest.

At the fully laminar boundary condition, x_A , we need the complex-lamellar velocity equation, Eq.(2.22) to match a fully laminar velocity. This means

$$\left[\vec{u}_{lam} + \nabla\phi + \tilde{E}\nabla\tau \right] \Big|_{x_A} = \vec{u}_{lam}|_{x_A} \quad (2.35)$$

To eliminate the potential term and hence any pressure effects, we can satisfy this velocity condition by satisfying the vorticity.

$$\left[\vec{\omega}_{lam} + \nabla\tilde{E} \times \nabla\tau \right] \Big|_{x_A} = \vec{\omega}_{lam}|_{x_A} \quad (2.36)$$

We see that for the complex-lamellar vorticity to match the laminar vorticity, then

$$\left[\nabla\tilde{E} \times \nabla\tau \right] \Big|_{x_A} = 0 \quad (2.37)$$

We can construct the difference in enstrophy, $\tilde{E} = E - E_{lam}$, as

$$\tilde{E} = \int_{x_{ref}}^x \int_{y_{ref}}^y (\omega^2 - \omega_{lam}^2) dy dx \quad (2.38)$$

where ω^2 is the enstrophy density found in the transitioning boundary layer, while ω_{lam}^2 is that which would otherwise be found in the baseline laminar flow. Thus at the boundary condition, $x = x_A$, the difference in enstrophy is $\tilde{E} \Big|_{x_A} = 0$ so the complex-lamellar vorticity matches the laminar vorticity at this location.

At the fully turbulent boundary condition, we require that the complex-lamellar velocity equation, Eq.(2.22), match the turbulent velocity.

$$\left[\vec{u}_{lam} + \nabla\phi + \tilde{E}\nabla\tau \right] \Big|_{x_B} = \vec{u}_{turb} \Big|_{x_B} \quad (2.39)$$

To satisfy this condition, we can again use the vorticity

$$\left[\vec{\omega}_{lam} + \nabla\tilde{E} \times \nabla\tau \right] \Big|_{x_B} = \vec{\omega}_{turb} \Big|_{x_B} \quad (2.40)$$

which can be rearranged into the following form

$$\left[\nabla\tilde{E} \times \nabla\tau \right] \Big|_{x_B} = (\vec{\omega}_{turb} - \vec{\omega}_{lam}) \Big|_{x_B} \quad (2.41)$$

To satisfy this velocity condition, we need to know how the enstrophy changes throughout the transition region and an expression for the drift function, τ .

2.5.1 Drift function

The transport of the drift function, as previously mentioned, is defined as

$$\frac{D\tau}{Dt} = 1 \quad (2.42)$$

and can be expanded using the definition of a material derivative, to obtain

$$\frac{D\tau}{Dt} = \frac{\partial\tau}{\partial t} + u(x, y, t) \frac{\partial\tau}{\partial x} + v(x, y, t) \frac{\partial\tau}{\partial y} = 1 \quad (2.43)$$

where we will assume that the unsteady flow can be represented by the separable form

$$u(x, y, t) = u(x, y)T(t) \quad (2.44)$$

2.5 Transitioning complex-lamellar equation boundary conditions

where $u(x, y)$ is the velocity dependent only on x and y and $T(t)$ is a function that depends only on t . We will write the function $T(t)$ as a Fourier series expansion in time so that the velocity can be written in the form

$$\begin{aligned} u(x, y, t) &= u(x, y) [1 + k_2 \sin(\alpha_1 t) + k_3 \cos(\alpha_2 t)] \\ &= u [1 + k_2 \sin(\alpha_1 t) + k_3 \cos(\alpha_2 t)] \end{aligned} \quad (2.45)$$

By using a flow described by Eq.(2.45), we are restricted to pulsed, unsteady flows. However even with this restriction, we can still obtain some significant insight. Then by adding this form of the velocity into the expanded transport equation, Eq.(2.43), we obtain

$$\frac{\partial \tau}{\partial t} + u \frac{\partial \tau}{\partial x} + u [k_2 \sin(\alpha_1 t) + k_3 \cos(\alpha_2 t)] \frac{\partial \tau}{\partial x} + v(x, y, t) \frac{\partial \tau}{\partial y} = 1 \quad (2.46)$$

We can factor the drift function into the following

$$u \frac{\partial \tau}{\partial x} = 1 \quad (2.47)$$

$$\frac{\partial \tau}{\partial t} = - [k_2 \sin(\alpha_1 t) + k_3 \cos(\alpha_2 t)] - v(x, y, t) \frac{\partial \tau}{\partial y} \quad (2.48)$$

and then obtain,

$$\tau = \int \frac{1}{u} dx \quad (2.49)$$

so that we can determine $\partial \tau / \partial y$ to be

$$\frac{\partial \tau}{\partial y} = \frac{\partial}{\partial y} \left(\int \frac{1}{u} dx \right) \quad (2.50)$$

Then, by using the 2D boundary layer approximations, $u \gg v$ and $\frac{\partial^2}{\partial y^2} \gg \frac{\partial^2}{\partial x^2}$ and assuming that we only consider cross-flow locations sufficiently far from the wall, the following drift

function approximations can be made

$$u \frac{\partial \tau}{\partial x} = 1 \tag{2.51}$$

$$\frac{\partial \tau}{\partial t} = - [k_2 \sin(\alpha_1 t) + k_3 \cos(\alpha_2 t)] \tag{2.52}$$

$$\frac{\partial \tau}{\partial y} = 0 \tag{2.53}$$

For this drift function approximation to be valid, we are limited to physical locations where $v \rightarrow 0$, $\frac{\partial \tau}{\partial y} \rightarrow 0$ and $u \neq 0$.

2.5.2 Difference in enstrophy across transition

Recall, that we want to match the potential/complex-lamellar velocity equation to the turbulent velocity at x_B . We will be considering the mean flow at both the laminar and turbulent boundary conditions to be steady which means the vorticity at x_B , Eq. (2.41), will be

$$\begin{aligned} \left[\frac{\partial \tilde{E}}{\partial x} \frac{\partial \tau}{\partial y} - \frac{\partial \tau}{\partial x} \frac{\partial \tilde{E}}{\partial y} \right] \Bigg|_{x_B} &= (\omega_{turb} - \omega_{lam})|_{x_B} \\ - \left[\frac{1}{u} \frac{\partial \tilde{E}}{\partial y} \right] \Bigg|_{x_B} &= (\omega_{turb} - \omega_{lam})|_{x_B} \end{aligned} \tag{2.54}$$

where $u = u(x, y)$. Then by using the difference in enstrophy, Eq.(2.38), we obtain

$$- \left[\frac{1}{u} \int_{x_{ref}}^x (\omega^2 - \omega_{lam}^2) dx \right] \Bigg|_{x_B} = (\omega_{turb} - \omega_{lam})|_{x_B} \tag{2.55}$$

which implies that in order to satisfy the velocity condition at x_B , we need to know the enstrophy density throughout the region between x_A and x_B so we can set the limits of integration to $x_{ref} = x_A$ and $x = x_B$. As we do not know how the enstrophy density will change throughout this region, we will approximate it using the following boundary conditions.

2.5 Transitioning complex-lamellar equation boundary conditions

$$(\omega^2 - \omega_{lam}^2) = \begin{cases} 0 & \text{when } x = x_A \\ (\omega_{turb}^2 - \omega_{lam}^2)|_{x_B} & \text{when } x = x_B \end{cases} \quad (2.56)$$

Then using a power series, we can approximate the difference in enstrophy density as

$$(\omega^2 - \omega_{lam}^2) = (\omega_{turb}^2 - \omega_{lam}^2)|_{x_B} \left(\sum_{n=1}^3 C_n \frac{(x - x_A)^n}{(x_B - x_A)^n} \right) \quad (2.57)$$

where

$$\sum_{n=1}^3 C_n = 1 \quad (2.58)$$

is needed to satisfy the boundary condition at $x = x_B$. We will only approximate the difference in enstrophy density using the first three terms of the power series. We chose to do this because the power series terms will be obtained from geometrical constraints and we do not want these constraints to be more significant than the physical conditions imposed by matching the laminar and turbulent velocities at the boundary. Further explanation will be provided in Chapter 3 when we discuss the geometrical constraints.

Then we can write

$$\int_{x_A}^{x_B} \left(\sum_{n=1}^3 C_n \frac{(x - x_A)^n}{(x_B - x_A)^n} \right) dx = \sum_{n=1}^3 \frac{C_n}{n+1} (x_B - x_A) \quad (2.59)$$

which is the measure of the total difference in enstrophy density between the end of the fully laminar region and the start of the fully turbulent region. Finally, when the approximate difference in enstrophy density, Eq. (2.57), is substituted into the vorticity at x_B , Eq. (2.55), and rearranged, we obtain the following equation

$$u|_{x_B} = - \sum_{n=1}^3 \frac{C_n}{n+1} (\omega_{turb} + \omega_{lam})|_{x_B} (x_B - x_A) \quad (2.60)$$

This equation states that the turbulent velocity at the fully turbulent location is a function

of the enstrophy growth between the fully laminar and fully turbulent regions, the sum of the resulting turbulent and otherwise laminar vorticity at the fully turbulent location, and the length of the fully laminar to fully turbulent region itself.

Finally, by solving the complex-lamellar velocity condition, Eq.(2.60), we will determine the location, x_A where the fully laminar velocity condition is met and the location, x_B , where the fully turbulent velocity condition is met. We will also have an approximation for how the difference in enstrophy density changes throughout the transition region.

CHAPTER 3

Boundary layer transition: Region modelling

Something that has been lacking in the study of transition is a clear definition of locations along the surface associated with transition. To better define these points we begin with what we know with a high degree of certainty regarding boundary layers. From the leading edge we can measure the thickness of the fully laminar flow. The boundary layer will remain in a fully laminar state until the laminar critical stability location, $Re_{x_{cr}}$ is obtained. This location is obtained from stability analysis and indicates where the disturbances, within the laminar flow, begin to grow. We know that before this point the laminar flow is stable. Then at some location much further downstream, the flow can be measured as being fully turbulent and the thickness of the turbulent boundary layer determined. The location of the effective leading edge of the turbulent boundary layer, Re_{x_t} , can be determined by extrapolating back from the measured data to the surface. We illustrate this pictorially in Figure 3.1, where we plot the laminar and turbulent boundary layer thickness versus the various x locations. A solid line means we know definitively the value of the boundary layer thickness and therefore

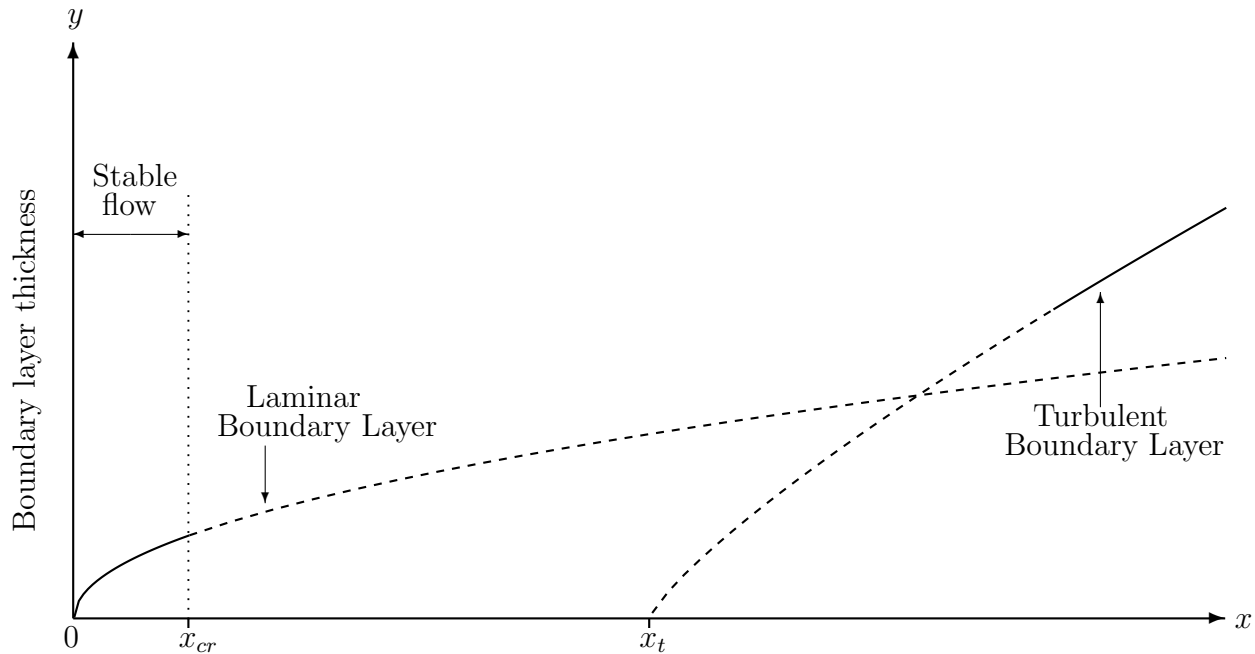


Figure 3.1 – Model of the laminar and turbulent laminar boundary layers

the shape of the boundary layer and a dashed line means we are extrapolating from the known value. The intersection point between the laminar and turbulent boundary layers is a consequence of the graphical representation and has no physical meaning.

In 1951, Emmons [26] performed a water table experiment and discovered that as the laminar boundary layer moved downstream patches of turbulent flow occurred intermittently within the laminar boundary layer. These patches or spots would grow as they moved downstream until eventually they covered the downstream region continuously. Emmons [26] did not make quantitative measurements and instead relied on visualization of the flow to determine the probability function for specifying the fraction of time the flow at each point would be turbulent. Emmons' [26] interpretation of transition is that initially a laminar boundary layer completely covers a given body. This boundary layer is disturbed and these disturbances amplify and damp until a critical amplitude is reached. Then at some point further downstream of this critical point, the boundary-layer disturbances will cause 'breaks' in the laminar boundary layer and turbulent spots will begin to occur. In Figure 3.2 we have inter-

puted Emmons' [26] transition model pictorially, with the laminar and turbulent boundary layer thickness plotted with the corresponding x locations. From Emmons' [26] description

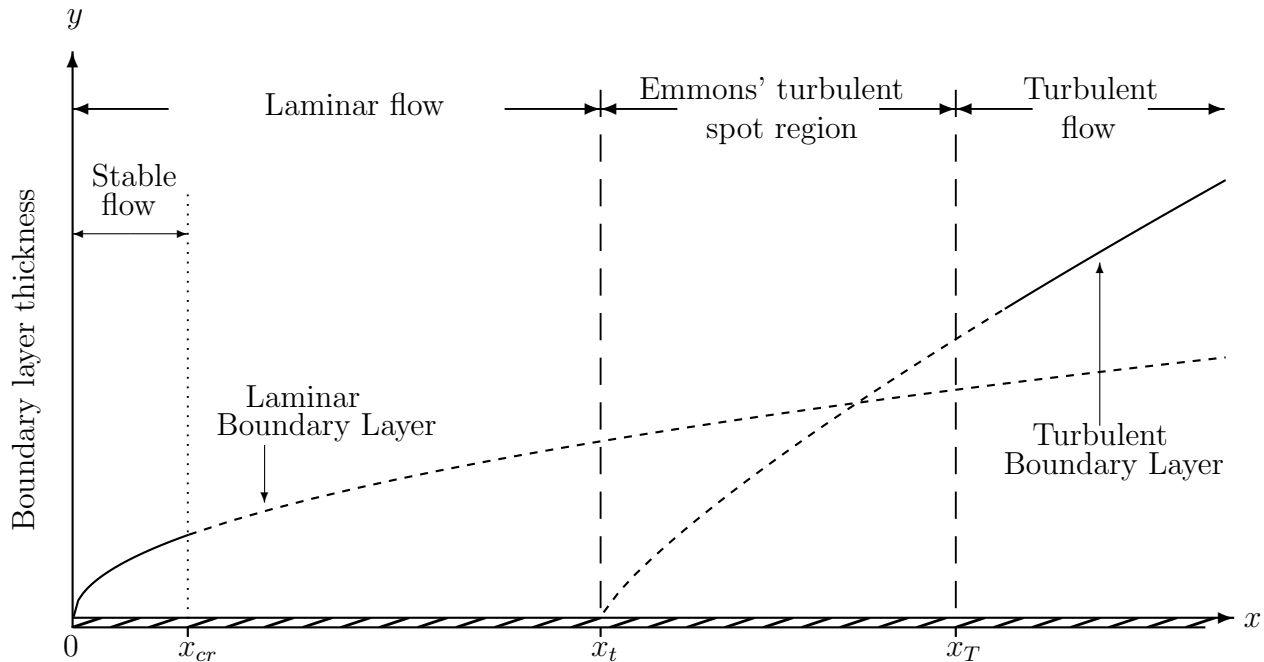


Figure 3.2 – Emmons model of a boundary layer that transitions across an intermittency region

of the boundary layer process we interpret that the start of the turbulent spot region is equal to the effective leading edge of the turbulent boundary layer, x_t . The end of the turbulent spot region corresponds to where the flow is only turbulent. We can expect this location to be somewhere downstream of the x_t and may or may not be where the fully turbulent flow is measured. Therefore, we have illustrated x_T between the effective leading edge of the turbulent boundary layer and where the fully turbulent flow is measured. The location where the disturbances within the laminar boundary layer reach the critical amplitude is illustrated as x_{cr} and is determined using stability analysis.

To verify Emmons' [26] model of transition, Schubauer and Klebanoff [2] conducted an experimental investigation of a boundary layer along a flat plate. They used hot-wire probes to measure the voltage fluctuations in the x direction and using calibration data, velocity fluctu-

tuations could be calculated. Then by taking photographs of the output on the oscilloscope screen, they made interpretations regarding laminar and turbulent flow. Regular sinusoidal oscillations described laminar flow and bursts of high frequency voltage represented turbulent flow. Then from the oscilloscope records they determined the fraction of time the flow was turbulent. This fraction is defined as an intermittency factor, γ . From the records, it was difficult to determine an intermittency of 0 and 1 so a Gaussian integral curve was fitted to the measured data in order to estimate the end points.

Based on these observations, Narasimha [27] introduced his universal intermittency distribution, which he based on the concept of concentrated breakdown. The idea of concentrated breakdown is that at a single point downstream of the critical stability location, the laminar flow will break down to form turbulent spots. The single location where breakdown occurred and intermittency began was defined as the location of the effective leading edge of the turbulent boundary layer. Then in 1985, Narasimha [3] expanded this concept by saying the laminar flow will actually breakdown over some distance across the flow where the total distance of breakdown would be small compared with what Narasimha [27] termed the measurable extent of the intermittency region. He defined the extent of the intermittency region as the length between where the intermittency, γ , is 0.75 and 0.25. This is written mathematically as $Re_{x|\gamma=0.75} - Re_{x|\gamma=0.25}$ where $\gamma = 0.75$ means the flow at the corresponding Reynolds number is 75% turbulent and $\gamma = 0.25$ means the flow is 25% turbulent. He used the experimental data within this region to fit the distribution as the intermittency factor could be accurately determined within this region [3]. He showed a pictorial representation, in Ref.[5], of where this break down region would occur along a flat plate when the external disturbances are low which we have reproduced in Figure 3.3. Based on this figure, we can assume that the laminar flow will begin to breakdown at the effective leading edge of the turbulent boundary layer and the start of intermittency will begin at some location slightly downstream of the effective leading edge. We have modelled Narasimha's [5] concept of breakdown for a boundary layer transition and have shown it pictorially in Figure 3.4.

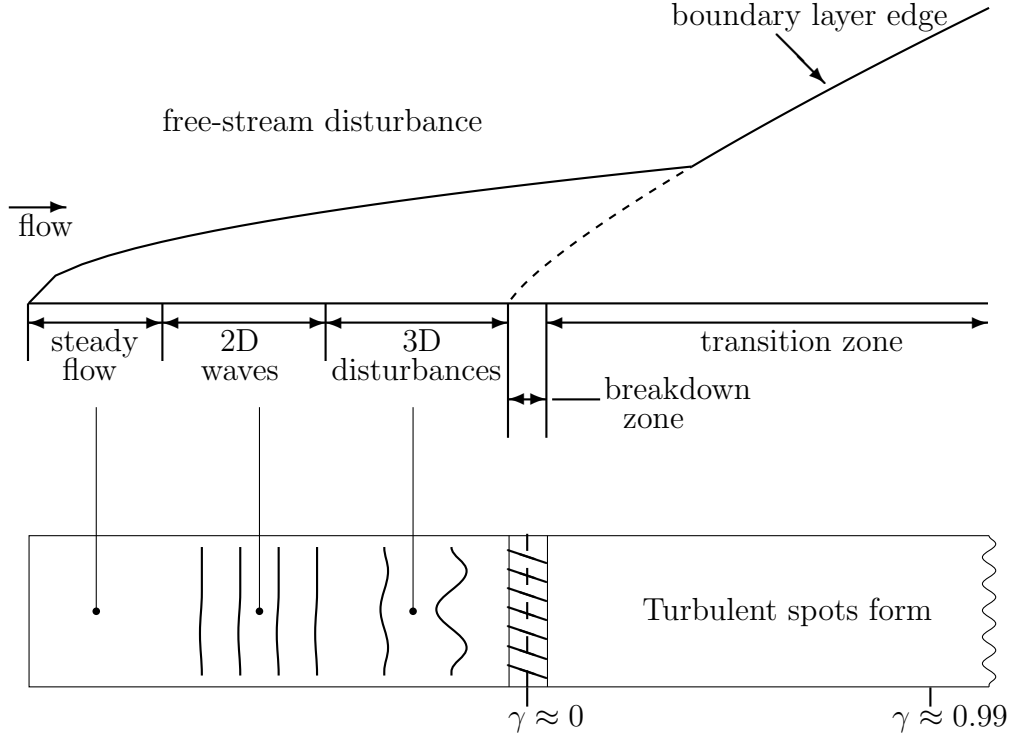


Figure 3.3 – Figure recreated from Narasimha and Dey [5] representing the stages from laminar to turbulent flow along a flat plate.

Again we plot the laminar and turbulent boundary layer thickness with the x locations. The x locations highlighted in Figure 3.4 are x_{cr} , the critical location determined from stability analysis, x_t , the effective leading edge of the turbulent boundary layer, x_0 , the start of intermittency and x_T , the end of intermittency. The measurable extent of intermittency is also illustrated as starting at $x|_{\gamma=0.25}$ and ending at $x|_{\gamma=0.75}$. We have also labelled the corresponding regions.

In our research, we believe that we can bound the breakdown and intermittency region in order to determine the location of the start and end of intermittency mathematically. In order to achieve this, we specify that at the upstream bounding location, x_A , a laminar velocity profile will be imposed and at the downstream location, x_B , a turbulent velocity profile will be imposed. These bounding locations will change in order to satisfy the complex-lamellar

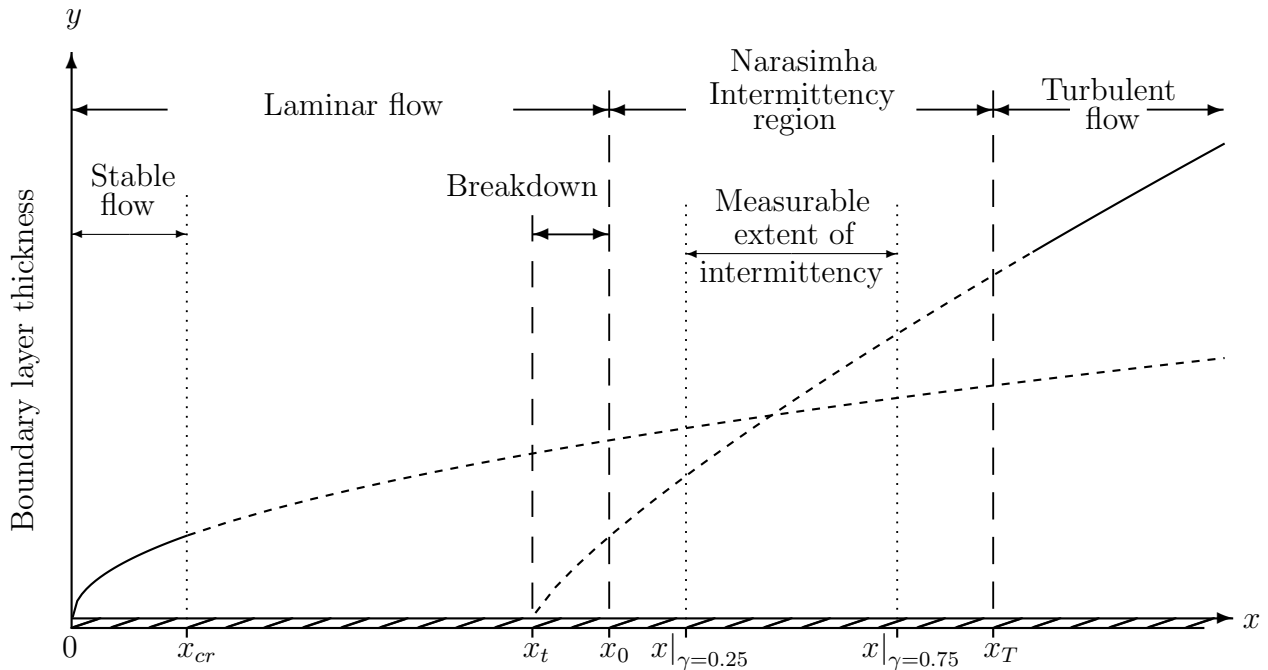


Figure 3.4 – Narasimha model of a boundary layer transitioning via breakdown and intermittency

velocity condition, Eq.(2.60). In Figure 3.5, we illustrate this transition model where the laminar and turbulent boundary layer thickness are represented along with the corresponding x locations. In Figure 3.5, we illustrate x_A between the critical stability location, $Re_{x_{cr}}$ and the effective leading edge of the turbulent boundary layer, x_t . However, it should be made clear that x_A will be located where the laminar velocity profile is satisfied, in theory this could be anywhere from the leading edge up until the effective leading edge of the turbulent boundary layer. The same applies for x_B , where we would expect the turbulent velocity profile to be satisfied anywhere downstream of the end of intermittency.

The final transition model we will consider is for a separated shear layer transitioning over a separation bubble. When a laminar boundary layer is subjected to a strong adverse pressure gradient, it can begin to separate from the surface. The flow within the free-stream layer near the surface may begin to transition and if this flow reattaches downstream as turbulent flow, a laminar separation bubble is formed on the surface [1]. Originally, the

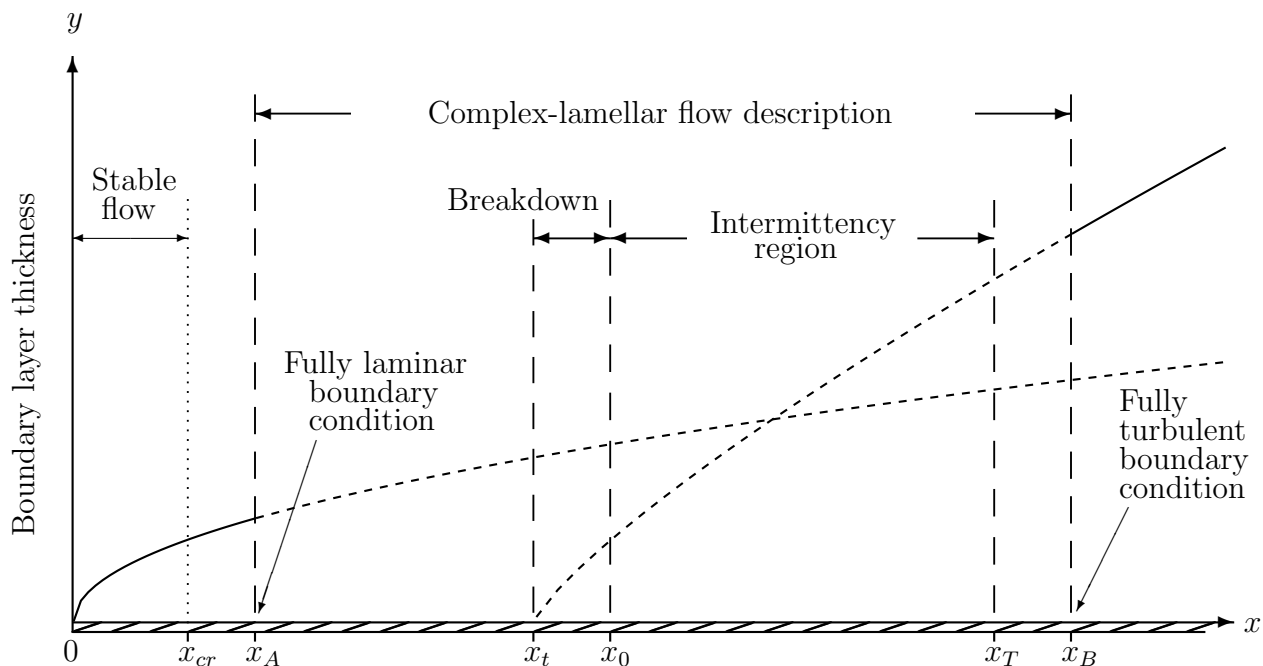


Figure 3.5 – Research model of boundary layer transition where breakdown and intermittency are bounded between x_A and x_B .

flow was divided into two main regions, an upstream region of nearly constant pressure and a downstream region of pressure recovery [4]. Mayle [1] further divided the upstream region into two regions, an unstable laminar shear region and a transition region, where the unstable laminar region ends with the formation of turbulent spots. This implies that the transition region is equivalent to an intermittency region. The start of the constant pressure region corresponded to the separation point and the start of the unstable laminar region. The end of the constant pressure region corresponded to the end of the intermittency region. The start of the intermittency region is determined using experimental intermittency measurements. Mayle [1] illustrated these regions over a separation bubble in his paper and it has been reproduced here in Figure 3.6, where x_s is the separation point, x_t is the start of the transition region, x_{Tp} is the the end of the transition region and x_r is the reattachment point.

To solve for a separation bubble case, we can bound the separation bubble between a laminar

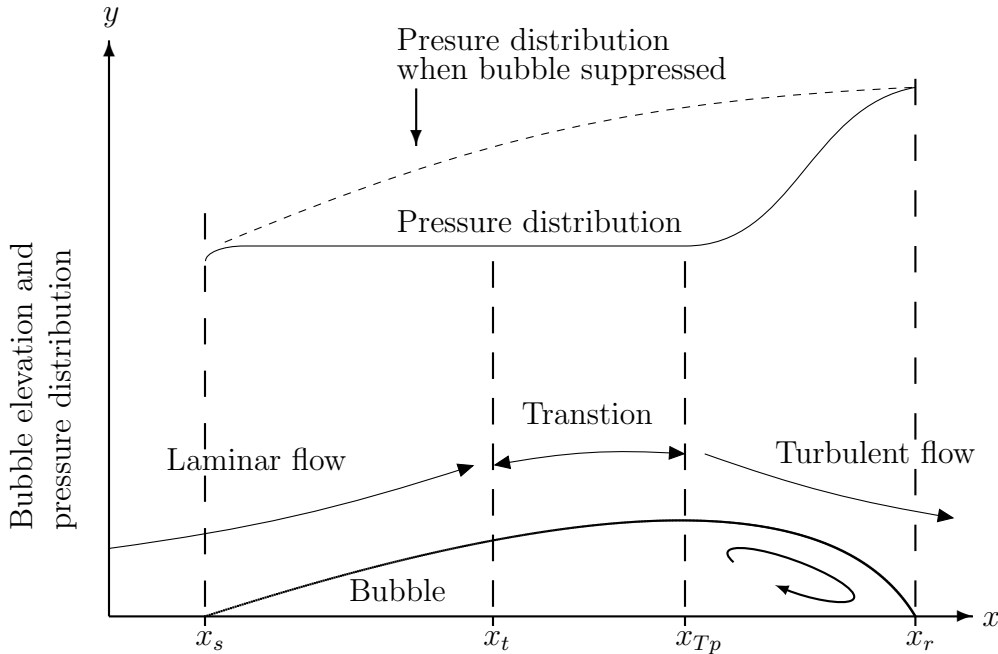


Figure 3.6 – Flow around a separation bubble recreated from Mayle [1]

and turbulent flow. Then at x_A , we will specify a laminar velocity profile that is on the verge of separation. We can achieve this using a laminar velocity profile equation that includes a term to account for the effect of a local pressure gradient. This will then allow us to impose the condition that $x_A = x_s$. At x_B , we will specify a turbulent velocity profile. Experiments [4, 44, 45] have shown that the flow at reattachment is turbulent. Therefore, we would expect that $x_B \approx x_r$. Transition over a separation bubble occurs within a small region and so to be consistent in our illustration of the various x locations, we show in our transition model, Figure 3.7, the laminar boundary layer beginning at an upstream location from the leading edge. We have plotted the laminar and turbulent boundary layer thickness with the various x locations, where x_0 is the start of intermittency and x_T is the end of intermittency.

3.1 Fully laminar boundary condition

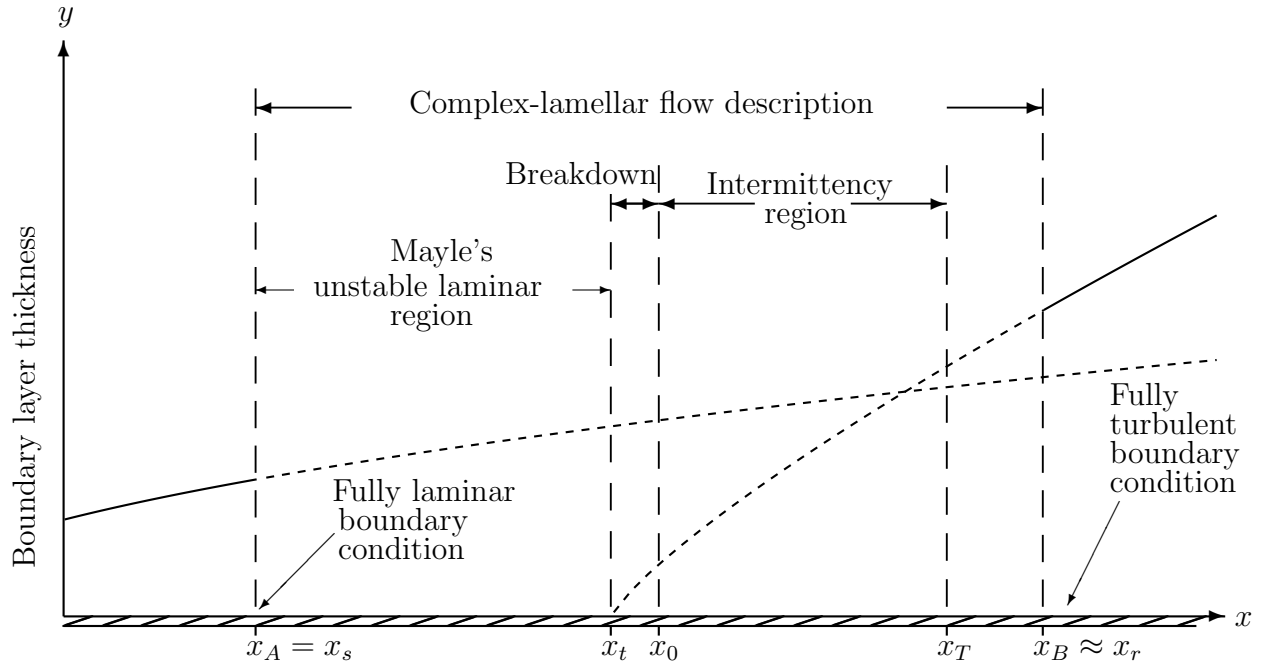


Figure 3.7 – Research model of boundary layer transition over a separation bubble bounded between x_A and x_B .

3.1 Fully laminar boundary condition

Within our first transition model, Figure 3.5, all we require is that the velocity profile at Re_{x_A} must satisfy a laminar boundary layer. However, for the second transition model, Figure 3.7, the velocity profile must satisfy a laminar boundary layer on the verge of separation. Therefore, to meet both of these requirements we need a laminar velocity profile that takes into account different pressure gradients. This can be achieved using the Pohlhausen velocity profile as different pressure gradients are included through the Pohlhausen parameter

$$\lambda = -\frac{\delta^2}{\mu U_\infty} \frac{\partial p}{\partial x} \quad (3.1)$$

where an adverse pressure gradient, $\frac{\partial p}{\partial x} > 0$, is represented by $\lambda < 0$ and a favourable pressure gradient, $\frac{\partial p}{\partial x} < 0$, is represented by $\lambda > 0$. Furthermore, the presence of flow separation exists when $\lambda = -12$ [14].

Pohlhausen's [46] velocity profile is

$$\frac{u}{U_\infty} = \left(2 + \frac{\lambda}{6}\right) \left(\frac{y}{\delta}\right) - \frac{\lambda}{2} \left(\frac{y}{\delta}\right)^2 - \left(2 - \frac{\lambda}{2}\right) \left(\frac{y}{\delta}\right)^3 + \left(1 - \frac{\lambda}{6}\right) \left(\frac{y}{\delta}\right)^4 \quad (3.2)$$

where U_∞ is the free-stream velocity and δ is the boundary layer thickness. Typically, the momentum thickness is determined by solving the momentum integral equation using the velocity profile for different values of λ . Then δ is determined through its relationship to the momentum thickness. We have chosen instead to keep δ fixed and to calculate it using the exact Blasius solution,

$$\delta_{lam} = 5xRe_x^{-1/2} \quad (3.3)$$

where Re_x is the Reynolds number based on the x location measured from the leading edge of the flat plate. The reason we chose not to change δ is that the location of the laminar boundary condition is not fixed and is determined from the solution of the complex-lamellar decomposition, Eq.(2.60). Therefore, x_A will correspond to the location where a boundary layer thickness represented by the Blasius solution is obtained.

The following expression for the laminar momentum thickness is determined by using the Pohlhausen velocity profile and Holstein and Bohlen's [14] analysis to solve the momentum integral equation.

$$\theta_{lam}^2 = A^2 \frac{\mu}{\rho} \int \frac{1}{U} dx \quad (3.4)$$

where

$$A^2 = 2 \left(\frac{37}{315} - \frac{\lambda}{945} + \frac{\lambda^2}{9072} \right) \left(2 - \frac{116\lambda}{315} + \left\{ \frac{2}{945} + \frac{1}{120} \right\} \lambda^2 + \frac{2\lambda^3}{9072} \right) \quad (3.5)$$

As A contains the Pohlhausen parameter, λ , this definition of the momentum thickness also allows for changes within the pressure gradient to be taken into account. Then we can model the mean flow as

$$U = U_\infty + u' \quad (3.6)$$

3.2 Fully turbulent boundary condition

and the momentum thickness equation becomes

$$\theta_{lam}^2 = A^2 \left(\frac{\mu}{\rho} \right) \frac{1}{U_\infty} \int \frac{1}{1 + u'/U_\infty} dx \quad (3.7)$$

Assuming that the presence of transition creates disturbances of the order

$$\frac{u'}{U_\infty} \ll 1 \quad (3.8)$$

allows us to construct the series approximation

$$\frac{1}{1 + u'/U_\infty} = 1 - \left(\frac{u'}{U_\infty} \right)^2 + \left(\frac{u'}{U_\infty} \right)^3 - \left(\frac{u'}{U_\infty} \right)^4 + O \left\{ \left(\frac{u'}{U_\infty} \right)^5 \right\} \quad (3.9)$$

and the resulting first order approximation for the laminar momentum thickness is

$$\theta_{lam} = Ax^{1/2} \left(\frac{\rho U_\infty}{\mu} \right)^{-1/2} \quad (3.10)$$

3.2 Fully turbulent boundary condition

We will use Prandtl-von Karman power law velocity profile for a flat plate [14] to describe the mean turbulent velocity, u_{turb}

$$\frac{u_{turb}}{U_\infty} = \left(\frac{y}{\delta_{turb}} \right)^{1/7} \quad (3.11)$$

This profile is valid for zero-pressure gradient flows however we will also use it for the separated flow transition over a separation bubble test case. For this test case, we expect the local pressure gradient at the location of the turbulent boundary condition to be minimal thereby making this choice of profile reasonable.

The boundary layer thickness is defined as

$$\delta_{turb} = 0.375x' Re_{x'}^{-1/5} \quad (3.12)$$

the Reynolds number based on x' is written as

$$Re_{x'} = \frac{\rho U_{\infty} x'}{\mu} \quad (3.13)$$

and the momentum thickness can be calculated from

$$\theta_{turb} = \frac{7}{72} \delta_{turb} \quad (3.14)$$

The turbulent boundary layer is coupled to the laminar one through the transformation $x = x' + x_t$, where the effective leading edge of the turbulent boundary layer is located at x_t .

It should be noted that no attempt is made to model either the viscous sublayer or the discontinuous nature of the log law since our approximate drift function, Eq.(2.51), restricts us from these regions.

3.3 Modelling the slope of the difference in enstrophy density function

Now that we have descriptions for the velocity profiles at Re_{x_A} and Re_{x_B} , we need to determine additional equations to solve for the power series coefficients within the difference in enstrophy density approximation. We can construct these equations using geometric conditions related to intermittency. To begin, let us define the difference in enstrophy density function, η

$$\eta = \left(\sum_{n=1}^3 C_n \frac{(x - x_A)^n}{(x_B - x_A)^n} \right) = \frac{(\omega^2 - \omega_{lam}^2)}{(\omega_{turb}^2 - \omega_{lam}^2)|_{x_B}} \quad (3.15)$$

3.3 Modelling the slope of the difference in enstrophy density function

which can then be rewritten as

$$\begin{aligned} \omega^2 = & (1 - \eta) \omega_{lam}^2 + \eta \omega_{turb}^2 \\ & + \eta \left[\left(\omega_{turb}^2|_{x_B} - \omega_{turb}^2 \right) - \left(\omega_{lam}^2|_{x_B} - \omega_{lam}^2 \right) \right] \end{aligned} \quad (3.16)$$

which tells us that the enstrophy density will change throughout the region from Re_{x_A} to Re_{x_B} as a linear combination of the laminar and turbulent enstrophy density plus an additional term involving the laminar and turbulent enstrophy density at Re_{x_B} .

Recall from Chapter 2, that Dhawan and Narasimha [30] used the following model to determine the velocity through the intermittency region

$$\vec{u} = (1 - \gamma) \vec{u}_{laminar} + \gamma \vec{u}_{turbulent} \quad (3.17)$$

where $\vec{u}_{laminar}$ is the laminar velocity and $\vec{u}_{turbulent}$ is the turbulent velocity with γ varying from 0 to 1. We can see that the enstrophy density equation, Eq.(3.16), looks similar to this model. We would expect that at the end points, u_{lam} used to calculate ω_{lam}^2 would be equivalent to $u_{laminar}$ and u_{turb} used to calculate ω_{turb}^2 would be equivalent to $u_{turbulent}$. However, between the end points these values may or may not be the same. As well, we don't know if η is equal to γ , however, as γ is the universal distribution it seems reasonable to match a couple of points and then rely on the complex-lamellar condition to determine where these points should be located.

Narasimha's universal intermittency distribution [27] is

$$\gamma = 1 - \exp \left(-0.412 \frac{(x - x_t)^2}{(x|_{\gamma=0.75} - x|_{\gamma=0.25})^2} \right) \quad (3.18)$$

where, as previously mentioned, $x|_{\gamma=0.25}$ and $x|_{\gamma=0.75}$ correspond to the locations where $\gamma = 0.25$ and 0.75 , respectively. x_t is the effective leading edge of the turbulent boundary

layer and also corresponds to the start of intermittency as this distribution is based on concentrated breakdown. The shape of the intermittency distribution was based on matching the experimental data between $\gamma = 0.25$ and $\gamma = 0.75$ so the shape at the end points is a result of the curve fit and not the experimental data. As well, this distribution does not cross the x axis and will never reach 1 since this function goes to infinity. Therefore, we chose to obtain our geometrical conditions by matching η to the slope of the intermittency distribution between $\gamma = 0.25$ and $\gamma = 0.75$ and not impose any conditions on the shape at the start and end of intermittency.

These conditions will not specify the physical location of where the slope of η is placed along the flat plate so by themselves these conditions just generate a shape. However, it is when we couple the geometrical conditions with the physical conditions, imposed by the complex-lamellar decomposition, that the slope will have a physical location within the region Re_{x_A} to Re_{x_B} .

The geometrical constraints we will use to determine the slope of η are two points and a slope. For the first equation, we chose a value of 0.5, as this is the midpoint. This is represented mathematically as

$$0.5 = \sum_{n=1}^3 C_n \frac{(Re_{x|\gamma=0.5} - Re_{x_A})^n}{(Re_{x_B} - Re_{x_A})^n} \quad (3.19)$$

We can determine $Re_{x|\gamma=0.5}$ by utilizing Narasimha's [27] universal intermittency distribution, Eq.(3.18) and rearranging to obtain

$$Re_{x|\gamma=0.5} = Re_{x_t} + 1.2971 \left(Re_{x|\gamma=0.75} - Re_{x|\gamma=0.25} \right) \quad (3.20)$$

where $\left(Re_{x|\gamma=0.75} - Re_{x|\gamma=0.25} \right)$ is the extent of the intermittency region [27], and Re_{x_t} , as previously stated, is the effective leading edge of the turbulent boundary layer. The extent of

3.3 Modelling the slope of the difference in enstrophy density function

the intermittency region is not universal for all types of transitioning boundary layers so this length will be obtained from experimental correlations related to the specific transitioning boundary layer.

The first equation to determine the slope of η is written as

$$0.5 = \sum_{n=1}^3 C_n \frac{(Re_{x_t} + 1.2971 (Re_{x|\gamma=0.75} - Re_{x|\gamma=0.25}) - Re_{x_A})^n}{(Re_{x_B} - Re_{x_A})^n} \quad (3.21)$$

It should be noted that in using Eq.(3.20) within the enstrophy growth function we are only specifying a length and not forcing η to be 0.5 at a specific x location.

For the second equation, we chose a value 0.25 as this value is the mid point between $\gamma = 0.5$ and the effective leading edge of the turbulent boundary layer, Re_{x_t} . This equation is written as

$$0.25 = \sum_{n=1}^3 C_n \frac{(Re_{x_t} + 0.8356 (Re_{x|\gamma=0.75} - Re_{x|\gamma=0.25}) - Re_{x_A})^n}{(Re_{x_B} - Re_{x_A})^n} \quad (3.22)$$

For the third equation, we chose the slope of the intermittency distribution, Eq.(3.18), at $\gamma = 0.5$ to scale with the slope the difference in enstrophy density function, η .

$$\left. \frac{d\gamma}{dx} \right|_{x\gamma=0.5} = \left. \frac{d}{dx} \left[\sum_{n=1}^3 C_n \frac{(Re_x - Re_{x_A})^n}{(Re_{x_B} - Re_{x_A})^n} \right] \right|_{x\gamma=0.5} \quad (3.23)$$

which when expanded produces

$$\frac{0.0983}{(Re_{x|\gamma=0.75} - Re_{x|\gamma=0.25})} = \sum_{n=1}^3 C_n \frac{n (Re_{x_t} + 1.2971 (Re_{x|\gamma=0.75} - Re_{x|\gamma=0.25}) - Re_{x_A})^{n-1}}{(Re_{x_B} - Re_{x_A})^n} \quad (3.24)$$

Additional geometrical conditions could have been chosen at $\gamma = 0.75$. However, since η spans the whole length between Re_{x_A} to Re_{x_B} and the measurable intermittency region is only a small portion of that length, we believe it is sufficient to use 3 geometrical conditions to determine the slope of η within this measurable region.

3.4 Expanded complex-lamellar velocity condition

We will expand the complex-lamellar velocity condition, Eq.(2.60), by substituting in the Prandtl turbulent velocity profile, Eqs. (3.11,3.12), and the Pohlhausen laminar velocity profile, Eqs. (3.2,3.3) to obtain

$$\begin{aligned} & \left[\frac{1}{7} \left(\frac{1}{0.375} \left(\frac{\rho U_\infty}{\mu} \right)^{\frac{1}{5}} (x_B - x_t)^{-\frac{4}{5}} \right)^{\frac{1}{7}} y^{-\frac{6}{7}} + \frac{(2 + \lambda/6)}{5(x_B)^{\frac{1}{2}}} \left(\frac{\rho U_\infty}{\mu} \right)^{\frac{1}{2}} - \frac{\lambda y}{(5)^2(x_B)} \left(\frac{\rho U_\infty}{\mu} \right) \right. \\ & \quad \left. - \frac{3(2 - \lambda/2)y^2}{(5)^3(x_B)^{\frac{3}{2}}} \left(\frac{\rho U_\infty}{\mu} \right)^{\frac{3}{2}} + \frac{4(1 - \lambda/6)y^3}{(5)^4(x_B)^2} \left(\frac{\rho U_\infty}{\mu} \right)^2 \right] (x_B - x_A) \sum_{n=1}^3 \frac{C_n}{n+1} \\ & \qquad \qquad \qquad = \left(\frac{y}{0.375} \left(\frac{\rho U_\infty}{\mu} \right)^{\frac{1}{5}} (x_B - x_t)^{-\frac{4}{5}} \right)^{\frac{1}{7}} \quad (3.25) \end{aligned}$$

Since the length of the region between x_A and x_B will be significantly larger than the height of the boundary layer, we can assume that changes to the cross-flow location will not significantly affect the location of x_A and x_B . Therefore, we will evaluate Eq.(3.25) at a single cross-flow location with the expectation that the resulting Reynolds number based on x will be accurate.

We will choose a cross-flow location that is equal to the momentum thickness at a specific x location,

3.5 Boundary layer transition model equations

$$y = \theta|_x \quad (3.26)$$

since the momentum thickness has been measured experimentally for various transition cases. When we substitute this cross-flow location into Eq.(3.25) and non-dimensionalize the equation, we obtain

$$\begin{aligned} & \left[\frac{1}{7} \left(\frac{1}{Re_{\theta|_x}} \right)^{\frac{6}{7}} \left(\frac{1}{0.375 (Re_{x_A} (R - R_L))^{\frac{4}{5}}} \right)^{\frac{1}{7}} + \frac{(2 + \lambda/6)}{5 (Re_{x_A} * R)^{\frac{1}{2}}} - \frac{\lambda Re_{\theta|_x}}{(5)^2 (Re_{x_A} * R)} \right. \\ & \quad \left. - \frac{3(2 - \lambda/2) Re_{\theta|_x}^2}{(5)^3 (Re_{x_A} * R)^{\frac{3}{2}}} + \frac{4(1 - \lambda/6) Re_{\theta|_x}^3}{(5)^4 (Re_{x_A} * R)^2} \right] \left[Re_{x_A} (R - 1) \sum_{n=0}^3 \frac{C_n}{n + 1} \right] \\ & \quad = \left(\frac{Re_{\theta|_x}}{0.375 (Re_{x_A} (R - R_L))^{\frac{4}{5}}} \right)^{\frac{1}{7}} \quad (3.27) \end{aligned}$$

where, for convenience, we chose to define two ratios across transition as

$$R = \frac{Re_{x_B}}{Re_{x_A}} \quad R_L = \frac{Re_{x_t}}{Re_{x_A}} \quad (3.28)$$

3.5 Boundary layer transition model equations

We will solve the expanded complex-lamellar equation, Eq.(3.27), along with the equations for determining the slope of η , Eqs.(3.21 - 3.24) and the boundary condition for the series coefficients, Eq. (2.58) to calculate location of Re_{x_A} and Re_{x_B} . We will term this set of non-linear, algebraic equations the boundary layer transition equations.

$$\begin{aligned}
 & \left[\frac{1}{7} \left(\frac{1}{Re_{\theta|x}} \right)^{\frac{6}{7}} \left(\frac{1}{0.375 (Re_{x_A} (R - R_L))^{\frac{4}{5}}} \right)^{\frac{1}{7}} + \frac{(2 + \lambda/6)}{5 (Re_{x_A} * R)^{\frac{1}{2}}} - \frac{\lambda Re_{\theta|x}}{(5)^2 (Re_{x_A} * R)} \right. \\
 & \quad \left. - \frac{3(2 - \lambda/2) Re_{\theta|x}^2}{(5)^3 (Re_{x_A} * R)^{\frac{3}{2}}} + \frac{4(1 - \lambda/6) Re_{\theta|x}^3}{(5)^4 (Re_{x_A} * R)^2} \right] \left[Re_{x_A} (R - 1) \sum_{n=1}^3 \frac{C_n}{n+1} \right] \\
 & \quad = \left(\frac{Re_{\theta|x}}{0.375 (Re_{x_A} (R - R_L))^{\frac{4}{5}}} \right)^{\frac{1}{7}} \\
 1 &= \sum_{n=1}^3 C_n \\
 0.5 &= \sum_{n=1}^3 C_n \frac{(Re_{x_t} + 1.2971 (Re_{x|\gamma=0.75} - Re_{x|\gamma=0.25}) - Re_{x_A})^n}{(Re_{x_B} - Re_{x_A})^n} \\
 0.25 &= \sum_{n=1}^3 C_n \frac{(Re_{x_t} + 0.8356 (Re_{x|\gamma=0.75} - Re_{x|\gamma=0.25}) - Re_{x_A})^n}{(Re_{x_B} - Re_{x_A})^n} \\
 \frac{0.0983}{(Re_{x|\gamma=0.75} - Re_{x|\gamma=0.25})} &= \sum_{n=1}^3 C_n \frac{n(Re_{x_t} + 1.2971 (Re_{x|\gamma=0.75} - Re_{x|\gamma=0.25}) - Re_{x_A})^{n-1}}{(Re_{x_B} - Re_{x_A})^n}
 \end{aligned} \tag{3.29}$$

The first and second equation are the physical conditions that are imposed through the complex-lamellar decomposition. The first equation ensures that the complex-lamellar velocity equation matches the turbulent velocity at x_B . By solving this equation, we obtain the locations of where the flow is fully laminar and fully turbulent. The second equation ensures that the power series coefficients add up to 1, thereby, satisfying the physical requirement that the difference in enstrophy density at x_B will be the difference between the turbulent enstrophy density and the laminar enstrophy density. The last three equations are the geometrical conditions related to intermittency. We determine the slope of the difference in enstrophy density function, η by matching the slope of intermittency at $\gamma = 0.5$, and two points at $\gamma = 0.25$ and $\gamma = 0.5$.

3.5.1 Numerical method

We solved the set of 5 non-linear algebraic equations using the numeric solver in Matlab and specified a termination tolerance on the function value to be 10^{-12} . The default algorithm, trust-region dogleg, was used to find the root of the system of equations. The advantage to using this algorithm is that each step is determined from a combination of a step along the steepest descent direction and a Newton step. This way if the Newton step is undefined, for instance when the Jacobian is singular, the next step is solely determined from the step in the steepest descent direction.

We solved the set of equations, using Matlab, to determine solutions for both a natural boundary layer transition and a separated flow transition over a separation bubble. For both cases, multiple solutions were obtained with some solutions being complex and some real. We interpreted the real solutions and their possible physical meaning by analyzing the locations of Re_{x_A} and Re_{x_B} compared to the effective leading edge of the turbulent boundary layer, Re_{x_t} , and by analyzing how the difference in enstrophy density function, η , changed between Re_{x_A} and Re_{x_B} . The solutions that are presented in Chapter 5 and 7 each have a physical interpretation in which experimental data exists for comparison. The other real solutions could be interpreted to have physical meanings such as relaminarization, however, we did not have experimental data for comparison.

When we solved the system of equations, Eq.(3.29), convergence occurred quickly. When we changed the configuration and used the point, $\gamma = 0.75$ instead of $\gamma = 0.25$ within the geometrical conditions, the algorithm had very slow convergence. A possible explanation for this is that if the Jacobian, for this set of equations, is nearly singular, the algorithm will only use a step in the steepest descent direction. A common characteristic of steepest descent methods is slow convergence and this is consistent with what we observe for this set of equations.

CHAPTER 4

Natural boundary layer transition

The first case we solved is that of a naturally transitioning boundary layer over a flat plate with zero pressure gradient flow. This test case has been studied extensively [26, 47, 2, 25, 29] and is the benchmark for all transition cases. Even so, there is still some ambiguity in terms of where transition begins and so by solving the boundary layer transition model equations, Eq.(3.29), we will be able to give a more concrete answer as to where the start and end of intermittency is located.

In order to solve the boundary layer transition model equations, Eq.(3.29), we need to know two things beforehand, 1) the location of the effective leading edge of the turbulent boundary layer, x_t , and 2) the length of the extent of the intermittency region. We will obtain this location and length for a natural boundary layer transition using the experimental correlations described below.

4.1 Determination of the effective leading edge of the turbulent boundary layer

The well established correlations developed by Abu-Ghannam and Shaw [25] were determined experimentally by placing boundary layer pitot tubes close to the surface at a fixed location and then determining the surface velocity for a range of wind tunnel speeds. They used a change in the surface velocity gradient to determine the start and end of transition. The location where this gradient began to increase, x_1 , was the start of transition. The location where the velocity gradient became zero, x_2 , was the end of transition. Then at these two locations they measured the momentum thickness by traversing the boundary layer with the pitot tube. They plotted the momentum thickness measurements at several different free-stream turbulence levels and compared them to the measurements of other researchers [25]. From this comparison, they determined the following correlation for the start of transition based on the momentum thickness Reynolds number and how it changes due to the free-stream turbulence level.

$$Re_{\theta}|_{x_1} = 163 + e^{6.91-Tu} \quad (4.1)$$

where the subscript x_1 is the location where the gradient of the surface velocity begins to increase and Tu is the the free-stream turbulence level. Abu-Ghannam and Shaw also determined a correlation relating the momentum thickness Reynolds number at the end of transition with the Reynolds number at the start of transition,

$$Re_{\theta}|_{x_2} = 2.667Re_{\theta}|_{x_1} \quad (4.2)$$

where the subscript x_2 is the location where the gradient of the surface velocity becomes zero. Abu-Ghannam and Shaw [25] determined that consistent results were obtained when the theoretical laminar relationship between the Reynolds number based on the momentum

thickness and x was used with Eq.(4.1) to determine $Re_{x|x_1}$ compared with $Re_{x|x_1}$ being determined from pitot-tube measurements. Therefore, we will determine $Re_{x|x_1}$ using Eq.(3.10) to obtain

$$Re_{x|x_1} = \left(\frac{Re_{\theta|x_1}}{A} \right)^2 \quad (4.3)$$

Similarly we will use Eq. (3.14), the turbulent relationship and Eq.(4.2) to determine $Re_{x|x_2}$

$$Re_{x|x_2} = \left[\frac{72}{7} \left(\frac{1}{0.375} \right) Re_{\theta|x_2} \right]^{\frac{5}{4}} + Re_{x_t} \quad (4.4)$$

It was noted [3, 48] that the start of transition determined by using surface measurements from pitot tubes did not correspond to the location of the effective leading edge of the turbulent boundary layer, x_t , or to the start of intermittency, x_0 . Narasimha and Dey [3] determined a conversion factor to relate the transition start and end, determined using surface measurements, to the effective leading edge of the turbulent boundary layer determined using intermittency measurements.

$$x_t \simeq x|x_1 - 0.26 (x|x_2 - x|x_1) \quad (4.5)$$

This relation is valid for surface pitot measurements taken at low-speed flows. However it may become invalid for high speed flows since surface pitot measurements are less accurate in high speed flow [3].

We can non-dimensionalize this conversion factor and make use of Abu-Ghannam and Shaw [25] experimental correlations, Eqs.(4.1) and (4.2) to determine the Reynolds number at the effective leading edge of the turbulent boundary layer.

$$Re_{x_t} = \left(\frac{Re_{\theta|x_1}}{A} \right)^2 - 12.95 \left(Re_{\theta|x_2} \right)^{\frac{5}{4}} \quad (4.6)$$

4.2 Length of intermittency correlation

For natural transition over a flat plate, Dhawan and Narasimha [30] initially specified the measurable extent of intermittency as

$$Re_{x|\gamma=0.75} - Re_{x|\gamma=0.25} \doteq 5Re_{x_t}^{0.8} \quad (4.7)$$

The coefficients were later updated by Narasimha [3], to obtain the following correlation.

$$Re_{x|\gamma=0.75} - Re_{x|\gamma=0.25} \doteq 9Re_{x_t}^{0.75} \quad (4.8)$$

We will use this correlation in the equations to determine the slope of the difference in enstrophy density function, η , and can therefore, update Eqs.(3.21-3.24) to be

$$0.5 = \sum_{n=1}^3 C_n \frac{(Re_{x_t} + 11.6736Re_{x_t}^{0.75} - Re_{x_A})^n}{(Re_{x_B} - Re_{x_A})^n} \quad (4.9)$$

$$0.25 = \sum_{n=1}^3 C_n \frac{(Re_{x_t} + 7.5206Re_{x_t}^{0.75} - Re_{x_A})^n}{(Re_{x_B} - Re_{x_A})^n} \quad (4.10)$$

$$\frac{0.0109}{Re_{x_t}^{0.75}} = \sum_{n=1}^3 C_n \frac{n(Re_{x_t} + 11.6736Re_{x_t}^{0.75} - Re_{x_A})^{n-1}}{(Re_{x_B} - Re_{x_A})^n} \quad (4.11)$$

CHAPTER 5

Natural boundary layer transition results

We will solve the following set of 5 non-linear, algebraic equations for a naturally occurring boundary layer transition over a flat plate with a zero pressure gradient flow.

$$\begin{aligned}
& \left[\frac{1}{7} \left(\frac{1}{Re_{\theta|x}} \right)^{\frac{6}{7}} \left(\frac{1}{0.375 \left(\frac{Re_{x_t}}{R_L} (R - R_L) \right)^{\frac{4}{5}}} \right)^{\frac{1}{7}} + \frac{(2 + \lambda/6)}{5 \left(\frac{Re_{x_t}}{R_L} * R \right)^{\frac{1}{2}}} - \frac{\lambda Re_{\theta|x}}{(5)^2 \left(\frac{Re_{x_t}}{R_L} * R \right)} \right. \\
& \quad \left. - \frac{3(2 - \lambda/2) Re_{\theta|x}^2}{(5)^3 \left(\frac{Re_{x_t}}{R_L} * R \right)^{\frac{3}{2}}} + \frac{4(1 - \lambda/6) Re_{\theta|x}^3}{(5)^4 \left(\frac{Re_{x_t}}{R_L} * R \right)^2} \right] \left[\frac{Re_{x_t}}{R_L} (R - 1) \sum_{n=1}^3 \frac{C_n}{n+1} \right] \\
& \qquad \qquad \qquad = \left(\frac{Re_{\theta|x}}{0.375 \left(\frac{Re_{x_t}}{R_L} (R - R_L) \right)^{\frac{4}{5}}} \right)^{\frac{1}{7}} \\
1 &= \sum_{n=1}^3 C_n \\
0.5 &= \sum_{n=1}^3 C_n \frac{\left(Re_{x_t} + 11.6736 Re_{x_t}^{0.75} - \frac{Re_{x_t}}{R_L} \right)^n}{\left(\frac{Re_{x_t}}{R_L} (R - 1) \right)^n} \\
0.25 &= \sum_{n=1}^3 C_n \frac{\left(Re_{x_t} + 7.5206 Re_{x_t}^{0.75} - \frac{Re_{x_t}}{R_L} \right)^n}{\left(\frac{Re_{x_t}}{R_L} (R - 1) \right)^n} \\
\frac{0.0109}{Re_{x_t}^{0.75}} &= \sum_{n=1}^3 C_n \frac{n \left(Re_{x_t} + 11.6736 Re_{x_t}^{0.75} - \frac{Re_{x_t}}{R_L} \right)^{n-1}}{\left(\frac{Re_{x_t}}{R_L} (R - 1) \right)^n}
\end{aligned} \tag{5.1}$$

We will use the numerical solver in Matlab, with the convergence criteria outlined in Chapter 3, to obtain the solution for the transition length ratios, $R = Re_{x_B}/Re_{x_A}$ and $R_L = Re_{x_t}/Re_{x_A}$ and the series coefficients, C_1, C_2 and C_3 . For the real solutions, R was always greater than 1. For this ratio to be less than 1 would imply that the fully turbulent flow occurs upstream of the fully laminar flow and this is not physically possible. However, there is no such physical restriction on R_L .

We will use the experimental correlations of Abu-Ghannam and Shaw [25], Eqs.(4.1 and 4.2), and Dey and Narasimha [49], Eq.(4.6), to calculate the effective leading edge of the

turbulent boundary layer, Re_{x_t} . We will consider two cases, the first in Section 5.1 evaluates this set of equations at a cross-flow location corresponding to Abu-Ghannam and Shaw's [25] experimental correlations for the momentum thickness Reynolds number, $Re_{\theta|_{x_1}}$. The second case, in Section 5.2, will evaluate this set of equations at a cross-flow location corresponding to Abu-Ghannam and Shaw's [25] maximum Reynolds number based on momentum thickness, $Re_{\theta|_{x_2}}$.

5.1 Boundary layer transition equations evaluated at $Re_{\theta|_{x_1}}$

We begin by solving the set of equations, Eq.(5.1) at $Re_{\theta|x} = Re_{\theta|_{x_1}}$. We use the assumptions that at Re_{x_A} the velocity is modelled with the Pohlhausen velocity profile, Eq.(3.2) and at Re_{x_B} the velocity is modelled with the Prandtl velocity profile, Eq.(3.11). We specify the Pohlhausen pressure parameter to be $\lambda = 0$. Then to calculate Re_{x_t} using Eq.(4.6), we need to specify a free-stream turbulence level, Tu . In a natural transition case, the free-stream disturbances are small so as to have as minimal effect as possible on where transition occurs. Experimentally [47] free-stream disturbances can not be eliminated completely and so the smallest value of Tu is 0.03%. Therefore, with $Tu = 0.03\%$, we can calculate $Re_{x_t} = 2.45 \times 10^6$. Upon solving this configuration, we produce the following results

$$\begin{aligned} C_1 &= -4.1996 & C_2 &= 9.6084 & C_3 &= -4.4088 \\ R_L &= 2.6303 & R &= 4.0518 \end{aligned} \tag{5.2}$$

where we obtain the fully laminar location, $Re_{x_A} = 9.33 \times 10^5$, and the fully turbulent location, $Re_{x_B} = 3.78 \times 10^6$.

The difference in enstrophy density function, η , Eq.(3.15) is plotted against the Reynolds number based on x from Re_{x_A} to Re_{x_B} and is shown in Figure 5.1. From this plot, we obtain the start of the intermittency, $Re_{x_0} = 2.65 \times 10^6$, as the location where the function

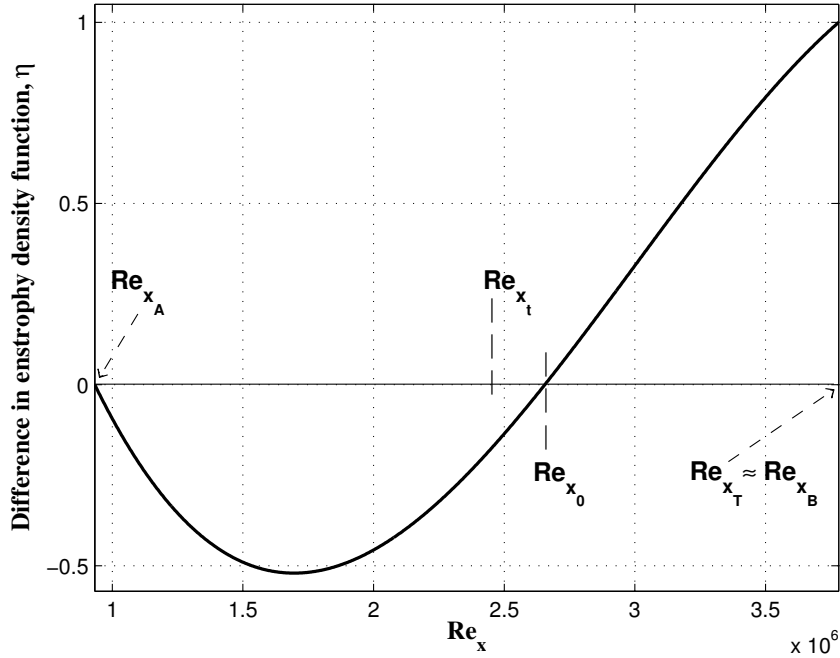


Figure 5.1 – Difference in enstrophy density versus Reynolds number based on x for natural boundary layer transition

is equal to zero downstream of Re_{x_A} and the end of intermittency, $Re_{x_T} = 3.78 \times 10^6$, as the location where the function is to equal 1. For this test case, Re_{x_B} is the same as Re_{x_T} , which implies that at the end of intermittency the flow is fully turbulent. This is consistent with experimental data [2, 30] for a natural boundary layer transition.

There may be some concern as to why η goes negative between Re_{x_A} and Re_{x_0} , especially since we related η to intermittency and intermittency only varies from 0 to 1. Recall from Chapter 3, that we only determined the shape of η by using 2 points and a slope of the intermittency. We did this because we did not expect the shape of η to be identical to γ . This was a fair assumption considering that η varies from Re_{x_A} to Re_{x_B} and not just within the intermittency region. As well, the intermittency values below $\gamma = 0.25$ and above $\gamma = 0.75$ are only estimates based on the distribution that was fitted to the experimental data.

Next, recall that the difference in enstrophy density function can be rewritten as

$$\begin{aligned} \omega^2 &= (1 - \eta) \omega_{lam}^2 + \eta \omega_{turb}^2 \\ &+ \eta \left[\left(\omega_{turb}^2|_{x_B} - \omega_{turb}^2 \right) - \left(\omega_{lam}^2|_{x_B} - \omega_{lam}^2 \right) \right] \end{aligned} \quad (5.3)$$

Now we can recognize that the third term on the RHS is a difference of a difference and we would expect this term to be at least an order of magnitude less than the other two terms.

Therefore, we can than say that

$$\omega^2 \approx (1 - \eta) \omega_{lam}^2 + \eta \omega_{turb}^2 \quad (5.4)$$

Furthermore, within the region, Re_{x_A} to Re_{x_0} , there will be no turbulent flow so Eq.(5.4) becomes

$$\omega^2 \approx (1 - \eta) \omega_{lam}^2 \quad (5.5)$$

Then in order for the RHS to be positive, $(1 - \eta) > 0$ or $\eta < 1$. However, between 0 and 1 turbulent flow is present so therefore when there is no turbulent flow, i.e. within the region Re_{x_A} to Re_{x_0} , $\eta < 0$.

For a possible physical reason why η would be less than zero, recall that

$$\eta = \frac{\omega^2 - \omega_{lam}^2}{(\omega_{turb}^2 - \omega_{lam}^2)|_{x_B}} \quad (5.6)$$

then for η to go negative, means that $\omega^2 < \omega_{lam}^2$ or that the local enstrophy density is less than the baseline laminar enstrophy density at the fixed perpendicular location $y = Re_{\theta_{x_1}}$. Since the enstrophy density is equal to $(\partial u / \partial y)^2$, a possible scenario for the local enstrophy density to less than the baseline would be if the boundary layer through this region was thinner than the baseline laminar boundary layer. Downstream of Re_{x_0} , where $\eta > 0$,

implies $\omega^2 > \omega_{lam}^2$ which could possibly result from a thickening of the boundary layer which would be consistent with the calculated and measured velocity profiles obtained by Dhawan and Narasimha [30] within the intermittency region.

In Figure 5.2 we illustrate a pictorial representation of the transition model where the boundary layer thickness for laminar and turbulent boundary layers are plotted against the x locations. In this figure, we include the critical stability location, $Re_{x_{cr}}$. For a Blasius boundary

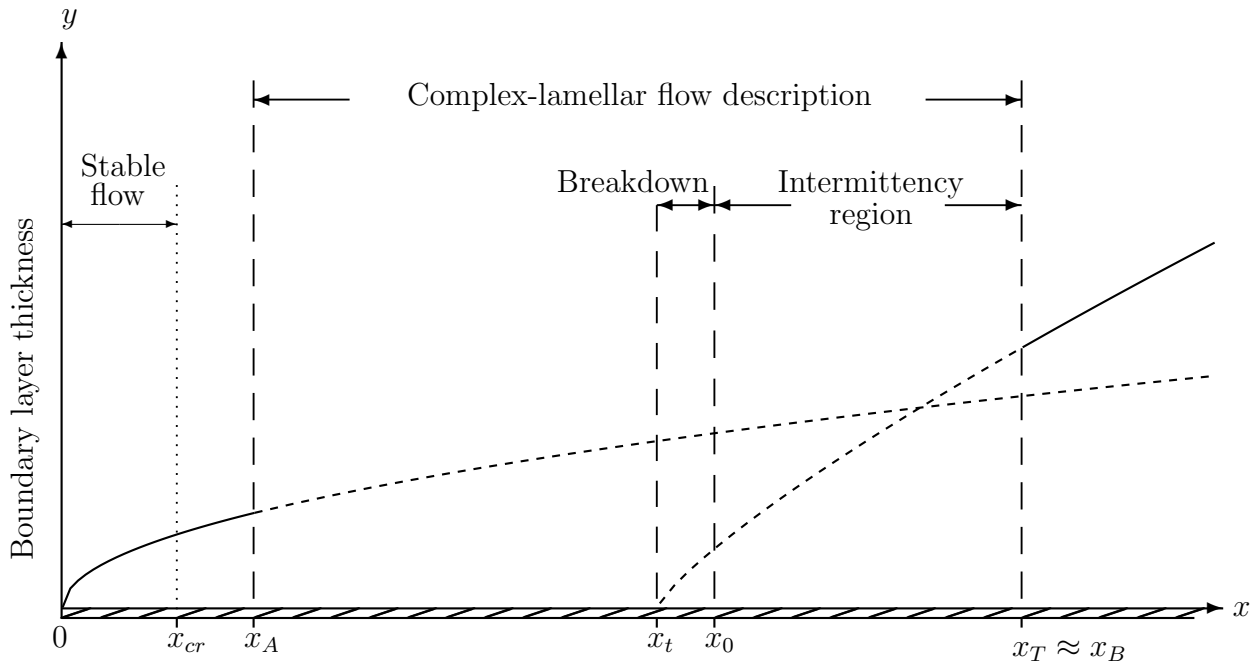


Figure 5.2 – A model of natural boundary layer transition along a flat plate with zero pressure gradient flow

layer, it is calculated from the stability equations to be $Re_{\delta^*} = 520$, where Re_{δ^*} is the Reynolds number based on displacement thickness [39]. We determined the corresponding value for the Reynolds number based on x using the relationship $Re_{\delta^*} = 1.721\sqrt{Re_x}$ [47] and obtained $Re_{x_{cr}} = 9.14 \times 10^4$. As illustrated, this value is upstream of the fully laminar location, Re_{x_A} . From this we could infer that between $Re_{x_{cr}}$ and Re_{x_A} 2D disturbances have begun to grow, however, are still minimal enough that the fully laminar flow is not yet affected.

Our solution provides a prediction of the start and end of intermittency so we can compare these locations with the experimental locations determined by Schubauer and Klebanoff [2]. This comparison is shown in Section 5.1.1. We can also use the difference in enstrophy density function, η , to calculate the Reynolds number location where $\eta = 0.25$ and $\eta = 0.75$ to determine the length of $Re_{x|\eta=0.75} - Re_{x|\eta=0.25}$. We can then compare this length with Dhawan and Narasimha's [30] experimental correlation. This comparison is shown in Section 5.1.2. Finally, we can calculate the length of breakdown, $Re_{x_0} - Re_{x_t}$ and compare this length with Narasimha's [3] estimate. This comparison is shown in Section 5.1.3.

5.1.1 Comparison of Reynolds numbers based on x with experimental data

In Table 5.1, we compare our results to the experimental data obtained by Schubauer and Klebanoff [2], for flat plate zero pressure gradient flow.

Table 5.1 – Start and end of intermittency location comparison between calculated results and the experimental data of Schubauer and Klebanoff [2] for natural boundary layer transition.

Re_x location	Schubauer and Klebanoff [2] Experimental data	Calculated	% Difference
Re_{x_0}	2.56×10^6	2.66×10^6	4
Re_{x_T}	3.90×10^6	3.79×10^6	3

The location of the start of intermittency, Re_{x_0} , that we calculated using the difference in enstrophy density function, η , is 4% further downstream than the experimental data of Schubauer and Klebanoff [2]. The location of the end of intermittency, Re_{x_T} , also calculated using η , is 3% upstream of the experimental data.

Schubauer and Klebanoff [47] used the same experimental set up as Schubauer and Skramstad [47], who determined that velocity fluctuations obtained from the hot-wire probes would have an accuracy of 1% if they were properly calibrated. If the measure of intermittency could be calculated directly from the hot-wire data, then it might be feasible for intermittency

measurements to have a similar level of accuracy. However, the measure of intermittency is interpreted from the velocity fluctuation records of the oscilloscope. Therefore, this adds an additional level of inaccuracy and is probably a reason why Narasimha [3] has noted that measuring intermittency at very high and low values does not produce accurate results. This implies that although the start and end of intermittency that we calculated is different from the experimental locations, this difference is not significant, thereby, permitting us to conclude that the difference in enstrophy density function predicts accurate locations of the start and end of intermittency.

For this test case, the location of the end of intermittency, Re_{x_T} is the same as the location of the fully turbulent flow, Re_{x_B} . This matches the experimental measurements made by Schubauer and Klebanoff [2], who measured the velocity profile at $\gamma = 1$ and determined a velocity profile consistent with a fully turbulent profile. Therefore, using Prandtl's velocity profile, Eq.(3.11), to model the fully turbulent flow at Re_{x_B} produced accurate results.

Our calculations predict the location for the fully laminar velocity to occur at $Re_{x_A} = 9.33 \times 10^5$. This location is between the critical stability location, $Re_{x_{cr}}$ and the start of intermittency Re_{x_0} . Based on experimental measurements of mean velocity profiles [2, 18], the velocity remains laminar up until the start of intermittency so we could infer from our calculations that between Re_{x_A} and Re_{x_0} the velocity profile is laminar however is no longer fully laminar as described by Pohlhausen's profile. Further experimental measurements would be needed to confirm this idea.

5.1.2 Comparison of the length of the intermittency region with experimental correlation

From the difference in enstrophy density function, η , we can determine $Re_{x|\eta=0.75}$ and $Re_{x|\eta=0.25}$ and compare this length with the approximate length obtained from Narasimha's [3] exper-

imental correlation.

$$Re_{x|\gamma=0.75} - Re_{x|\gamma=0.25} \doteq 9Re_{x_t}^{0.75} \quad (5.7)$$

This comparison is shown in Table 5.2.

Table 5.2 – Comparison of the length of the intermittency region between the experimental correlation of Narasimha [3] and our analysis for a natural boundary layer transition.

Intermittency Region Length	Narasimha [3] Experimental Correlation, Eq.(4.8)	Calculated from Figure 5.1	% Difference
$Re_{x \gamma=0.75} - Re_{x \gamma=0.25}$	5.57×10^5	5.34×10^5	4

Our calculation of the measurable length of the intermittency region is 4% shorter than obtained by Narasimha’s [3] correlation. This difference is acceptable and considering the experimental data used by Narasimha [3] had significant scatter, he could only determine an approximate correlation, these values may be within the same accuracy and therefore, for all intents and purposes, the same. Since this difference is within an acceptable accuracy range, our calculations of the length, $Re_{x|\eta=0.75} - Re_{x|\eta=0.25}$ verifies Dhawan and Narasimha’s [30] idea that a correlation between $Re_{x|\gamma=0.75} - Re_{x|\gamma=0.25}$ and Re_{x_t} exists.

5.1.3 Comparison of the length of breakdown with experimental observation

For the length of breakdown, $Re_{x_0} - Re_{x_t}$, Narasimha [27] estimated that

$$Re_{x_0} - Re_{x_t} \sim \frac{Re_{x|\gamma=0.75} - Re_{x|\gamma=0.25}}{3} \quad (5.8)$$

Based on the Reynolds numbers we achieved from the difference in enstrophy density function, η , we can calculate the length of breakdown to be

$$\frac{Re_{x_0} - Re_{x_t}}{Re_{x|\eta=0.75} - Re_{x|\eta=0.25}} = 0.38 \quad (5.9)$$

The length of breakdown within our analysis is 38% of the extent of intermittency, which compares well with Narasimha's [3] estimate of 1/3. Therefore, from this analysis we can infer that using experimental correlations and intermittency equations that are based on the assumption that Re_{x_t} is the Re_{x_0} will result in some discrepancy within the location of the start of intermittency. For this particular case, Re_{x_0} differs from Re_{x_t} by about 8%.

5.1.4 Conclusions

We solved a set of 5 non-linear equations for natural boundary layer transition flow over a flat plate. Two equations were obtained from the physical constraints imposed by the complex-lamellar decomposition of the flow and three from geometrical constraints. The geometrical constraints imposed that the slope of the difference in enstrophy density function, η , matches the slope of the intermittency, γ . The location of where this slope is placed along the flat plate is determined from the physical constraints imposed on the flow. This results in multiple solutions. We interpreted a possible physical meaning for the solutions and presented the solution in which experimental data exists for comparison.

From the solution of this set of equations, we determined the locations of the start of intermittency, Re_{x_0} , and the end of intermittency, Re_{x_T} . These locations compared well with the experimental data of Schubauer and Klebanoff [2]. From the difference in enstrophy density function, η , we calculated the length of measurable extent of intermittency, $Re_{x_{\eta=0.75}} - Re_{x_{\eta=0.25}}$, and this length compared well with the experimental correlation of Dhawan and Narasimha [30]. Finally, we calculated the length of breakdown, $Re_{x_0} - Re_{x_t}$, and this length compared well with the experimental estimate of Narasimha [3].

Overall, along the flat plate, our analysis produced both locations and lengths associated with intermittency. We verified the locations and lengths using the experimental data of Schubauer and Klebanoff [2], Dhawan and Narasimha [30], and Narasimha [3]. From these comparisons, we can conclude that our model of a natural boundary layer transition, that

bounds the intermittency region between a fully laminar and fully turbulent flow is valid. We illustrated that the derived complex-lamellar condition, Eq. (3.27), when evaluated at a cross-flow location of $Re_{\theta|_{x_1}}$ produces correct results. Finally, the assumption that the difference in enstrophy density function could be modelled using the slope and two points of the universal intermittency function was correct.

5.2 Boundary layer transition equations evaluated at $Re_{\theta|_{x_2}}$

For this test case, we solved the same set of non-linear equations, Eq.(5.1), however, in this test case, we used a different cross-flow location, specified as $Re_{\theta|_x} = Re_{\theta|_{x_2}}$. We used the assumptions that at Re_{x_A} the velocity is modelled with the Pohlhausen velocity profile, Eq.(3.2), and at Re_{x_B} the velocity is modelled with the Prandtl velocity profile, Eq.(3.11) We specified the Pohlhausen pressure parameter to be $\lambda = 0$, the free-stream turbulence level to be $Tu = 0.03$, and calculated $Re_{x_t} = 2.45 \times 10^6$. Upon solving this configuration, we produced the following results

$$\begin{aligned}
 C_1 &= -4.1957 & C_2 &= 9.6029 & C_3 &= -4.4072 \\
 R_L &= 2.6252 & R &= 4.0444 & &
 \end{aligned}
 \tag{5.10}$$

which corresponds to $Re_{x_A} = 9.35 \times 10^6$ and $Re_{x_B} = 3.78 \times 10^6$. In Table 5.3, we compare the results obtained using the cross-flow location at $Re_{\theta|_{x_1}}$ and $Re_{\theta|_{x_2}}$.

Table 5.3 – Comparison of the results obtained at a cross-flow location $Re_{\theta|_{x_1}}$ and $Re_{\theta|_{x_2}}$

Reynolds number	Results obtained with $Re_{\theta _{x_1}}$	Results obtained with $Re_{\theta _{x_2}}$	% Difference
Re_{x_A}	9.3290×10^5	9.3290×10^5	0.2
Re_{x_B}	3.7799×10^6	3.7801×10^6	0.01

5.2 Boundary layer transition equations evaluated at $Re_{\theta|_{x_2}}$

We see that the difference in Re_{x_A} between the two cases is 0.2% and the difference in Re_{x_B} is 0.01%. Since these values correspond to locations where the fully laminar and fully turbulent velocity profiles are achieved, they could be measured experimentally. If these values were obtained experimentally using pitot tubes the best possible accuracy would effectively be 1%, therefore, since these values are less than 1%, we can say that Re_{x_A} and Re_{x_B} are the same for both cases.

From the difference in enstrophy density function, Eq.(3.15), we can calculate the start of intermittency to be $Re_{x_0} = 2.66 \times 10^6$ and the end of intermittency to be $Re_{x_0} = 3.78 \times 10^6$. In Table 5.4, we compare these results with those obtained using the cross-flow location at $Re_{\theta|_{x_1}}$.

Table 5.4 – Comparison of start and end of intermittency locations obtained at a cross-flow location $Re_{\theta|_{x_1}}$ and $Re_{\theta|_{x_2}}$

Reynolds number	Results obtained with $Re_{\theta _{x_1}}$	Results obtained with $Re_{\theta _{x_2}}$	% Difference
Re_{x_0}	2.65553×10^6	2.65551×10^5	0.001
Re_{x_T}	3.7799×10^6	3.7801×10^6	0.01

The difference in Re_{x_0} is 0.001% and the difference in Re_{x_T} is 0.01%. These values are well within any accuracy range that could be achieved experimentally and therefore indicate that the start and end of intermittency are the same for both cases.

We see that the difference in the results between the two test cases is insignificant. With that said, it is interesting to note that the largest difference within the results occurs for the fully laminar location, Re_{x_A} . As an initial interpretation, this could imply that the fully laminar location is the most sensitive to external factors. This would definitely be consistent with experimental observations and data that have shown how free-stream turbulence, pressure gradients, surface roughness, etc, affects the laminar boundary layer thickness causing transition to be hastened or delayed.

In conclusion, we evaluated the derived complex-lamellar velocity condition at two different cross-flow locations and obtained the same results for the fully laminar location, the start of intermittency, the end of intermittency and the fully turbulent location. This verifies that our assumption of using a single cross-flow location to solve the complex-lamellar condition is correct. It also verifies that solving the complex-lamellar condition at a cross-flow location above the flat plate achieves the correct surface locations.

CHAPTER 6

Separated flow transition over a separation bubble

Since we achieved consistent results for the natural boundary layer transition case, we decided to try solving our boundary layer transition equations for a more difficult case, separated flow transition over a separation bubble. Utilizing separated flow transition through separation bubbles is crucial in compressor and low-pressure turbine design, since controlling where transition occurs can increase the performance of compressors and the efficiencies of low-pressure turbines [1]. The difficulty in using separation bubbles to control performance by forcing transition is that bubbles can exist in either a short form or long form. A short bubble will have only a local displacement on the pressure distribution, where as a long bubble will interact with the exterior flow causing significant changes in the overall pressure distribution [4, 1]. So for a short bubble, the pressure distribution before and after separation will be similar to a pressure distribution obtained without the presence of a separation bubble. On

the other hand, the long bubble effects the exterior flow so significantly that the extent of the pressure distribution over the whole surface is completely different from a pressure distribution obtained without the bubble. Therefore, since small changes in Reynolds number can cause a short bubble to ‘burst’ and become long and cause dramatic losses in lift, it is important to be able to predict where short and long bubbles will occur.

To solve this type of transition using the transition model outlined in Chapter 3, requires that, at Re_{x_A} , the velocity profile must be on the verge of separation. To satisfy this condition, we will use the Pohlhausen velocity profile, Eq.(3.2) with the Pohlhausen pressure parameter, $\lambda = -12$ as this term models the effect of the local adverse pressure gradient. For the turbulent flow, we will again make use of Prandtl’s velocity profile, Eq.(3.11). By analyzing the pressure distributions Gaster [4] obtained for his short and long bubble experiments, we can justify this choice. For a short separation bubble, the pressure recovery region happens over a short distance. Since the Prandtl velocity profile does not account for local pressure gradients, we would expect the velocity profile to be satisfied near the end of the constant pressure region. This would mean that the location of the turbulent velocity condition, x_B , will be located upstream of x_r , however, since the distance between x_r and the end of the constant pressure region is short, we would expect the location of x_B to still provide acceptable results.

For a long separation bubble, the pressure recovery happens over a longer distance. As well, the pressure peak is decreased resulting in the slope of the pressure distribution at the reattachment point being more shallow. Therefore, since the slope at the reattachment point is near zero, the pressure gradient would be minimal and we would expect Prandtl’s velocity profile to provide an acceptable estimate of the turbulent velocity at this location.

To solve the separated flow test case, we will also use experimental correlations to determine the effective leading edge of the turbulent boundary layer, Re_{x_t} and Narasimha’s [27] extent of the intermittency region, $Re_{x|\gamma=0.75} - Re_{x|\gamma=0.25}$.

6.1 Determination of the effective leading edge of the turbulent boundary layer

For a separated shear layer transitioning over a separation bubble, the pressure distribution measured along the surface is used to determine the locations associated with separation, the end of transition and reattachment [4, 1, 21]. The location where the constant pressure region begins is the separation point and the location where the constant region ends is the end of transition, and according to Mayle [1] the end of transition corresponds to the end of intermittency. He determined the onset of transition to be located where the formation of turbulent spots begin. To determine this location, he used the turbulence measurements of Gaster [4] and Bellows [50] to determine a corresponding measure of the intermittency, $\gamma(x)$. With these intermittency measurements, he could use Narasimha [27] universal intermittency distribution,

$$\gamma = 1 - \exp\left(-0.412 \frac{(x - x_t)^2}{(x|_{\gamma=0.75} - x|_{\gamma=0.25})^2}\right) \quad (6.1)$$

to determine a function based on γ , $F(\gamma)$,

$$F(\gamma) = \sqrt{-\ln(1 - \gamma(x))} \quad (6.2)$$

which can be calculated within the measurable region, $0.25 < \gamma < 0.75$. Then by plotting $F(\gamma)$ versus x , a straight line is achieved. When this function is extrapolated to zero, the corresponding x location is the onset of transition. This method was first introduced by Narasimha [27], who stated that this is the most accurate definition of the onset of transition as it happens to also be the effective leading edge of the fully turbulent boundary layer. Therefore, Mayle [1] based his correlations on the concept of concentrated breakdown, where the effective leading edge is at the same location as the start of intermittency, we can use his correlation and experimental data from Gaster [4] to determine the effective leading edge of the turbulent boundary layer, Re_{x_t} .

Mayle's [1] experimental correlation for the length of the effective leading edge of the turbulent boundary layer to the end of the constant pressure region, x_{Tp} is

$$Re_{x_{Tp}} - Re_{x_t} = 400Re_{\theta_s}^{0.7} \quad (6.3)$$

Using the pressure distribution curve provided by Gaster [4] that corresponds to a measured momentum thickness at separation, θ_s , we can locate the end of the constant pressure region and calculate $Re_{x_{Tp}}$. By rearranging Eq.(6.3), we will determine the effective leading edge of the turbulent boundary layer,

$$Re_{x_t} = Re_{x_{Tp}} - 400Re_{\theta_s}^{0.7} \quad (6.4)$$

6.2 Length of the intermittency region with laminar separation bubble present

In order to use Eqs.(3.21-3.24) to determine the slope of the difference in enstrophy density function, η , we need to relate Mayle's [1] transition region length, $Re_{x_{Tp}} - Re_{x_t}$ to Narasimha's [3] extent of the intermittency region, $Re_{x|\gamma=0.75} - Re_{x|\gamma=0.25}$. This is achieved by using the relation [25]

$$Re_{x|\gamma=0.75} - Re_{x|\gamma=0.25} = \frac{(Re_{x_{Tp}} - Re_{x_t})}{3.36} \quad (6.5)$$

$$= 119.05Re_{\theta_s}^{0.7} \quad (6.6)$$

Then the equations to determine the slope of the difference in enstrophy density function

6.2 Length of intermittency region

become

$$0.5 = \sum_{n=1}^3 C_n \frac{(Re_{x_t} + 154.42Re_{\theta_s}^{0.7} - Re_{x_A})^n}{(Re_{x_B} - Re_{x_A})^n} \quad (6.7)$$

$$0.25 = \sum_{n=1}^3 C_n \frac{(Re_{x_t} + 99.476Re_{\theta_s}^{0.7} - Re_{x_A})^n}{(Re_{x_B} - Re_{x_A})^n} \quad (6.8)$$

$$\frac{8.257 \times 10^{-4}}{Re_{\theta_s}^{0.7}} = \sum_{n=1}^3 C_n \frac{n(Re_{x_t} + 154.42Re_{\theta_s}^{0.7} - Re_{x_A})^{n-1}}{(Re_{x_B} - Re_{x_A})^n} \quad (6.9)$$

We now have enough information to solve for Re_{x_A} and Re_{x_B} and then determine the locations of the start and end of intermittency, Re_{x_0} and Re_{x_T} , for a separated shear layer transitioning over a separation bubble.

CHAPTER 7

Separation flow transition over a separation bubble: Results

We will solve the following set of 5 non-linear algebraic equations for separated flow over a separation bubble.

$$\begin{aligned}
& \left[\frac{1}{7} \left(\frac{1}{Re_{\theta|_x}} \right)^{\frac{6}{7}} \left(\frac{1}{0.375 \left(\frac{Re_{x_t}}{R_L} (R - R_L) \right)^{\frac{4}{5}}} \right)^{\frac{1}{7}} + \frac{(2 + \lambda/6)}{5 \left(\frac{Re_{x_t}}{R_L} * R \right)^{\frac{1}{2}}} - \frac{\lambda Re_{\theta|_x}}{(5)^2 \left(\frac{Re_{x_t}}{R_L} * R \right)} \right. \\
& \quad \left. - \frac{3(2 - \lambda/2) Re_{\theta|_x}^2}{(5)^3 \left(\frac{Re_{x_t}}{R_L} * R \right)^{\frac{3}{2}}} + \frac{4(1 - \lambda/6) Re_{\theta|_x}^3}{(5)^4 \left(\frac{Re_{x_t}}{R_L} * R \right)^2} \right] \left[\frac{Re_{x_t}}{R_L} (R - 1) \sum_{n=1}^3 \frac{C_n}{n+1} \right] \\
& \qquad \qquad \qquad = \left(\frac{Re_{\theta|_x}}{0.375 \left(\frac{Re_{x_t}}{R_L} (R - R_L) \right)^{\frac{4}{5}}} \right)^{\frac{1}{7}} \\
1 &= \sum_{n=1}^3 C_n \\
0.5 &= \sum_{n=1}^3 C_n \frac{(Re_{x_t} + 154.42 Re_{\theta_s}^{0.7} - \frac{Re_{x_t}}{R_L})^n}{\left(\frac{Re_{x_t}}{R_L} (R - 1) \right)^n} \tag{7.1} \\
0.25 &= \sum_{n=1}^3 C_n \frac{(Re_{x_t} + 99.476 Re_{\theta_s}^{0.7} - \frac{Re_{x_t}}{R_L})^n}{\left(\frac{Re_{x_t}}{R_L} (R - 1) \right)^n} \\
\frac{8.257 \times 10^{-4}}{Re_{\theta_s}^{0.7}} &= \sum_{n=1}^3 C_n \frac{n(Re_{x_t} + 154.42 Re_{\theta_s}^{0.7} - \frac{Re_{x_t}}{R_L})^{n-1}}{\left(\frac{Re_{x_t}}{R_L} (R - 1) \right)^n}
\end{aligned}$$

Just like in the natural boundary layer transition case, we will use the numerical solver in Matlab, with the convergence criteria outlined in Chapter 3, to obtain the solution for the transition length ratios, $R = Re_{x_B}/Re_{x_A}$ and $R_L = Re_{x_t}/Re_{x_A}$ and the series coefficients, C_1, C_2 and C_3 .

For the cross-flow location, we chose a momentum thickness Reynolds number at separation of $Re_{\theta|_s} = 394$ as Gaster [4] has experimental data for a short separation bubble occurring at this momentum thickness. To calculate the effective leading edge of the turbulent boundary layer, Re_{x_t} , we used the experimental correlation of Mayle [1], Eq.(6.4) along with the location of the end of the constant pressure region from Gaster's [4] experimental data. We

will evaluate the complex-lamellar velocity condition, the first equation in the set, at a cross-flow location corresponding to the momentum thickness at separation, $Re_{\theta|_x} = Re_{\theta|_s} = 394$. As previously discussed in Chapter 3, multiple solutions were obtained when the set of 5 equations, Eq.(7.1) was solved. We determined that two of these solutions could represent transition over a separation bubble. Both of these solutions had the same location for the start and end of intermittency, however, they differed in locations of Re_{x_A} and Re_{x_B} . In the one solution, the location of Re_{x_A} was further upstream and the location of Re_{x_B} was further downstream. These observations are characteristics of a long separation bubble compared to a short separation bubble. Therefore, it appeared that we obtained a short bubble and long bubble solution at a single momentum thickness Reynolds number at separation. In Gaster's experimental data, he only obtained a single solution at the specified Reynolds number however Mayle's correlations can be used to obtain both a short and long bubble solution at a single Reynolds number. Therefore, in Section 7.1 we compare the locations and lengths associated with the short bubble solution to the experimental data of Gaster [4], Mayle [1] and Narasimha [3]. Then in Section 7.2, we will compare only lengths associated with the long bubble solution to the experimental correlations of Mayle [1] and Narasimha [3].

7.1 Short separation bubble

We begin by solving the set of equations, Eq.(7.1), at $Re_{\theta|_x} = Re_{\theta|_s} = 394$. We will use the assumptions that at Re_{x_A} , the velocity is modelled with the Pohlhausen velocity profile corresponding to separation, Eq.(3.2), at Re_{x_B} , the velocity is modelled with the Prandtl velocity profile, Eq.(3.11). We will specify $\lambda = -12$. From Gaster's [4] experimental data, the end of the constant pressure region occurs at $Re_{x_{Tp}} = 5.49 \times 10^5$, then using this and Mayle's [1] correlation, Eq.(6.4) we can calculate the effective leading edge of the turbulent boundary layer, $Re_{x_t} = 5.22 \times 10^5$. We do not specify a value for the free-stream turbulence

7.1 Short separation bubble

for this test case as it is not required within the equations to determine Re_{x_t} . However, this test case is for a flow with low free-stream turbulence levels since Mayle's correlations are only valid at low levels. Upon solving this configuration, we obtain the following short bubble solution

$$\begin{aligned}
 C_1 &= -3.7525 & C_2 &= 9.0025 & C_3 &= -4.2500 \\
 R_B &= 1.0368 & R &= 1.0741 & & (7.2)
 \end{aligned}$$

which corresponds to the fully laminar location at separation, $Re_{x_A} = 5.04 \times 10^5$ and the fully turbulent location, $Re_{x_B} = 5.41 \times 10^5$.

The difference in enstrophy density function, Eq.(3.15), is plotted against the Reynolds number based on x between Re_{x_A} and Re_{x_B} . This is shown in Figure 7.1. From this

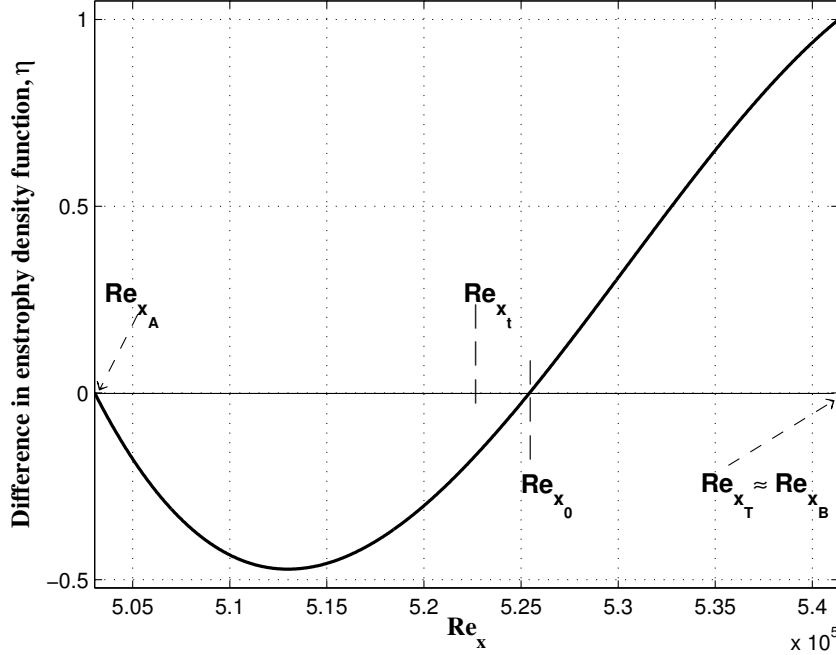


Figure 7.1 – Difference in enstrophy density between Re_{x_A} and Re_{x_B} for short separation bubble

function, we obtain the start of intermittency to be at $Re_{x_0} = 5.25 \times 10^5$ and the end of intermittency at $Re_{x_T} = 5.41 \times 10^5$. For this test case, the end of intermittency is at the same location as the fully turbulent boundary condition.

In Figure 7.2, we illustrate a pictorial representation of the separated flow transition over a short separation, where the laminar and turbulent boundary layer thickness is shown with the corresponding x locations. This figure illustrates that we impose a fully laminar velocity

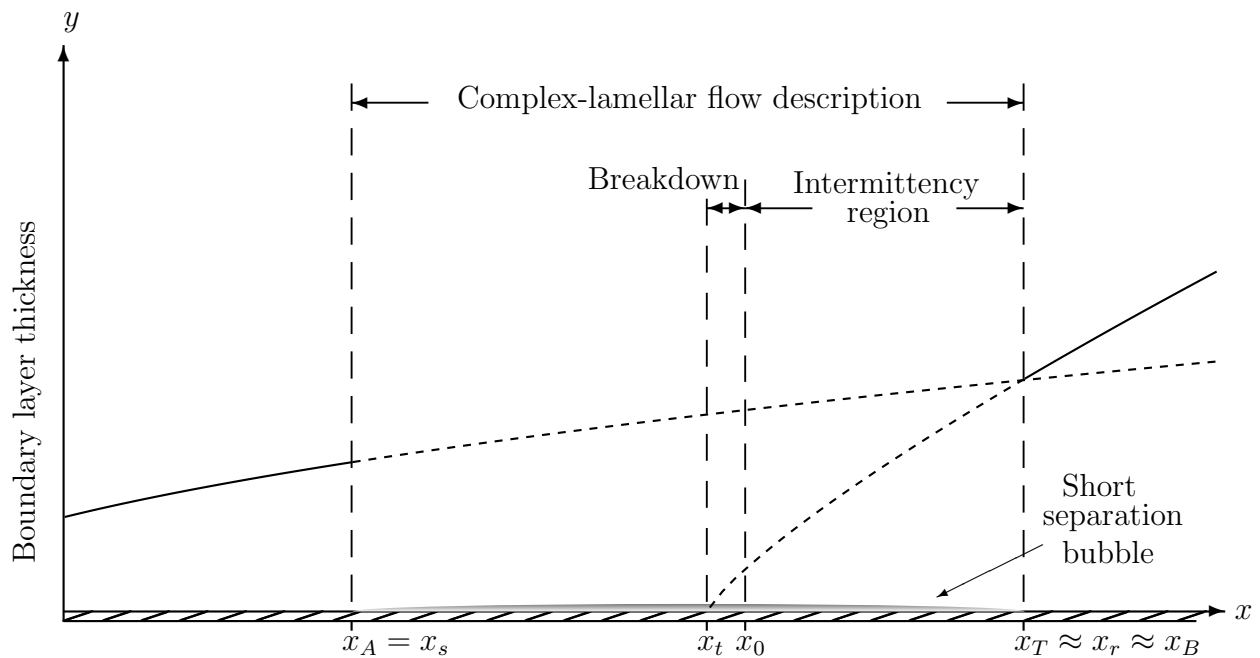


Figure 7.2 – Pictorial representation of the locations of the Reynolds number based on x associated with the short separation bubble results

profile at separation, however, nothing is imposed at the reattachment location. The flow at reattachment is assumed to be fully turbulent based on experimental results [4]. Therefore we can infer from our results, that the end of intermittency, the location of Prandtl’s fully turbulent flow and reattachment, will occur at approximately the same location and the pressure recovery from the end of intermittency to reattachment will occur very rapidly.

7.1 Short separation bubble

7.1.1 Comparison of Reynolds number based on x with experimental data

In Table 7.1, we compare our results with the experimental data taken from Gaster [4].

Table 7.1 – Comparison between calculated results and Gaster’s [4] experimental data for a short separation bubble at $Re_{\theta|_s} = 394$

Reynolds number	Gaster [4] Experimental data	Calculated	% Difference
Re_{x_s}	4.99×10^5	5.04×10^5	1
$Re_{x_{Tp}}$	5.49×10^5	5.41×10^5	1
Re_{x_r}	5.59×10^5	5.41×10^5	3

The location of separation, Re_{x_A} , that we obtained from the solution of the set of equations, is 1% further downstream than the value corresponding to the start of the constant pressure region in Gaster’s [4] experimental data. The location of the end of intermittency, Re_{x_T} , that we obtained from the difference in enstrophy density function, η , is 1% upstream of the value corresponding to the end of the constant pressure region in Gaster’s [4] experimental data. The location of the reattachment point, Re_{x_B} , that we obtained from the solution of the set of equations, is 3% upstream from the measured reattachment point in Gaster’s [4] experimental data.

Unfortunately, Gaster [4] does not mention the accuracy range for the pressure measurements. However, he did use inclined manometers for the measurements which would have required an approximation of the reading. As such, we could interpret the results we obtained for separation and the end of the intermittency region to be the same as those obtained by Gaster [4] for the start and end of the constant pressure region, respectively. It is not surprising that there is a slightly larger difference in the reattachment locations, since, Gaster [4] was unable to measure the mean velocity due to the reverse flow region just above the reattachment point. There was no instrument at the time that could determine the true mean velocity in this region, therefore, Gaster [4] approximated the reattachment point using con-

four plots of constant velocity. Other experimentalists [21, 1] approximate the reattachment point by measuring the pressure distribution with the separation bubble present and without the separation bubble. When these two pressure distributions are plotted, the point where the pressure distribution with the separation bubble matches the pressure distribution without the bubble is the reattachment point. For short separation bubbles, the pressure recovery from the end of the constant pressure region to the reattachment point is very rapid. We also determined that the flow would also be fully turbulent at the end of intermittency as $Re_{x_B} \approx Re_{x_T}$ and so can conclude that the flow reattaches at the same streamwise location as the end of intermittency. This is consistent with the experimental data for short bubbles that shows a sharp pressure recovery [4].

To illustrate that the local pressure gradient for the short bubble is minimal at x_B we reproduced Gaster's [4] pressure distribution for the short bubble test case, which is shown in Figure 7.3. Since x_B is located within the constant pressure region, using Prandtl's velocity profile at x_B is acceptable. As well, since the pressure recovery between x_{Tp} and x_r occurs over a minimal distance, using Prandtl's velocity profile at x_B still provided an accurate measure of where reattachment would occur.

7.1.2 Comparison of the start of intermittency with experimental observation

From the previous analysis, we determined that the calculated locations of separation, the end of intermittency and reattachment, were all the same as those measured experimentally. The only location that could not be determined from the experimental data is the start of intermittency. Mayle [1] determined correlations for the length of the constant pressure region, the unstable laminar flow region, and the intermittency region. However, these correlations are based on concentrated breakdown and therefore are most accurately applied from the effective leading edge of the turbulent boundary layer. Therefore, since we are in a nearly constant pressure region and experimental data for attached boundary layers has

7.1 Short separation bubble

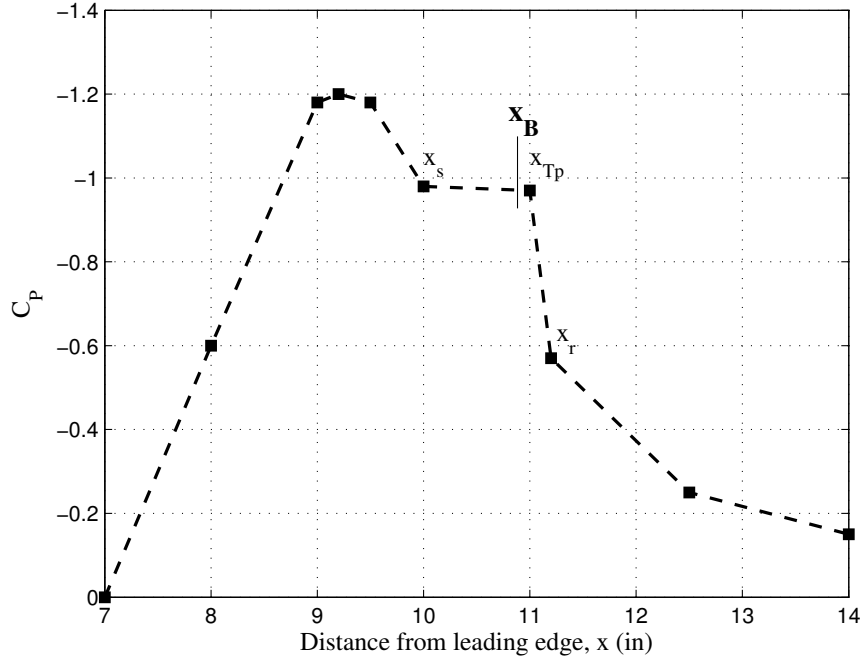


Figure 7.3 – Pressure distribution for short bubble reproduced from Gaster’s [4] experimental data.

been used [1], we will make use of Narasimha’s estimate for the length of breakdown to verify that the location of the start of intermittency is valid.

From the difference in enstrophy density function, η , we can determine the extent of the intermittency region, $Re_{x_{\eta=0.75}} - Re_{x_{\eta=0.75}} = 7.44 \times 10^4$ and the location of the start of intermittency, $Re_{x_0} = 5.25 \times 10^5$.

Then we can determine the length of breakdown, $Re_{x_0} - Re_{x_t}$ as a percent of the extent of intermittency

$$\frac{Re_{x_0} - Re_{x_t}}{Re_{x_{\eta=0.75}} - Re_{x_{\eta=0.75}}} = 0.37 \quad (7.3)$$

The length of breakdown, $Re_{x_0} - Re_{x_t}$, that we obtain from the difference in enstrophy density function, η , is 37% of the extent of intermittency. This is consistent with Narasimha’s [3] estimate of 1/3. Therefore, we can infer that the location we obtain for the start of

intermittency would be the same as expected from experimental observation.

7.1.3 Mayle [1] correlations for short separation bubbles

Since we will be using Mayle's [1] experimental correlations in determining the accuracy of the long separation bubble results, we will determine how well the correlations predict the lengths associated with the short bubble.

Mayle [1] has three length correlations for the different Reynolds numbers based on x of the various regions. These lengths are all correlated with the momentum thickness Reynolds number at separation. The correlation length of the entire constant pressure region for a short separation bubble is,

$$Re_{x_{Tp}} - Re_{x_s} = 700Re_{\theta_s}^{0.7} \quad (7.4)$$

the length of the unstable laminar region is,

$$Re_{x_t} - Re_{x_s} = 300Re_{\theta_s}^{0.7} \quad (7.5)$$

and the length of the transition region is

$$Re_{x_{Tp}} - Re_{x_t} = 400Re_{\theta_s}^{0.7} \quad (7.6)$$

In Table 7.2 we compare Mayle's correlations with the results we obtained.

The length from separation to the end of intermittency that we calculated from our results is 19% shorter than estimated from Mayle's correlation, Eq.(7.4). In determining this correlation, Mayle [1] stated that 'most of the data' fell along the line corresponding to Eq.(7.4). The length from separation to the effective leading edge of the turbulent boundary layer that we calculated is 6% shorter than estimated from Mayle's correlation, Eq.(7.5). The length

7.1 Short separation bubble

Table 7.2 – Short bubble length comparison between calculated lengths and Mayle’s [1] experimental correlations

Region length	Mayle [1] Experimental Correlation	Calculated	% Difference
$Re_{x_{Tp}} - Re_{x_s}$	4.59×10^4	3.73×10^4	19
$Re_{x_t} - Re_{x_s}$	1.97×10^4	1.85×10^4	6
$Re_{x_{Tp}} - Re_{x_t}$	2.63×10^4	1.88×10^4	29

from the effective leading edge to the end of the intermittency region that we calculated is 29% shorter than estimated from Mayle’s correlation, Eq.(7.6). For this correlation, Mayle [1] stated there was ‘considerable scatter’ in the data that was used to determine Eq.(7.6).

Since Mayle’s correlations were developed as approximations to scattered data and since other researchers [51] found that these correlations provide a rough estimate of the region lengths, the percent differences we obtained are not unexpected. For a rough estimate, we could expect values to vary by 30%. This means that within the long separation bubble results, we can expect similar differences.

7.1.4 Conclusions for short separation bubble

We determined the location of the fully laminar velocity at separation, Re_{x_A} , and the fully turbulent velocity, Re_{x_B} , by solving the set of 5 non-linear equations, Eq.(7.1). These values were the same as the experimental locations for separation and reattachment determined by Gaster [4]. We determined the location of the end of intermittency, Re_{x_T} , from the difference in enstrophy difference function, η , and this value corresponded to the end of the constant pressure region from the experimental data of Gaster [4].

From the difference in enstrophy density function, η , we were able to determine the start of the intermittency, Re_{x_0} . Since the start of intermittency can not be identified from the pressure distribution, we calculated the length of breakdown, $Re_{x_0} - Re_{x_t}$, and verified that the location we achieved for the start of intermittency is consistent with experimental

observation of Narasimha [3].

Using Re_{x_A} , determined from the solution of the set of non-linear equations, Eq.(7.1), Re_{x_T} , determined from the difference in enstrophy density function, η , and Re_{x_t} specified from experimental data, we were able to compare lengths of the various regions to the experimental correlations of Mayle [1]. The length of the unstable laminar region, $Re_{x_t} - Re_{x_A}$ compared well with the experimental correlation. The length of the upstream region, $Re_{x_T} - Re_{x_A}$, and the length of the transition region, $Re_{x_T} - Re_{x_t}$, did vary by 19% and 29%, respectively. However, due to the scatter in the experimental data, Mayle's correlations are only estimates so we would expect higher percent differences.

Overall, we solved for the x locations and lengths associated with transition over a separation bubble. By comparing these with the experimental data and correlations by Gaster [4], Mayle [1] and Narasimha [3], we can conclude that solving the set of equations, Eq.(7.1), produces consistent results for a short separation bubble.

7.2 Long separation bubble

Using the same set up, as outlined in Section 7.1, we obtained a long bubble solution by solving the set of non-linear equations, Eq.(7.1),

$$\begin{aligned}
 C_1 &= -16.9806 & C_2 &= 48.0815 & C_3 &= -30.1009 \\
 R_B &= 1.1333 & R &= 1.2652 & & (7.7)
 \end{aligned}$$

This result corresponds to the location of the fully laminar boundary condition at $Re_{x_A} = 4.61 \times 10^5$ and the location of the fully turbulent boundary condition at $Re_{x_B} = 5.83 \times 10^5$.

We can plot the difference in enstrophy density function, η , against the Reynolds number based on x between Re_{x_A} and Re_{x_B} . This is shown in Figure 7.4. From this plot, we

7.2 Long separation bubble

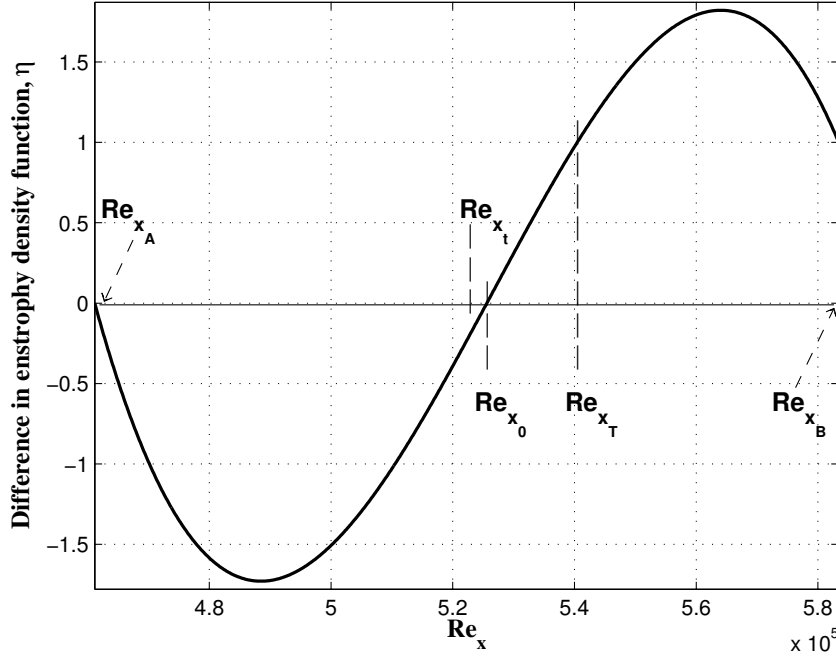


Figure 7.4 – Difference in enstrophy density between Re_{x_A} and Re_{x_B} for long separation bubble

obtain the start of the intermittency, $Re_{x_0} = 5.25 \times 10^5$ and the end of intermittency, $Re_{x_T} = 5.40 \times 10^5$. Between Re_{x_T} and Re_{x_B} , η goes above 1, this means that at the perpendicular location, $y = Re_{\theta_s}$,

$$\omega^2 > \left[\omega_{lam}^2 + (\omega_{turb}^2 - \omega_{lam}^2)|_{x_B} \right] \quad (7.8)$$

This means that the local enstrophy density is greater than baseline laminar enstrophy density plus a scaling term. Since the enstrophy density is calculated as $(\partial u / \partial y)^2$, a possible explanation for why the local enstrophy density is be greater is that the boundary layer becomes thicker through the region between Re_{x_T} and Re_{x_B} . This thickening could be the result of the long separation bubble becoming thinner as it reattaches. A similar possibility exists for why η is a larger negative between Re_{x_A} and Re_{x_0} . Through this region it could be possible that the presence of the bubble cause the boundary layer to become thinner.

When we compare the locations obtained for the long separation bubble with those obtained for the short bubble, we see that the location of start of intermittency is the same, as is the location of the end of intermittency. This is consistent with the experimental observation made by Mayle [1], who noted that the length of the intermittency region depended on the momentum thickness Reynolds number at separation and not whether the bubble length was short or long.

Figure 7.4 also indicates that the fully turbulent boundary condition location, Re_{x_B} is upstream of the end of intermittency. This implies that the turbulent flow at the end of intermittency takes longer to develop into a fully turbulent state. This is consistent with the experimental observations [1, 4] regarding long separation bubbles.

In Figure 7.5, we illustrate a pictorial representation of the separated flow transition over a long separation, where the laminar and turbulent boundary layer thickness is shown with the corresponding x locations. This figure illustrates that similar to the short separation

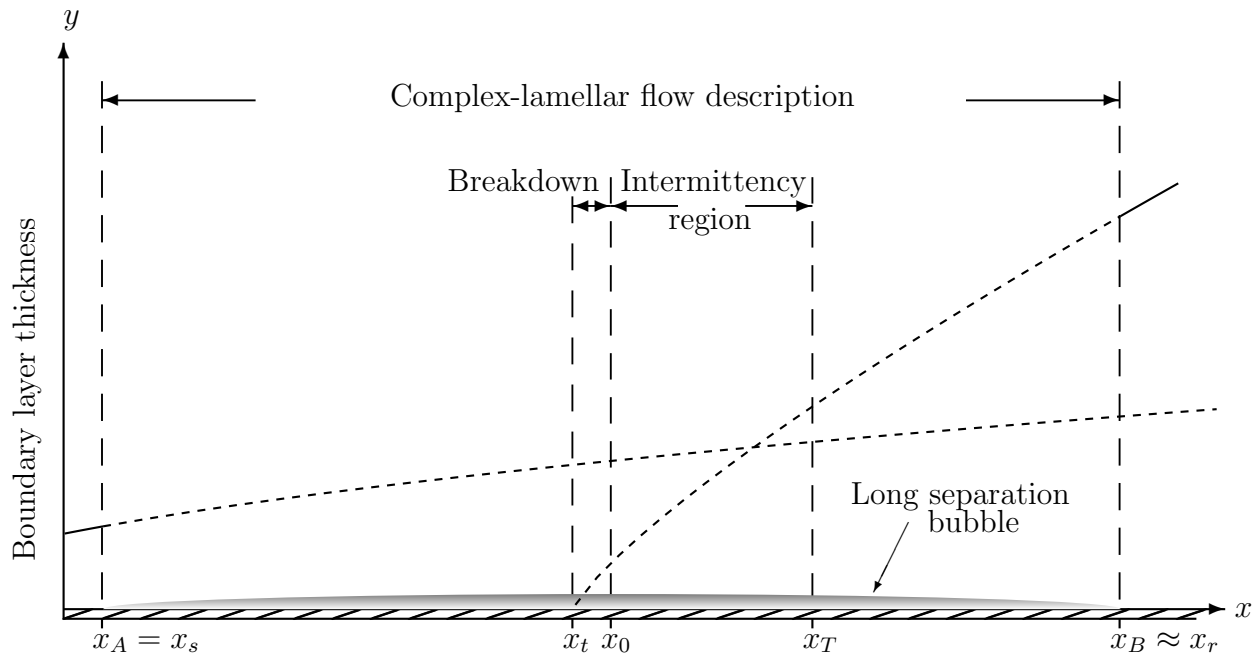


Figure 7.5 – Pictorial representation of the x locations associated with the long separation bubble results

7.2 Long separation bubble

bubble, we impose a fully laminar velocity profile at separation, however, nothing is imposed at the reattachment location. For the short separation bubble, we determined that the fully turbulent location was approximately the same as the experimental reattachment location. Therefore, we could infer that for the long separation bubble, $Re_{x_B} \approx Re_{x_r}$ and that the pressure recovery will occur over a greater distance compared to the short bubble. In Gaster's [4] long bubble test cases the reattachment point was located where the local pressure gradient was minimal, therefore, it seems reasonable to have used Prandtl's velocity profile at Re_{x_B} .

7.2.1 Comparison with Mayle [1] experimental correlations for long separation bubble

For long separation bubbles, Mayle [1] determined the experimental correlation for the length of the constant pressure region to be

$$Re_{x_{Tp}} - Re_{x_s} = 1300Re_{\theta_s}^{0.7} \quad (7.9)$$

the length of the unstable laminar region to be

$$Re_{x_t} - Re_{x_s} = 1000Re_{\theta_s}^{0.7} \quad (7.10)$$

and the length of the transition region to be

$$Re_{x_{Tp}} - Re_{x_t} = 400Re_{\theta_s}^{0.7} \quad (7.11)$$

Since we do not know the Reynolds number based on the momentum thickness at the long bubble separation location, Re_{x_A} , we will still use the value, $Re_{\theta_s} = 394$ from the experimental data of Gaster [4]. We expect this to still provide us with an accurate comparison,

since, the momentum thickness Reynolds number between separation and transition varies only slightly [1] so $Re_{\theta_t} \approx Re_{\theta_s}$. Therefore, since the long bubble is transitioning at the same location as the short bubble, we can use the same momentum thickness Reynolds number to obtain consistent results.

In Table 7.3 we compare Mayle's [1] correlations with the results we obtained.

Table 7.3 – Long bubble lengths calculated from our results comparison with Mayle's [1] experimental correlations

Region length	Mayle [1] Experimental Correlation	Calculated	% Difference
$Re_{x_{Tp}} - Re_{x_s}$	8.53×10^4	7.93×10^4	7
$Re_{x_t} - Re_{x_s}$	6.56×10^4	6.15×10^4	6
$Re_{x_{Tp}} - Re_{x_t}$	2.63×10^4	1.78×10^4	32

The length of the upstream region that we calculated from our results is 7% shorter than estimated from Mayle's correlation, Eq.(7.4). The length from separation to the effective leading edge of the turbulent boundary layer that we calculated is 6% shorter than estimated from Mayle's correlation, Eq.(7.5). Finally, the length from the effective leading edge to the end of the intermittency region that we calculated is 32% shorter than estimated from Mayle's correlation, Eq.(7.6).

Similar to the short bubble test case in Section 7.1.3, the length of the transition region, $Re_{x_T} - Re_{x_t}$, that we obtain is much shorter than predicted from Mayle's [1] correlation. The interesting factor is that there is only a 3% difference between our calculated length for the short bubble and the long bubble. Mayle [1] noted that even though there was considerable scatter in the data for determining the correlation for the length of transition, he was convinced that the length of transition was independent of whether the bubble was short or long. With the results we obtained from the derived complex-lamellar decomposition and the difference in enstrophy density function, we can also infer that the length of transition

7.2 Long separation bubble

is independent of the bubble length.

Obtaining consistent results for the various lengths associated with transition over a separation bubble, only tells us that the lengths are correct not that the x locations are correct. It is the fact that the location of the start and end of intermittency, Re_{x_0} and Re_{x_T} , are the same for the short and long bubble results that implies that because the lengths are consistent, then the x locations obtained from the long bubble results are also correct.

7.2.2 Conclusions regarding the long separation bubble

By solving the set of non-linear equations, Eq.(7.1), we obtained a solution that corresponded to a long separation bubble. We determined the separation point, Re_{x_A} and the reattachment point, Re_{x_B} from the solution of these equations, and the start of intermittency, Re_{x_0} , and the end of intermittency, Re_{x_T} , from the difference in enstrophy density function, η . Since Gaster only has a single solution at the specified momentum thickness Reynolds number at separation, we could not compare the location obtained for the long bubble. However, we were able to compare the region lengths we obtained with the experimental correlations of Mayle [1] for long separation bubbles. All of the region lengths were consistent with the experiment correlations which implied that this second solution was indeed a long bubble solution.

7.2.3 Conclusions regarding the comparison of short and long bubbles

When we compare the results we obtained for the short bubble with those for the long bubble, we see that our results are consistent with several experimental observations. We determined that the separation point, Re_{x_A} , for the long bubble was further upstream than the separation point for the short bubble. We determined the reattachment point, Re_{x_B} , for the long bubble was further downstream from the reattachment point of the short bubble. The location of the end of intermittency, Re_{x_T} , for a long bubble occurred upstream of the

reattachment point, Re_{x_B} , where as for a short bubble the end of intermittency coincides with the reattachment point. This implies that the pressure recovery for a long bubble occurs over a longer distance than for a short bubble. All of these results are consistent with experimental data and observation by many researchers, such as Gaster [4], Mayle [1] and Roberts [52]. Finally, our results imply that the length of the transition region, $Re_{x_T} - Re_{x_I}$, is independent of whether the separation bubble was short or long, just as Mayle [1] observed. Overall, our analysis provided the locations of separation, the start of intermittency, the end of intermittency and reattachment. From these locations, we could determine the lengths of the different regions associated with separation bubble transition. To verify these locations and lengths, we compared our results with the experimental data of Gaster [4], experimental correlations of Mayle [1] and experimental observations of Narasimha [3].

Therefore, we can conclude that solving the set of equations, Eq.(7.1), produces consistent results for both short and long separation bubbles. This implies that at a fixed location for the effective leading edge of the turbulent boundary layer, the complex-lamellar velocity condition provides the Reynolds number locations of where the short and long bubbles will separate. This is something experimentalists [4, 1] have tried to predict in order to use short bubbles to force transition and control gas turbine performance. The assumed slope of the difference in enstrophy density function can be accurately determined using equations, Eqs.(6.7 - 6.8). Finally, we obtain consistent locations for the start and end of intermittency by bounding the intermittency region between a fully laminar velocity profile on the verge of separation and a fully turbulent velocity profile, thereby indicating that our transition model for separated flow in the presence of a separation bubble is correct.

CHAPTER 8

Conclusions and Future work

8.1 Conclusions

From the results presented in the preceding chapters, we can make some conclusions regarding the objectives outlined in Chapter 1. By deriving the complex-lamellar decomposition of the velocity field across transition, we obtained a complex-lamellar velocity condition at the fully turbulent boundary condition. This condition provided us with an equation that identifies the locations of the fully laminar and fully turbulent boundary conditions. Furthermore, it provided us with a method for identifying the start and end of intermittency. In order to use this model, the location of the effective leading edge of the turbulent boundary layer needs to be known beforehand.

For the natural boundary layer transition we identified the location of the start and end of intermittency and these locations compared well with experimental data of Schubauer

and Klebanoff [2]. We were also able to identify the breakdown region between the effective leading edge of the turbulent boundary layer and the start of intermittency. This length compared well with the experimental observation of Narasimha [3]. Finally, we obtained the same results at two different cross-flow locations, thereby, indicating that evaluating the complex-lamellar velocity condition above the flat plate achieves the correct surface locations.

For separated flow transition over a separation bubble, we obtained solutions for both a short and long bubble. We identified the start and end of intermittency and these locations remained the same for both the short and long bubble. The end of intermittency corresponded with the end of the constant pressure region from Gaster's [4] experimental data. There was no experimental data for the start of intermittency, however, we compared the length of breakdown with Narasimha's [3] experimental estimate and it compared well. We also identified the location of separation and reattachment for the short and long bubble. The location of separation for the short bubble corresponded to the start of the constant pressure region from Gaster's [4] experimental data. Using Prandtl's turbulent velocity profile at the fully turbulent boundary condition produced consistent results for the short bubble reattachment location as compared with Gaster's [4] experimental data. There was no experimental data to compare with the locations for the long bubble solution, however, we compared the lengths of the unstable laminar region, transition region and constant pressure region, with Mayle's [1] experimental correlations. The length of regions were all within an acceptable accuracy range. Therefore, with the lengths of the regions being consistent with experimental correlations and since the start and end of intermittency were the same for both the short and long bubble, we could infer that the locations of separation and reattachment for the long bubble were correct. For a long separation bubble, we illustrated that using Prandtl's velocity profile at the fully turbulent boundary condition was justified and would provide a good estimate of the reattachment location.

Overall, the results illustrated that our boundary layer transition model that bounds the intermittency region between a fully laminar and fully turbulent boundary condition provides

consistent results for the start and end of intermittency for natural boundary layer transition and separated flow transition over a separation bubble.

8.2 Future work

Currently, by describing the laminar velocity with the Pohlhausen velocity profile we are able to take into account changes in pressure gradient of the laminar flow. Ideally it would also be useful to have another parameter that could model the effects of surface roughness and upstream disturbances. The commonality between these effects is a thinning of the laminar boundary layer. Therefore, the first attempt to model these effects would be to add a scaling parameter to the laminar boundary layer thickness and determine how the transition locations are affected.

Both the natural boundary layer transition and separated flow transition over a separation bubble cases were along a flat plate. The next step would be to implement a transition model for an airfoil and turbine blade. A first attempt would be to determine the effective leading edge of the turbulent boundary layer from experimental or CFD data. The Pohlhausen pressure parameter could then be obtained from the pressure distribution and the laminar velocity profile to be satisfied at Re_{x_A} could be determined. Based on the results from the current research, we can conclude that the turbulent velocity profile that is satisfied at Re_{x_B} has little influence on the location of the start and end of intermittency. Therefore, we would still describe the turbulent velocity profile on an airfoil or turbine blade using the Prandtl turbulent profile.

We would also like to consider implementing this model within a RANS solver. As our model requires knowing the location of the effective leading of the turbulent boundary layer this might have to be an iterative process. In theory we may be able to use the height of the wake to determine possible locations for the effective leading edge. Once we have this location, we could then determine the location of the start of intermittency and the η function from

our model and use this within an algebraic transition model.

APPENDIX A

Matlab code

```
% This program using part of CsandRsol2.m and runnested2.m to experiment
% with differnt Cn values. The purposes is to find different xL values.
% *** For disseration , only Type 3 is used, other types are incomplete!! **

%————— CsandRsol2.m —————
% This program is set up to solve for 3 different situations.
% ***** Type 1 *****
% Here we assume that RexL is the AGS correlation for the start of
% transition. We solve the program for R0 and RexT.
%
% ***** Type 2 *****
% Here we assume that R0 is the AGS correlation for the start of
% transition. We solve the program for RexL and RexT.
%
% ***** Type 3 *****
% This version is the most complex and includes some different parameters.
```



```

% ***** 2:  $C_n(x-x_L)/(x_T-x_L) = \gamma dw/dw_f$  ***** %
intermittency = 1;
% ***** cntype - 1: solving for  $C_n$ , cntype - 2: preset  $C_n$  values, ***** %
% ***** cntype - 3: using solve ***** %
Cntype = 1;
% ***** pres - 0, figures print out for dissertation, pres - 1, figures * %
% ***** print out for presentation
pres = 0;
% ***** sep - 0: zero pressure gradient flow, 1: separated flow ***** %
sep = 0;
testa = 1;

% ***** Parameters for zero pressure and separated bubble cases ***** %
for testa = 1
    if sep == 0 % Zero pressure
        L=0;
        Ks=1;
        t=0.03;
        L2=0;
        % Case 1 For  $y=\theta_{min}$  and  $y=\theta_{max}$ 
        x0 = [2,4,-4,9,-4]
        %x0 = [2.6,4.0,-4.1,9.6,-4.4]
        %x0 = [2.62,4.04,-4.19,9.60,-4.40]
        % Case 2 at both y values
        %x0 = [0.1,1.01,-1.6,2,0.6]
        % Case 3
        %x0 = [0.1,5,20,-65,46]
        %x0 = [170,300,-17,48,-30]

        %x0 = [0.89,15,12,-40,29]
        %x0 = [2,4,-3,9,-5]

        %x0 = [2.637409,4.304669,-6.139714,15.428341,-8.288729]
    end
end

```

```

    %x0=[3.4874,5.8623,-6.2676,15.8109,-8.5432]
elseif sep == 1 % Separation bubble
    L=-12;

    % Separation case 1
    % * NOTE: if you use the initial value below, you will obtain *** %
    % * a different enstrophy function shape! Proving that there **** %
    % * are different solutions from our equations. *** %
    % * If you use the initial values, x0, specified below *** %
    % * along with a Ks=1, then our results match Mayle's ** %
    % * correlation for the length of the intermittency region and ** %
    % * for the length of the laminar region for a short bubble. *** %

    % short bubble y = theta_s=394, 268, 232
    x0 = [1.04,1.1,-4,10,-5];
    Ks = 2.298;
    % long bubble y=theta_s=394, 268, 232
    %
    x0 = [1.2,1.5,-17,48,-30];
    %
    Ks = 1;

    % Separation case 2
    % Re_theta_s = 268, 232
    %
    x0 = [0.4,1.2,-1.6,1.93,0.67]
    %
    Ks = 1

    % Separation case 3
    % * NOTE 2: if you use the initial values given below and a ** %
    % * Ks = 1, you get the solution of xL = x0! This is 3 different %
    % * solutions.
    % y = theta_turb
    %
    x0 = [0.8, 1.1, 1.2,-0.9,0.6]

```

```

%           Ks = 1.1;
% Case 3
% theta_s = 268
%           x0 = [0.99,3.70,59.7,-182.2,123.5]
%           Ks = 1.0;

% Separation case 4
% Re_theta_s = 232
%           x0 = [0.4,1.2,-1.6,1.93,0.67]
%           Ks = 1.0

end
% ***** %
if sep==0
    Flam=6.91+12.75*L2+63.64*L2^2;
    Retheta_lam=(163+exp(Flam-Flam/6.91*t));

elseif sep==1
    % short bubble
%           Rethetax=268;
%           Rexmax=12.6*458.4/0.023;

    % long bubble
%           Rethetax=232;
%           Rexmax=12*516/0.023;

    % shortest bubble
    Rethetax=394;
    Rexmax=11*1147.2/0.023;

    % longest bubble
%           Rethetax=136;
%           Rexmax=14.5*211.2/0.023;

end

```

```

A=(2*(37/315-L/945-L^2/9072)*(2-(116*L)/315 ...
    +(2/945+1/120)*L^2+(2*L^3)/9072))^0.5;
k=2.667;
Cs=30.2;
b = 3.36;
G25 = (log(1-0.25)/(-0.412*b^2))^0.5;
G50 = (log(1-0.5)/(-0.412*b^2))^0.5;
G75 = (log(1-0.75)/(-0.412*b^2))^0.5;
G40 = (log(1-0.7)/(-0.412*b^2))^0.5;
A/(37/315-L/945-L^2/9072)

if sep == 0
    Res=(Retheta_lam/A)^2; %Rexmin
    Rethetae=k*Retheta_lam;
    RexagsEp = (72/7*(1/0.375)*Rethetae)^(5/4);
    if testa == 1
        Rethetax=Retheta_lam;
    elseif testa == 2
        Rethetax=Rethetae;
    end
    if type == 1
        Rexl = Res;
    elseif type == 2
        R0 = Res;
    elseif type == 3
        RagsS = Res;
        R0 = (1.26*RagsS - 0.26*RexagsEp)/1.26;
    end

    ReLT = Cs*R0^0.75;
elseif sep == 1
    ReLT = 400*((Rethetax))^0.7;

```

```

R0 = Rexmax - ReLT;
Res = R0;
RexagsEp= ReLT;

end

% This can be ignored for now. However, if changing 'type' changes %
% than this will need to be uncommented. %
%%Establishing type
% if Cntype == 1
%     if type == 1
%         x0=[1.11,2.5,-3,7,-3]
%         %x0=[1.17,1.8,-0.0004,-0.7,3.4,-1.6]
%     elseif type == 2
%         x0=[1.11,1.5,-3,7,-3] %works with eqn 1,3,5,6,7
%         %x0=[1.17,1.8,-0.0004,-0.7,3.4,-1.6]
%     elseif (type == 3)
%         x0 = [2,3,-4,10,-5] % solves zero pressure gradient case
%         %x0 = [2,5,-16,49,-32] % solves separation bubble case
%         %x0 = [42,85,-16,46,-29]
%         %x0 = [0.8,1.5,1.4,0.6,0.9,-1.9]
%     elseif (type == 4)
%         x0 = [1*10^6,3.9*10^6,-15,20,2,-6]
%     end
% elseif (Cntype == 2)
%     if type == 3
%         x0 = [1.06,1.5]
%     elseif type ==4
%         x0 = [2.6*10^6,3.9*10^6]
%     end
% end

options=optimset('Algorithm','trust-region-reflective','Display'...
```

```

    , 'iter' , 'MaxFunEvals' , 100000 , 'MaxIter' , 100000);

if (Cntype == 2)
    [x C0 C1 C2 C4 C6 fval]=...
        runnestedRLRT(type , yvalue , intermittency , L, Ks, ...
            k, A, Rethetax , RexagsEp , Res , Cs , x0)
elseif (Cntype == 1)
    [x C0 C1 C2 C3 C4 fval exitflag]=...
        runnested2(type , yvalue , intermittency , ...
            L, Ks, k, A, Rethetax , RexagsEp , Res , Cs , x0 , G25 , G50 , G75 , ReLT , G40 , R0)
elseif (Cntype == 3)
    syms RB R C1 C2 C3
    [RB R C0 C1 C2 C3 C4] = runnested3(type , yvalue , intermittency , L, ...
        Ks, k, A, Rethetax , RexagsEp , Res , Cs , G25 , G50 , G75 , ReLT , G40)
end

x(1);
x(2);
R = x(2);
RB = x(1);
if type == 1
    R0 = x(1)*Rexl;
elseif type == 2
    Rexl = R0/x(1)
    C6=0;
elseif type == 3
    Rexl = R0/x(1)
    RexagsE = RexagsEp + R0;
elseif type == 4

end
Rexft=x(2)*Rexl
syms a

```

```

Gamma_0 = solve((a - Rexl)/(Rexft-Rexl)*C1 ...
    +(a - Rexl)^2/(Rexft-Rexl)^2*C2 + (a - Rexl)^3/(Rexft-Rexl)^3*C3...
    +(a - Rexl)^4/(Rexft-Rexl)^4*C4 - 0);
Rex0_mj = Gamma_0(2)
Gamma_1 = solve((a - Rexl)/(Rexft-Rexl)*C1 ...
    +(a - Rexl)^2/(Rexft-Rexl)^2*C2 + (a - Rexl)^3/(Rexft-Rexl)^3*C3...
    +(a - Rexl)^4/(Rexft-Rexl)^4*C4 - 1);
Rext_mj = Gamma_1(2)
Gamma_25 = solve((a - Rexl)/(Rexft-Rexl)*C1 ...
    +(a - Rexl)^2/(Rexft-Rexl)^2*C2 + (a - Rexl)^3/(Rexft-Rexl)^3*C3...
    +(a - Rexl)^4/(Rexft-Rexl)^4*C4 - 0.25);
Rexg25_mj = Gamma_25(2)
Gamma_75 = solve((a - Rexl)/(Rexft-Rexl)*C1...
    +(a - Rexl)^2/(Rexft-Rexl)^2*C2 + (a - Rexl)^3/(Rexft-Rexl)^3*C3...
    +(a - Rexl)^4/(Rexft-Rexl)^4*C4 - 0.75);
Rexg75_mj = Gamma_75(2)

Relen = Rexft - Rexl;
% Rlen0T = Rext - R0
i=1;
for Rex = Rexl:Relen/1000:Rexft
    Gamma_dmj(i) = C0 + (Rex - Rexl)/(Rexft-Rexl)*C1...
        + (Rex - Rexl)^2/(Rexft-Rexl)^2*C2...
        + (Rex - Rexl)^3/(Rexft-Rexl)^3*C3...
        + (Rex - Rexl)^4/(Rexft-Rexl)^4*C4;
    Rex_plot(i) = Rex;

    if sep==0
        if type ==3
            if yvalue == 1
                ydivdelta(i) = (k*A*RagsS^(1/2))/(5*Ks*Rex^(1/2));
                ydivdeltat(i) = (0.375*(7/72)*RexagsEp^(4/5))/...

```

```

(0.375*(Rex-R0)*(Rex-R0)^(-1/5));

% enstrophy/vorticity through out region
dw_f = (1/(7*k*A))^2*(7/72)^(2/7)*...
((RexagsEp/Rexl)/(R-RB))^(8/35)...
- ((2+L/6)^2*(RagsS/Rexl))/((5*Ks)^2*R)...
+ (2*L*(2+L/6)*k*A*...
(RagsS/Rexl)^(3/2))/((5*Ks)^3*(R)^(3/2)) ...
+ (6*(2+L/6)*(2-L/2)-L^2)*k^2*A^2*...
(RagsS/Rexl)^2/((5*Ks)^4*(R)^2)...
- (8*(2+L/6)*(1-L/6)+6*L*(2-L/2))*k^3*A^3*...
(RagsS/Rexl)^(5/2)/((5*Ks)^5*(R)^(5/2))...
+ (8*L*(1-L/6)-9*(2-L/2)^2)*k^4*A^4*...
(RagsS/Rexl)^3/((5*Ks)^6*(R)^3)...
+ 24*(2-L/2)*(1-L/6)*k^5*A^5*...
(RagsS/Rexl)^(7/2)/((5*Ks)^7*(R)^(7/2))...
- 16*(1-L/6)^2*k^6*A^6*...
(RagsS/Rexl)^4/((5*Ks)^8*(R)^4);

dw_f2 = (1/(7*k*A)*(7/(72))^(1/7)*...
((RexagsEp/Rexl)/(R-RB))^(4/35))^2 ...
-(((2+L/6)*(RagsS/Rexl)^0.5)/(5*Ks*R^0.5))...
-(L*k*A*(RagsS/Rexl))/((5*Ks)^2*R) ...
- (3*(2-L/2)*k^2*A^2*...
(RagsS/Rexl)^1.5)/((5*Ks)^3*R^1.5)...
+ (4*(1-L/6)*k^3*A^3*...
(RagsS/Rexl)^2)/((5*Ks)^4*R^2))^2;

if ydivdelta(i) > 1
    w2_lam(i) = 0;
else
    w2_lam(i)=-(-(2+L/6)^2*(RagsS))/((5*Ks)^2*(Rex))...
    + (2*L*(2+L/6)*k*A*...
    (RagsS)^(3/2))/((5*Ks)^3*(Rex)^(3/2)) ...

```

```

+ (6*(2+L/6)*(2-L/2)-L^2)*k^2*A^2*...
(RagsS)^2/((5*Ks)^4*(Rex)^2)...
- (8*(2+L/6)*(1-L/6)+6*L*(2-L/2))*k^3*A^3*...
(RagsS)^(5/2)/((5*Ks)^5*(Rex)^(5/2))...
+ (8*L*(1-L/6)-9*(2-L/2)^2)*k^4*A^4*...
(RagsS)^3/((5*Ks)^6*(Rex)^3)...
+ 24*(2-L/2)*(1-L/6)*k^5*A^5*...
(RagsS)^(7/2)/((5*Ks)^7*(Rex)^(7/2))...
- 16*(1-L/6)^2*k^6*A^6*...
(RagsS)^4/((5*Ks)^8*(Rex)^4);
w2_lam2(i) = (((2+L/6)*...
(RagsS)^0.5)/(5*Ks*Rex^0.5)...
-(L*k*A*(RagsS))/((5*Ks)^2*Rex) ...
- (3*(2-L/2)*k^2*A^2*...
(RagsS)^1.5)/((5*Ks)^3*Rex^1.5)...
+ (4*(1-L/6)*k^3*A^3*...
(RagsS)^2)/((5*Ks)^4*Rex^2))^2;
end
if ((Rex > R0) & (ydivdeltat(i) < 1))
w2_turb(i) = (1/(7*k*A))^2*(7/72)^(2/7)*...
((RexagsEp)/(Rex-R0))^(8/35);
else
w2_turb(i) = 0;
end
elseif yvalue == 2
ydivdelta(i) = (A*RagsS^(1/2))/(5*Ks*Rex^(-1/2)*Rex);
ydivdeltat(i) = (0.375*(7/(72*k)))*...
RexagsEp^(4/5)/(0.375*(Rex-R0)*(Rex-R0)^(-1/5));

dw_f = (1/(7*A))^2*(7/(72*k))^(2/7)*...
((RexagsEp/Rexl)/(R-RB))^(8/35)...
- ((2+L/6)^2*(RagsS/Rexl))/((5*Ks)^2*R)...
+ (2*L*(2+L/6)*A*...

```

```

(RagsS/Rexl)^(3/2)/((5*Ks)^3*(R)^(3/2)) ...
+ (6*(2+L/6)*(2-L/2)-L^2)*A^2*...
(RagsS/Rexl)^2/((5*Ks)^4*(R)^2)...
- (8*(2+L/6)*(1-L/6)+6*L*(2-L/2))*A^3*...
(RagsS/Rexl)^(5/2)/((5*Ks)^5*(R)^(5/2))...
+ (8*L*(1-L/6)-9*(2-L/2)^2)*A^4*...
(RagsS/Rexl)^3/((5*Ks)^6*(R)^3)...
+ 24*(2-L/2)*(1-L/6)*A^5*...
(RagsS/Rexl)^(7/2)/((5*Ks)^7*(R)^(7/2))...
- 16*(1-L/6)^2*A^6*(RagsS/Rexl)^4/((5*Ks)^8*(R)^4);
if ydivdelta(i) > 1
    w2_lam(i) = 0;
else
    w2_lam(i) = -((2+L/6)^2*...
        (RagsS))/((5*Ks)^2*(Rex))...
        + (2*L*(2+L/6)*A*...
        (RagsS)^(3/2))/((5*Ks)^3*(Rex)^(3/2)) ...
        + (6*(2+L/6)*(2-L/2)-L^2)*A^2*...
        (RagsS)^2/((5*Ks)^4*(Rex)^2)...
        - (8*(2+L/6)*(1-L/6)+6*L*(2-L/2))*A^3*...
        (RagsS)^(5/2)/((5*Ks)^5*(Rex)^(5/2))...
        + (8*L*(1-L/6)-9*(2-L/2)^2)*A^4*...
        (RagsS)^3/((5*Ks)^6*(Rex)^3)...
        + 24*(2-L/2)*(1-L/6)*A^5*...
        (RagsS)^(7/2)/((5*Ks)^7*(Rex)^(7/2))...
        - 16*(1-L/6)^2*A^6*...
        (RagsS)^4/((5*Ks)^8*(Rex)^4);
end
if ((Rex > R0) & (ydivdeltat(i) < 1))
    w2_turb(i) = (1/(7*A))^2*(7/(72*k))^(2/7)*...
        ((RexagsEp)/(Rex-R0))^(8/35);
else
    w2_turb(i) = 0;

```

```

        end
    end
    % enst and vort are without U/nu and xagsS terms
    if intermittency == 1
        enst(i) = Gamma_dmj(i) +w2_lam(i)/dw_f;
        enst_lin(i) =(1- Gamma_dmj(i))*w2_lam(i)...
            + Gamma_dmj(i)*w2_turb(i);
        enst_nonlin(i) = Gamma_dmj(i)*(dw_f -(w2_turb(i)...
            - w2_lam(i)));
    elseif intermittency == 2
        enst(i) = Gamma_dmj(i)*dw_f +w2_lam(i);
    end
    vort(i) = sqrt(enst(i));
    vort2(i) = -vort(i);
    enst_lam(i) = w2_lam(i);
end
end
i=i+1;
end

j=1;
for Rextn = R0:(Rext_mj-R0)/1000:Rext_mj
    if intermittency == 1
        Gamma_dnr(j) = 1-exp(-(0.412*3.36^2*(Rextn-R0)^2)/(ReLT)^2);
        Rextn_plot(j) = Rextn;
        j=j+1;
    elseif intermittency == 2
        if (type == 3 && yvalue == 1)
            dw_f = (1/(7*k*A))^2*(7/72)^(2/7)*...
                ((RextagsEp/Rextl)/(R-RB))^(8/35)...
                - ((2+L/6)^2*(RagsS/Rextl))/((5*Ks)^2*R)...
                + (2*L*(2+L/6)*k*A*...

```

```

(RagsS/Rexl)^(3/2)/((5*Ks)^3*(R)^(3/2)) ...
+ (6*(2+L/6)*(2-L/2)-L^2)*k^2*A^2*...
(RagsS/Rexl)^2/((5*Ks)^4*(R)^2)...
- (8*(2+L/6)*(1-L/6)+6*L*(2-L/2))*k^3*A^3*...
(RagsS/Rexl)^(5/2)/((5*Ks)^5*(R)^(5/2))...
+ (8*L*(1-L/6)-9*(2-L/2)^2)*k^4*A^4*...
(RagsS/Rexl)^3/((5*Ks)^6*(R)^3)...
+ 24*(2-L/2)*(1-L/6)*k^5*A^5*...
(RagsS/Rexl)^(7/2)/((5*Ks)^7*(R)^(7/2))...
- 16*(1-L/6)^2*k^6*A^6*(RagsS/Rexl)^4/((5*Ks)^8*(R)^4);
enst_turb(j) = (1/(7*k*A))^2*(7/72)^(2/7)*...
((RexagsEp)/(Rexn - R0))^(8/35);
if Rexn == R0
dw(j) = - ((2+L/6)^2*(RagsS))/((5*Ks)^2*(Rexn))...
+ (2*L*(2+L/6)*k*A*...
(RagsS)^(3/2))/((5*Ks)^3*(Rexn)^(3/2)) ...
+ (6*(2+L/6)*(2-L/2)-L^2)*k^2*A^2*...
(RagsS)^2/((5*Ks)^4*(Rexn)^2)...
- (8*(2+L/6)*(1-L/6)+6*L*(2-L/2))*k^3*A^3*...
(RagsS)^(5/2)/((5*Ks)^5*(Rexn)^(5/2))...
+ (8*L*(1-L/6)-9*(2-L/2)^2)*k^4*A^4*...
(RagsS)^3/((5*Ks)^6*(Rexn)^3)...
+ 24*(2-L/2)*(1-L/6)*k^5*A^5*...
(RagsS)^(7/2)/((5*Ks)^7*(Rexn)^(7/2))...
- 16*(1-L/6)^2*k^6*A^6*...
(RagsS)^4/((5*Ks)^8*(Rexn)^4);

else
dw(j) = (1/(7*k*A))^2*(7/72)^(2/7)*...
((RexagsEp)/(Rexn - R0))^(8/35)...
- ((2+L/6)^2*(RagsS))/((5*Ks)^2*(Rexn))...
+ (2*L*(2+L/6)*k*A*...
(RagsS)^(3/2))/((5*Ks)^3*(Rexn)^(3/2)) ...

```

$$\begin{aligned}
& + (6*(2+L/6)*(2-L/2)-L^2)*k^2*A^2*... \\
& (\text{RagsS})^2/((5*Ks)^4*(\text{Rexn})^2)... \\
& - (8*(2+L/6)*(1-L/6)+6*L*(2-L/2))*k^3*A^3*... \\
& (\text{RagsS})^{5/2}/((5*Ks)^5*(\text{Rexn})^{5/2})... \\
& + (8*L*(1-L/6)-9*(2-L/2)^2)*k^4*A^4*... \\
& (\text{RagsS})^3/((5*Ks)^6*(\text{Rexn})^3)... \\
& + 24*(2-L/2)*(1-L/6)*k^5*A^5*... \\
& (\text{RagsS})^{7/2}/((5*Ks)^7*(\text{Rexn})^{7/2})... \\
& - 16*(1-L/6)^2*k^6*A^6*... \\
& (\text{RagsS})^4/((5*Ks)^8*(\text{Rexn})^4);
\end{aligned}$$

end

elseif (type == 3 && yvalue == 2)

$$\begin{aligned}
\text{dw}_f & = (1/(7*A))^2*(7/(72*k))^{2/7}*... \\
& ((\text{RexagsEp}/\text{Rexl})/(\text{R-RB}))^{8/35}... \\
& - ((2+L/6)^2*(\text{RagsS}/\text{Rexl}))/((5*Ks)^2*R)... \\
& + (2*L*(2+L/6)*A*... \\
& (\text{RagsS}/\text{Rexl})^{3/2})/((5*Ks)^3*(R)^{3/2})... \\
& + (6*(2+L/6)*(2-L/2)-L^2)*A^2*... \\
& (\text{RagsS}/\text{Rexl})^2/((5*Ks)^4*(R)^2)... \\
& - (8*(2+L/6)*(1-L/6)+6*L*(2-L/2))*A^3*... \\
& (\text{RagsS}/\text{Rexl})^{5/2}/((5*Ks)^5*(R)^{5/2})... \\
& + (8*L*(1-L/6)-9*(2-L/2)^2)*A^4*... \\
& (\text{RagsS}/\text{Rexl})^3/((5*Ks)^6*(R)^3)... \\
& + 24*(2-L/2)*(1-L/6)*A^5*... \\
& (\text{RagsS}/\text{Rexl})^{7/2}/((5*Ks)^7*(R)^{7/2})... \\
& - 16*(1-L/6)^2*A^6*(\text{RagsS}/\text{Rexl})^4/((5*Ks)^8*(R)^4);
\end{aligned}$$

if Rexn == R0

$$\begin{aligned}
\text{dw}(j) & = - ((2+L/6)^2*(\text{RagsS}))/((5*Ks)^2*(\text{Rexn}))... \\
& + (2*L*(2+L/6)*A*... \\
& (\text{RagsS})^{3/2})/((5*Ks)^3*(\text{Rexn})^{3/2})... \\
& + (6*(2+L/6)*(2-L/2)-L^2)*A^2*... \\
& (\text{RagsS})^2/((5*Ks)^4*(\text{Rexn})^2)...
\end{aligned}$$

```

- (8*(2+L/6)*(1-L/6)+6*L*(2-L/2))*A^3*...
  (RagsS)^(5/2)/((5*Ks)^5*(Rexn)^(5/2))...
+ (8*L*(1-L/6)-9*(2-L/2)^2)*A^4*...
  (RagsS)^3/((5*Ks)^6*(Rexn)^3)...
+ 24*(2-L/2)*(1-L/6)*A^5*...
  (RagsS)^(7/2)/((5*Ks)^7*(Rexn)^(7/2))...
- 16*(1-L/6)^2*A^6*(RagsS)^4/((5*Ks)^8*(Rexn)^4);

else
  dw(j) = (1/(7*A))^2*(7/(72*k))^(2/7)*...
    ((RexagsEp)/(Rexn - R0))^(8/35)...
    - ((2+L/6)^2*(RagsS))/((5*Ks)^2*(Rexn))...
    + (2*L*(2+L/6)*A*...
      (RagsS)^(3/2))/((5*Ks)^3*(Rexn)^(3/2)) ...
    + (6*(2+L/6)*(2-L/2)-L^2)*A^2*...
      (RagsS)^2/((5*Ks)^4*(Rexn)^2)...
    - (8*(2+L/6)*(1-L/6)+6*L*(2-L/2))*A^3*...
      (RagsS)^(5/2)/((5*Ks)^5*(Rexn)^(5/2))...
    + (8*L*(1-L/6)-9*(2-L/2)^2)*A^4*...
      (RagsS)^3/((5*Ks)^6*(Rexn)^3)...
    + 24*(2-L/2)*(1-L/6)*A^5*...
      (RagsS)^(7/2)/((5*Ks)^7*(Rexn)^(7/2))...
    - 16*(1-L/6)^2*A^6*(RagsS)^4/((5*Ks)^8*(Rexn)^4);

end

enst_turb(j) = (1/(7*A))^2*(7/(72*k))^(2/7)*...
  ((RexagsEp)/(Rexn - R0))^(8/35);

end

Gamma_dnr(j) = (1-exp(-(0.412*3.36^2*(Rexn-R0)^2)/...
  (Cs*R0^0.75)^2))*dw(j)/dw_f;

Rexn_plot(j) = Rexn;
j=j+1;

end

end

```

```

if sep == 1
    Retheta_st = Retheta_x;
    Rex0T_Mayle = 400*Retheta_st^0.7 % Mayle's intermittency length
    RextT_mj = Rext_mj - R0 % Our intermittency length
    Rex0T_mj = Rext_mj - Rex0_mj
    RexL0_Mayle_sb = 300*Retheta_st^0.7 % Mayle's sb lam length
    RexL0_Mayle_lb = 1000*Retheta_st^0.7 % Mayle's lb lam length
    RexLt_mj = R0 - Rexl % Our laminar region length
    RexL0_mj = Rex0_mj - Rexl
    RexST_Mayle_sb = 700*Retheta_st^0.7
    ResST_Mayle_lb = 1300*Retheta_st^0.7
    RexST_mj = Rext_mj - Rexl
end

% Plots for the proposal/dissertation
if pres == 1
    if (R0 < Rexl)
        figure(3)
        plot(Rexn_plot, Gamma_dnr, 'r--', 'LineWidth', 1.5)
        %semilogx(Rex_plot, Gamma_dmj, Rexn_plot, Gamma_dnr)
        legend('Difference in enstrophy density', ...
            'Narasimha Intermittency Distribution');...
        %, 'fontname', 'Times New Roman', 'fontsize', 12)
        %xlabel('Reynolds Number', 'fontname', 'Times New Roman', ...
            'fontsize', 12)
        ylabel('Enstrophy density function', ...
            'fontname', 'Times New Roman', 'fontsize', 12)
        %axis([10^0 4*10^6 -0.7 1.2])
        axis([R0 Rexft 0 2])
        % set(gca, 'XTick', [R0 Rexl Rexft])
        % set(gca, 'XTickLabel', {'Re_x0p', 'Re_xFL', 'Re_xFT'})
    end
end

```

```

grid on
figure(4)
plot(Rex_plot , Gamma_dmj,'-r' , 'LineWidth' ,1.5)
xlabel('Re_x' , 'fontname' , 'Times New Roman' , 'fontsize' ,12)
ylabel('Difference in enstrophy density' , 'fontname' ,...
      'Times New Roman' , 'fontsize' ,12)
%axis([9*10^5 3.9*10^6 -0.7 1])
axis([Rexl Rexft min(Gamma_dmj)-0.1 max(Gamma_dmj)+0.1])
% set(gca , 'XTick' , [Rexl Rexft])
% set(gca , 'XTickLabel' , { 'Re_xL' , 'Re_xFT' })
% set(gca , 'GridLineStyle' , '-' )
else
if sep == 0
figure(3)
plot(Rexn_plot(352:772) , Gamma_dnr(352:772) ,...
      'k-' , 'LineWidth' ,1.5)
%semilogx(Rex_plot , Gamma_dmj , Rexn_plot , Gamma_dnr)
%legend('Difference in enstrophy density' ,...
% 'Narashima Intermittency Distribution ');...
% % , 'fontname' , 'Times New Roman' , 'fontsize' ,12)
% xlabel('Reynolds Number' , 'fontname' , 'Times New Roman' ,...
% 'fontsize' ,12)
ylabel('Intermittency , \gamma' , 'fontname' ,...
      'Times New Roman' , 'fontsize' ,16)
axis([2.6555*10^6 Rexft 0 1])
% if sep == 0
% axis([Rex0_mj Rexft 0 1])
% elseif sep == 1
% axis([Rex0_mj Rexft 0 2])
% end
set(gca , 'XTick' , [2.6555*10^6 Rexn_plot(352)...
Rexn_plot(772) Rexft])
set(gca , 'XTickLabel' , { '' , '' , '' , '' })

```

```

text(2.6555*10^6,-0.06,'x_0','fontname',...
     'Times New Roman','fontsize',16);
text(Rexn_plot(352),-0.06,'x-|_{\gamma=0.25}',...
     'fontname','Times New Roman','fontsize',16);
text(Rexn_plot(772),-0.06,'x-|_{\gamma=0.75}',...
     'fontname','Times New Roman','fontsize',16);
text(Rexft,-0.06,'x_T','fontname','Times New Roman',...
     'fontsize',16);
grid on
figure(6)
plot(Rex_plot, Gamma_dmj,'r--',...
     Rexn_plot(352),Gamma_dnr(352),'*k',...
     Rexn_plot(546),Gamma_dnr(546),'*k',...
     Rexn_plot(510:580),Gamma_dnr(510:580),...
     'k-','LineWidth',1.5)
%semilogx(Rex_plot, Gamma_dmj,Rexn_plot, Gamma_dnr)
legend('\eta','\gamma','location','NorthWest')
%xlabel('Reynolds Number','fontname','Times New Roman',...
%      'fontsize',12)
ylabel('\eta','fontname','Times New Roman','fontsize',16)
axis([Rexl Rexft min(Gamma_dmj)-0.05 max(Gamma_dmj)+0.05])
%   if sep == 0
%       axis([Rex0_mj Rexft 0 1])
%   elseif sep == 1
%       axis([Rex0_mj Rexft 0 2])
%   end
set(gca,'XTick',[Rexl 2.6555*10^6 Rexn_plot(352)...
     Rexn_plot(772) Rexft])
set(gca,'XTickLabel',{' ',' ',' ',' ',' '})
text(Rexl,-0.65,'x_A','fontname','Times New Roman',...
     'fontsize',16)
text(2.6555*10^6-5*10^4,-0.65,'x_0','fontname',...
     'Times New Roman','fontsize',16);

```

```

text (Rexn_plot(352)-6*10^4,-0.65,'x|_{\gamma=0.25}',...
      'fontname','Times New Roman','fontsize',16);
text (Rexn_plot(772)-2*10^5,-0.65,'x|_{\gamma=0.75}',...
      'fontname','Times New Roman','fontsize',16);
text (Rexft-7*10^4,-0.65,'x_T \approx x_B','fontname',...
      'Times New Roman','fontsize',16);
annotation('line',[0.135 0.9],[0.397 0.397],'LineStyle',...
           '-','LineWidth',1.0);
annotation('line',[0.599 0.599],[0.12 0.39],'LineStyle',...
           '- -','LineWidth',1.0);
annotation('line',[0.67 0.67],[0.12 0.51],'LineStyle',...
           '- -','LineWidth',1.0);
annotation('line',[0.823 0.823],[0.12 0.78],'LineStyle'...
           '- -','LineWidth',1.0);
grid on
end
figure(4)
plot(Rex_plot, Gamma_dmj,'--k','LineWidth',1.5)
grid on
if sep == 0
    xlabel('Re_x','fontname','Times New Roman','FontSize',...
           12,'FontWeight','BOLD')
    ylabel('Difference in enstrophy density function, \eta',...
           'fontname','Times New Roman',...
           'fontsize',12,'FontWeight','BOLD')
    axis([Rexl Rexft min(Gamma_dmj)-0.05 max(Gamma_dmj)+0.05])
    annotation('arrow',[0.175,0.135],[0.495,0.407],...
              'HeadStyle','vback3','HeadLength',3,'HeadWidth',7,...
              'LineStyle','- -')
    text(Rexl+6*10^4,0.23,'Re_{x_A}','FontSize',16)
    text(R0-3.5*10^4,0.23,'Re_{x_t}','FontSize',16)
    text(R0-2.5*10^4,0.0,'\mid');...
        text(R0-2.5*10^4,0.1,'\mid');...

```

```

        text(R0-2.5*10^4,0.2,'\mid')

text(2.66*10^6-5*10^4,-0.35,'Re_{x_0}','FontSize',16)
text(2.66*10^6-2.5*10^4,0.05,'\mid');...
    text(2.66*10^6-2.5*10^4,-0.05,'\mid')
text(2.66*10^6-2.5*10^4,-0.15,'\mid')
text(Rexft-7*10^5,-0.35,'Re_{x_T}\approx Re_{x_B}',...
    'FontSize',16)
annotation('arrow',[0.79,0.90],[0.29,0.39],...
    'HeadStyle','vback3','HeadLength',3,'HeadWidth',7,...
    'LineStyle','--')
annotation('line',[0.13 0.9],[0.3975 0.3975],...
    'LineStyle','--')
elseif (sep == 1 && Rexft <5.8*10^5)
    legend('short bubble')
    axis([4.6118*10^5 5.8341*10^5 -1.7794 1.8717])
    set(gca,'XTicklabelMode','manual','XTickLabel',[])
    set(gca,'YTicklabelMode','manual','YTickLabel',[])
    grid off

    annotation('arrow',[0.4,0.4],[0.57,0.52],...
        'HeadStyle','vback3','HeadLength',3,'HeadWidth',7,...
        'LineStyle','--')
    text(Rexl-5*10^3,0.21,'Re_{x_A}','FontSize',16)
elseif (sep == 1 && Rex0_mj == Rexl)
    %axis([Rexl Rexft 0 1])
    %    set(gca,'XTick',[Rexl Rexft])
    %    set(gca,'XTickLabel',{'Re_xFL','Re_xFT'})
    %    set(gca,'GridLineStyle','--')
elseif (sep == 1 && Rexft>Rex0_mj)
    legend('long bubble')
    min(Gamma_dmj)-0.05
    max(Gamma_dmj)+0.05

```

```

xlabel('Re_x', 'fontname', 'Times New Roman', 'FontSize', ...
      12, 'FontWeight', 'BOLD')
ylabel('Difference in enstrophy density function, \eta', ...
      'fontname', 'Times New Roman', ...
      'fontsize', 12, 'FontWeight', 'BOLD')
axis([Rexl Rexft min(Gamma_dmj)-0.05 max(Gamma_dmj)+0.05])
annotation('arrow', [0.17, 0.14], [0.595, 0.51], ...
          'HeadStyle', 'vback3', 'HeadLength', 3, ...
          'HeadWidth', 7, 'LineStyle', '--')
%arrow([0 0], [0.1 0.1])
text(Rexl+1*10^3, 0.45, 'Re_{x_A}', 'FontSize', 16, 'color', 'r')
text(R0-4*10^3, 0.45, 'Re_{x_t}', 'FontSize', 16)
text(R0-8*10^2, 0.0, '\mid'); text(R0-8*10^2, 0.2, '\mid');
text(R0-8*10^2, 0.4, '\mid'); % text(R0, 0.29, '\mid');

text(5.25398*10^5-2*10^3, -0.83, 'Re_{x_0}', 'FontSize', 16)
text(5.25398*10^5-1*10^3, 0.05, '\mid'); ...
text(5.25398*10^5-1*10^3, -0.15, '\mid');
text(5.25398*10^5-1*10^3, -0.35, '\mid');

text(5.40246*10^5-2*10^3, -0.83, 'Re_{x_T}', 'FontSize', 16)
text(5.40246*10^5-1*10^3, 0.05, '\mid'); ...
text(5.40246*10^5-1*10^3, -0.15, '\mid');
text(5.40246*10^5-1*10^3, -0.35, '\mid');
text(5.40246*10^5-1*10^3, 0.25, '\mid'); ...
text(5.40246*10^5-1*10^3, 0.45, '\mid');
text(5.40246*10^5-1*10^3, 0.65, '\mid'); ...
text(5.40246*10^5-1*10^3, 0.85, '\mid');
text(5.40246*10^5-1*10^3, 1.05, '\mid');
annotation('arrow', [0.86, 0.90], [0.39, 0.5], ...
          'HeadStyle', 'vback3', 'HeadLength', 3, ...
          'HeadWidth', 7, 'LineStyle', '--')
text(Rexft-1.5*10^4, -0.83, 'Re_{x_B}', 'FontSize', ...

```

```

        16,'color','r')
        annotation('line',[0.135 0.9],[0.505 0.505],...
        'LineStyle','-')

    end
    %hold on
end
elseif pres == 0
    if sep == 0
        figure(1)
        i=1
        for x=0:0.01:3.5
            int(i) = 1-exp(-0.412*x^2);
            plot_int(i) = x;
            i=i+1;
        end
        plot(plot_int,int,'k-','LineWidth',1.5)
        ylabel('Intermittency , \gamma','fontname',...
        'Times New Roman','fontsize',12)
        xlabel('\xi','fontname','Times New Roman','fontsize',12)
        %xlabel('{(x-x_t)}/{(x|_{\gamma=0.75} - x|_{\gamma=0.25})}')
        grid on
        figure(3)
        plot(Rexn_plot(352:772),Gamma_dnr(352:772),'k-','LineWidth',1.5)
        ylabel('Intermittency , \gamma','fontname','Times New Roman','fontsize',12)
        axis([2.6555*10^6 Rexft 0 1])
        %     if sep == 0
        %         axis([Rex0_mj Rexft 0 1])
        %     elseif sep == 1
        %         axis([Rex0_mj Rexft 0 2])
        %     end
        set(gca,'XTick',[2.6555*10^6 Rexn_plot(352) Rexn_plot(772) Rexft])
        set(gca,'XTickLabel',{' ',' ',' ',' '})

```

```

text(2.6555*10^6,-0.06,'x_0','fontname','...
    'Times New Roman','fontsize',12);
text(Rexn_plot(352),-0.06,'x|_{\gamma=0.25}','...
    'fontname','Times New Roman','fontsize',12);
text(Rexn_plot(772),-0.06,'x|_{\gamma=0.75}','...
    'fontname','Times New Roman','fontsize',12);
text(Rexft,-0.06,'x_T','fontname','Times New Roman',...
    'fontsize',12);
grid on
figure(6)
plot(Rex_plot, Gamma_dmj,'r-',Rexn_plot(352:772),...
    Gamma_dnr(352:772),'k--','LineWidth',1.5)
%semilogx(Rex_plot, Gamma_dmj,Rexn_plot, Gamma_dnr)
legend('\eta','\gamma');
ylabel('\eta','fontname','Times New Roman','fontsize',12)
axis([Rexl Rexft min(Gamma_dmj)-0.05 max(Gamma_dmj)+0.05])
%     if sep == 0
%         axis([Rex0_mj Rexft 0 1])
%     elseif sep == 1
%         axis([Rex0_mj Rexft 0 2])
%     end
set(gca,'XTick',[Rexl 2.6555*10^6 Rexn_plot(352) Rexn_plot(772) Rexft])
set(gca,'XTickLabel',{' ',' ',' ',' ',' '})
text(Rexl,-0.65,'x_A','fontname','Times New Roman',...
    'fontsize',12)
text(2.6555*10^6-5*10^4,-0.65,'x_0','fontname',...
    'Times New Roman','fontsize',12);
text(Rexn_plot(352)-5*10^4,-0.65,'x|_{\gamma=0.25}','...
    'fontname','Times New Roman','fontsize',12);
text(Rexn_plot(772)-2*10^5,-0.65,'x|_{\gamma=0.75}','...
    'fontname','Times New Roman','fontsize',12);
text(Rexft-5*10^4,-0.65,'x_T \approx x_B','fontname',...
    'Times New Roman','fontsize',12);

```

```

        grid on
    end
    figure(4)
    plot(Rex_plot, Gamma_dmj, '-k', 'LineWidth', 1.5)
    xlabel('Re_x', 'fontname', 'Times New Roman', 'FontSize', 12, ...
        'FontWeight', 'BOLD')
    ylabel('Difference in enstrophy density function, \eta', ...
        'fontname', 'Times New Roman', ...
        'fontsize', 12, 'FontWeight', 'BOLD')
    %legend('y=Re_{\theta |_{min}}', 'y=Re_{\theta |_{max}}')
    %grid off
    axis([Rexl Rexft min(Gamma_dmj)-0.05 max(Gamma_dmj)+0.05])
    if sep == 0
        annotation('arrow', [0.175, 0.135], [0.495, 0.407], ...
            'HeadStyle', 'vback3', 'HeadLength', 3, 'HeadWidth', 7, ...
            'LineStyle', '- -')
        text(Rexl+6*10^4, 0.23, 'Re_{x_A}', 'FontSize', 12, ...
            'FontWeight', 'BOLD')
        text(R0-3.5*10^4, 0.23, 'Re_{x_t}', 'FontSize', 12, ...
            'FontWeight', 'BOLD')
        text(R0, 0.0, '\mid'); text(R0, 0.1, '\mid'); ...
            text(R0, 0.2, '\mid')

        text(2.66*10^6-5*10^4, -0.3, 'Re_{x_0}', 'FontSize', 12, ...
            'FontWeight', 'BOLD')
        text(2.66*10^6, 0.05, '\mid'); ...
            text(2.66*10^6, -0.05, '\mid')
        text(2.66*10^6, -0.15, '\mid')
        text(Rexft-5.7*10^5, -0.3, 'Re_{x_T}\approx Re_{x_B}', ...
            'FontSize', 12, 'FontWeight', 'BOLD')
        annotation('arrow', [0.79, 0.90], [0.29, 0.39], ...
            'HeadStyle', 'vback3', 'HeadLength', 3, 'HeadWidth', 7, ...
            'LineStyle', '- -')
    end

```

```

        annotation('line',[0.13 0.9],[0.3975 0.3975],'LineStyle','-')
elseif (sep == 1 & Rexft <5.83*10^5)
    annotation('arrow',[0.175,0.135],[0.49,0.385],...
        'HeadStyle','vback3','HeadLength',3,'HeadWidth',7,...
        'LineStyle','--')
%arrow([0 0],[0.1 0.1])
text(Rexl+5*10^2,0.21,'Re- $x_A$ ','FontSize',12,'FontWeight',...
    'BOLD')
text(R0-6*10^2,0.21,'Re- $x_t$ ','FontSize',12,'FontWeight',...
    'BOLD')
text(R0,0.0,'\mid');text(R0,0.1,'\mid');...
    text(R0,0.2,'\mid')

text(5.25213*10^5-4.5*10^2,-0.3,'Re- $x_0$ ','FontSize',12,...
    'FontWeight','BOLD')
text(5.25213*10^5,0.05,'\mid');...
    text(5.25213*10^5,-0.05,'\mid')
text(5.25213*10^5,-0.15,'\mid')
text(Rexft-0.71*10^4,-0.3,'Re- $x_T$ \approx Re- $x_B$ ','...
    'FontSize',12,'FontWeight','BOLD')
annotation('arrow',[0.79,0.90],[0.28,0.36],...
    'HeadStyle','vback3','HeadLength',3,'HeadWidth',7,...
    'LineStyle','--')
    annotation('line',[0.13 0.9],[0.37 0.37],'LineStyle','-')
elseif (sep == 1 & Rex0_mj == Rexl)
    %axis([Rexl Rexft 0 1])
    %    set(gca,'XTick',[Rexl Rexft])
    %    set(gca,'XTickLabel',{'Re_xFL','Re_xFT'})
    %    set(gca,'GridLineStyle','-')
elseif (sep == 1 & Rexft>Rext_mj)
    annotation('arrow',[0.17,0.14],[0.595,0.51],...
        'HeadStyle','vback3','HeadLength',3,...
        'HeadWidth',7,'LineStyle','--')

```

```

%arrow([0 0],[0.1 0.1])
text(Rexl+1*10^3,0.45,'Re_{x_A}','FontSize',12,...
      'FontWeight','BOLD')
text(R0-1.5*10^3,0.45,'Re_{x_t}','FontSize',12,...
      'FontWeight','BOLD')
text(R0,0.0,'\mid');text(R0,0.2,'\mid');
text(R0,0.4,'\mid');%text(R0,0.29,'\mid');

text(5.25398*10^5-2*10^3,-0.75,'Re_{x_0}','FontSize',12,...
      'FontWeight','BOLD')
text(5.25398*10^5,0.05,'\mid');...
text(5.25398*10^5,-0.15,'\mid');
text(5.25398*10^5,-0.35,'\mid');

text(5.40246*10^5-2*10^3,-0.75,'Re_{x_T}','FontSize',12,...
      'FontWeight','BOLD')
text(5.40246*10^5,0.05,'\mid');...
text(5.40246*10^5,-0.15,'\mid');
text(5.40246*10^5,-0.35,'\mid');
text(5.40246*10^5,0.25,'\mid');...
text(5.40246*10^5,0.45,'\mid');
text(5.40246*10^5,0.65,'\mid');...
text(5.40246*10^5,0.85,'\mid');
text(5.40246*10^5,1.05,'\mid');
annotation('arrow',[0.86,0.90],[0.39,0.5],...
          'HeadStyle','vback3','HeadLength',3,...
          'HeadWidth',7,'LineStyle','--')
text(Rexft-1.1*10^4,-0.75,'Re_{x_B}','FontSize',12,...
      'FontWeight','BOLD')
annotation('line',[0.135 0.9],[0.505 0.505],'LineStyle','--')

end
end

```

```

        testa= testa+1;
end

if sep == 0
    figure(5)
    plot(Rex_plot ,enst ,'-k' , 'LineWidth' ,1.5)
    axis([Rexl Rexft -5 3])
    xlabel('Re_x' , 'fontname' , 'Times New Roman' , 'fontsize' ,12)
    ylabel('enstrophy' , 'fontname' , 'Times New Roman' , 'fontsize' ,12)
    grid on
end

figure(7)
t = [0 -0.6 -1.18 -1.2 -1.18 -0.98 -0.97 -0.57 -0.25 -0.15];
s = [7 8 9 9.2 9.5 10 11 11.2 12.5 14];
%t=[0, 1.38, 2.72, 2.77, 2.72, 2.26, 2.26, 1.85, 1.32, 0.35]'
%s=[0.44 0.88 1.33 1.42 1.56 1.78 2.22 2.22 2.31 3.55]'
plot(s,t,'--ks' , 'LineWidth' ,1.5 , 'markerfacecolor' , 'k' , 'markersize' ,5)
set(gca , 'YDir' , 'reverse ')
ylabel('C_P' , 'fontname' , 'Times New Roman' , 'fontsize' ,12)
xlabel('Distance from leading edge, x (in)' , 'fontname' , ...
        'Times New Roman' , 'fontsize' ,12)
text(10,-1.025,'x_s' , 'fontname' , 'Times New Roman' , 'fontsize' ,12)
text(11,-1.025,'x_{Tp}' , 'fontname' , 'Times New Roman' , 'fontsize' ,12)
text(11.25,-0.605,'x_{r}' , 'fontname' , 'Times New Roman' , 'fontsize' ,12)
annotation('line' ,[0.56 0.56],[0.65 0.75] , 'linestyle' , '-')
text(10.8,-1.13,'x_B' , 'fontname' , 'Times New Roman' , 'fontsize' ,14 ,...
        'fontweight' , 'BOLD')

% ***** check velocity profile for separated flow ***** %
U = 80;

```

```

nu = 1.61*10^(-4);
xagsS = Res*nu/U;
j=1;
delta_l = 5*Ks*Res^(-1/2)*xagsS;
for yl = 0:delta_l/50:delta_l
    ulamp(j) = (2+L/6)*yl/(delta_l) - L/2*(yl/(delta_l))^2 ...
        - (2-L/2)*(yl/(delta_l))^3 + (1-L/6)*(yl/(delta_l))^4;
    yl_plot(j) = yl/delta_l;
    j=j+1;
end
figure(8)
plot(ulamp,yl_plot)
legend('laminar velocity profile')

```

```

%function to solve system of equations

function [x C0 C1 C2 C3 C4 fval exitflag] = runnested2(type,yvalue,...
    intermittency ,L,Ks,k,A,Rethetax ,RagsEp ,Res ,Cs ,x0 ,G25 ,...
    G50 ,G75 ,ReLT ,G40 ,R0)
options=optimset('MaxFunEvals',500,'MaxIter',500,'Tolfun',10^(-12),...
    'TolX',10^(-10),'Display','iter');% ,...
    %,'Algorithm','trust-region-reflective');% 'levenberg-marquardt');
[x,fval,exitflag] = fsolve(@nestedfun,x0,options); % Nested function
function F = nestedfun(x)

    C0 = 0;
    C1 = x(3);
    C2 = x(4);
    C3 = x(5);
    C4 = 0;
    b=3.36;
    R = x(2);
    RB = x(1);

```

```

if intermittency == 1
    if type == 1
        Rex = Res;
        R0 = RB*Rex;
        if yvalue == 1
            eqn5 = (1/(7*k*A))*(7/72)^(1/7)+...
                (2+L/6)/(5*Ks*R^0.5) - (L*k*A)/((5*Ks)^2*R) ...
                - (3*(2-L/2)*k^2*A^2)/((5*Ks)^3*R^1.5)...
                + (4*(1-L/6)*k^3*A^3)/((5*Ks)^4*R^2))*...
                (C0+C1/2+C2/3+C3/4+C4/5) ...
                - (7/72)^(1/7)*A*((R-1)*Rethetax)^(-1);
        elseif yvalue == 2
            eqn5 = (1/(7*A))*(7/(72*k))^(1/7)...
                +(2+L/6)/(5*Ks*R^0.5) - (L*A)/((5*Ks)^2*R) ...
                - (3*(2-L/2)*A^2)/((5*Ks)^3*R^1.5)...
                + (4*(1-L/6)*A^3)/((5*Ks)^4*R^2))*...
                (C0+C1/2+C2/3+C3/4+C4/5) ...
                - (7/(72*k))^(1/7)*A*((R-1)*Rethetax)^(-1);
        end
    elseif type == 2
        %R0 = Res;
        Rex = R0/RB;
        eqn5 = (1/(7*k*A))*(7/72)^(1/7)+...
            ((2+L/6)*RB^0.5)/(5*Ks*R^0.5)...
            -(L*k*A*RB)/((5*Ks)^2*R)...
            - (3*(2-L/2)*k^2*A^2*RB^1.5)/((5*Ks)^3*R^1.5) ...
            + (4*(1-L/6)*k^3*A^3*RB^2)/((5*Ks)^4*R^2))*...
            (C0+C1/2+C2/3+C3/4+C4/5) ...
            - (7/72)^(1/7)*A*((1/RB)*(R-1)*Rethetax)^(-1);
    elseif type == 3
        Rex = R0/RB;
        eqn5 = ((1/7)*(1/(0.375*(Rex*(R-RB))^(4/5))))^(1/7)*...
            (1/Rethetax)^(6/7)...

```

$$\begin{aligned}
& + ((2+L/6))/(5*Ks*(Rex*R)^{0.5}) \dots \\
& - (L*Rethetax)/((5*Ks)^2*Rex*R) \dots \\
& - (3*(2-L/2)*(Rethetax)^2)/((5*Ks)^3*(Rex*R)^{1.5}) \dots \\
& + (4*(1-L/6)*(Rethetax)^3)/((5*Ks)^4*(Rex*R)^2) * \dots \\
& Rex*(R-1)*(C0/1+C1/2+C2/3+C3/4+C4/5) \dots \\
& - ((Rethetax)/(0.375*(Rex*(R-RB))^{(4/5)}))^{(1/7)};
\end{aligned}$$

elseif type == 4

$$RT = x(2);$$

$$Rex = x(1);$$

$$R = RT/Rex;$$

$$R0 = Rex;$$

$$\begin{aligned}
eqn5 = & (1/(7*A)*(7/(72*k))^{(1/7)}+(2+L/6)/(5*Ks*R^{0.5}) \dots \\
& - (L*A)/((5*Ks)^2*R) \dots \\
& - (3*(2-L/2)*A^2)/((5*Ks)^3*R^{1.5}) \dots \\
& + (4*(1-L/6)*A^3)/((5*Ks)^4*R^2) * \dots \\
& (C0+C1/2+C2/3+C3/4+C4/5) \dots \\
& - (7/(72*k))^{(1/7)}*((R-1)*Rex^{0.5})^{(-1)};
\end{aligned}$$

end

$$eqn1 = C0+C1+C2+C3+C4-1;$$

$$\begin{aligned}
eqn2 = & C0+C1*((R0+G75*ReLT-Rex)/(Rex*(R-1))) \dots \\
& + C2*((R0+G75*ReLT-Rex)/(Rex*(R-1)))^2 \dots \\
& + C3*((R0+G75*ReLT-Rex)/(Rex*(R-1)))^3 \dots \\
& + C4*((R0+G75*ReLT-Rex)/(Rex*(R-1)))^4-0.75;
\end{aligned}$$

$$\begin{aligned}
eqn2b = & C0+C1*((R0+G40*ReLT-Rex)/(Rex*(R-1))) \dots \\
& + C2*((R0+G40*ReLT-Rex)/(Rex*(R-1)))^2 \dots \\
& + C3*((R0+G40*ReLT-Rex)/(Rex*(R-1)))^3 \dots \\
& + C4*((R0+G40*ReLT-Rex)/(Rex*(R-1)))^4-0.7;
\end{aligned}$$

$$\begin{aligned}
eqn3 = & C0+C1*((R0+G25*ReLT-Rex)/(Rex*(R-1))) \dots \\
& + C2*((R0+G25*ReLT-Rex)/(Rex*(R-1)))^2 \dots \\
& + C3*((R0+G25*ReLT-Rex)/(Rex*(R-1)))^3 \dots
\end{aligned}$$

$$\begin{aligned}
 & + C4 * ((R0 + G25 * ReLT - Rex) / (Rex * (R - 1))) ^ 4 - 0.25; \\
 \text{eqn4} = & C0 * (R0 + G75 * ReLT - Rex) \dots \\
 & + (C1 * (R0 + G75 * ReLT - Rex) ^ 2) / (2 * Rex * (R - 1)) \dots \\
 & + (C2 * (R0 + G75 * ReLT - Rex) ^ 3) / (3 * Rex ^ 2 * (R - 1) ^ 2) \dots \\
 & + (C3 * (R0 + G75 * ReLT - Rex) ^ 4) / (4 * Rex ^ 3 * (R - 1) ^ 3) \dots \\
 & + (C4 * (R0 + G75 * ReLT - Rex) ^ 5) / (5 * Rex ^ 4 * (R - 1) ^ 4) \dots \\
 & - C0 * (R0 + G25 * ReLT - Rex) \dots \\
 & - (C1 * (R0 + G25 * ReLT - Rex) ^ 2) / (2 * Rex * (R - 1)) \dots \\
 & - (C2 * (R0 + G25 * ReLT - Rex) ^ 3) / (3 * Rex ^ 2 * (R - 1) ^ 2) \dots \\
 & - (C3 * (R0 + G25 * ReLT - Rex) ^ 4) / (4 * Rex ^ 3 * (R - 1) ^ 3) \dots \\
 & - (C4 * (R0 + G25 * ReLT - Rex) ^ 5) / (5 * Rex ^ 4 * (R - 1) ^ 4) \dots \\
 & - ((G75 - G25) * ReLT - 1.381 * ReLT / b * \text{erf}(0.642 * (G75 * b))) \dots \\
 & + 1.381 * ReLT / b * \text{erf}(0.642 * (G25 * b)); \\
 \text{eqn4c} = & C0 * (R0 + G40 * ReLT - Rex) \dots \\
 & + (C1 * (R0 + G40 * ReLT - Rex) ^ 2) / (2 * Rex * (R - 1)) \dots \\
 & + (C2 * (R0 + G40 * ReLT - Rex) ^ 3) / (3 * Rex ^ 2 * (R - 1) ^ 2) \dots \\
 & + (C3 * (R0 + G40 * ReLT - Rex) ^ 4) / (4 * Rex ^ 3 * (R - 1) ^ 3) \dots \\
 & + (C4 * (R0 + G40 * ReLT - Rex) ^ 5) / (5 * Rex ^ 4 * (R - 1) ^ 4) \dots \\
 & - C0 * (R0 + G25 * ReLT - Rex) \dots \\
 & - (C1 * (R0 + G25 * ReLT - Rex) ^ 2) / (2 * Rex * (R - 1)) \dots \\
 & - (C2 * (R0 + G25 * ReLT - Rex) ^ 3) / (3 * Rex ^ 2 * (R - 1) ^ 2) \dots \\
 & - (C3 * (R0 + G25 * ReLT - Rex) ^ 4) / (4 * Rex ^ 3 * (R - 1) ^ 3) \dots \\
 & - (C4 * (R0 + G25 * ReLT - Rex) ^ 5) / (5 * Rex ^ 4 * (R - 1) ^ 4) \dots \\
 & - ((G40 - G25) * ReLT - 1.381 * ReLT / b * \text{erf}(0.642 * (G40 * b))) \dots \\
 & + 1.381 * ReLT / b * \text{erf}(0.642 * (G25 * b)); \\
 \text{eqn4b} = & (C1 * (R0 + 0.546 * Cs * R0 ^ 0.75 - Rex) ^ 2) / (2 * Rex * (R - 1)) \dots \\
 & + (C2 * (R0 + 0.546 * Cs * R0 ^ 0.75 - Rex) ^ 3) / (3 * Rex ^ 2 * (R - 1) ^ 2) \dots \\
 & + (C3 * (R0 + 0.546 * Cs * R0 ^ 0.75 - Rex) ^ 4) / (4 * Rex ^ 3 * (R - 1) ^ 3) \dots \\
 & + (C4 * (R0 + 0.546 * Cs * R0 ^ 0.75 - Rex) ^ 5) / (5 * Rex ^ 4 * (R - 1) ^ 4) \dots \\
 & - (C1 * (R0 + 0.249 * Cs * R0 ^ 0.75 - Rex) ^ 2) / (2 * Rex * (R - 1)) \dots \\
 & - (C2 * (R0 + 0.249 * Cs * R0 ^ 0.75 - Rex) ^ 3) / (3 * Rex ^ 2 * (R - 1) ^ 2) \dots \\
 & - (C3 * (R0 + 0.249 * Cs * R0 ^ 0.75 - Rex) ^ 4) / (4 * Rex ^ 3 * (R - 1) ^ 3) \dots \\
 & - (C4 * (R0 + 0.249 * Cs * R0 ^ 0.75 - Rex) ^ 5) / (5 * Rex ^ 4 * (R - 1) ^ 4) \dots
 \end{aligned}$$

```

- (0.297*Cs*R0^0.75 - 1.381*Cs/b*(R0^1.5)^0.5*...
erf(0.642*b/Cs*((1/R0^1.5)^0.5*(R0+0.546*Cs*R0^0.75) ...
-(R0^0.5)^0.5))+ 1.381*Cs/b*(R0^1.5)^0.5*...
erf(0.642*b/Cs*((1/R0^1.5)^0.5*(R0+0.249*Cs*R0^0.75) ...
-(R0^0.5)^0.5));
eqn6 = C0+C1*((R0+G50*ReLT-Rex)/(Rex*(R-1))) ...
+ C2*((R0+G50*ReLT-Rex)/(Rex*(R-1)))^2 ...
+ C3*((R0+G50*ReLT-Rex)/(Rex*(R-1)))^3 ...
+ C4*((R0+G50*ReLT-Rex)/(Rex*(R-1)))^4-0.5;
eqn7 = C1/((R-1)*Rex) ...
+ (2*C2*(R0+G50*ReLT-Rex))/(Rex^2*(R-1)^2) ...
+ (3*C3*(R0+G50*ReLT-Rex)^2)/(Rex^3*(R-1)^3) ...
+ (4*C4*(R0+G50*ReLT-Rex)^3)/(Rex^4*(R-1)^4) ...
- 2*(0.412*(3.36)^2)*(G50)/(ReLT)*exp(-0.412*3.36^2*G50^2);
F=[eqn1;
eqn3;
eqn5;
eqn6;
eqn7];
elseif intermittency == 2
if type == 1
Rex = Res;
R0 = RB*Rex;
if yvalue == 1
eqn5 = 1/(7*k*A)*(7/72)^(1/7)+(2+L/6)/(5*Ks*R^0.5)...
-(L*k*A)/((5*Ks)^2*R) ...
- (3*(2-L/2)*k^2*A^2)/((5*Ks)^3*R^1.5) ...
+ (4*(1-L/6)*k^3*A^3)/((5*Ks)^4*R^2) ...
- (7/72)^(1/7)*A*((R-1)*Rethetax*...
(C1/2+C2/3+C3/4+C4/5))^( -1);
elseif yvalue == 2
eqn5 = 1/(7*A)*(7/(72*k))^(1/7)+(2+L/6)/(5*Ks*R^0.5)...
-(L*A)/((5*Ks)^2*R) ...

```

```

- (3*(2-L/2)*A^2)/((5*Ks)^3*R^1.5) ...
+ (4*(1-L/6)*A^3)/((5*Ks)^4*R^2) ...
- (7/(72*k))^(1/7)*A*((R-1)*Rethetax*...
(C1/2+C2/3+C3/4+C4/5))^( -1);

end

elseif type == 2
R0 = Res;
Rex = R0/RB;
eqn5 = 1/(7*k*A)*(7/72)^(1/7)+...
((2+L/6)*RB^0.5)/(5*Ks*R^0.5)-(L*k*A*RB)/((5*Ks)^2*R) ...
- (3*(2-L/2)*k^2*A^2*RB^1.5)/((5*Ks)^3*R^1.5) ...
+ (4*(1-L/6)*k^3*A^3*RB^2)/((5*Ks)^4*R^2) ...
- (7/72)^(1/7)*A*((1/RB)*(R-1)*Rethetax*...
(C1/2+C2/3+C3/4+C4/5))^( -1);

elseif type == 3
RagsS = Res;
R0 = (1.26*RagsS - 0.26*RagsEp)/1.26;
Rex = R0/RB;
if yvalue == 1
dw_f = (1/(7*k*A))^2*(7/72)^(2/7)*...
((RagsEp/Rex)/(R-RB))^(8/35)...
- ((2+L/6)^2*(RagsS/Rex))/((5*Ks)^2*R)...
+ (2*L*(2+L/6)*k*A*(RagsS/Rex)^(3/2))/((5*Ks)^3*...
(R)^(3/2)) ...
+ (6*(2+L/6)*(2-L/2)-L^2)*k^2*A^2*...
(RagsS/Rex)^2/((5*Ks)^4*(R)^2)...
- (8*(2+L/6)*(1-L/6)+6*L*(2-L/2))*k^3*A^3*...
(RagsS/Rex)^(5/2)/((5*Ks)^5*(R)^(5/2))...
+ (8*L*(1-L/6)-9*(2-L/2)^2)*k^4*A^4*...
(RagsS/Rex)^3/((5*Ks)^6*(R)^3)...
+ 24*(2-L/2)*(1-L/6)*k^5*A^5*...
(RagsS/Rex)^(7/2)/((5*Ks)^7*(R)^(7/2))...
- 16*(1-L/6)^2*k^6*A^6*...

```

$$\begin{aligned}
& (\text{RagsS}/\text{Rex})^4 / ((5 * \text{Ks})^8 * (\text{R})^4); \\
\text{dw}_{25} = & (1 / (7 * \text{k} * \text{A}))^2 * (7 / 72)^{(2/7)} * \dots \\
& ((\text{RagsEp}) / (0.249 * \text{Cs} * \text{R0}^{0.75}))^{(8/35)} \dots \\
& - ((2 + \text{L}/6)^2 * (\text{RagsS})) / ((5 * \text{Ks})^2 * \dots \\
& (\text{R0} + 0.249 * \text{Cs} * \text{R0}^{0.75})) \dots \\
& + (2 * \text{L} * (2 + \text{L}/6) * \text{k} * \text{A} * (\text{RagsS})^{(3/2)}) / ((5 * \text{Ks})^3 * \dots \\
& (\text{R0} + 0.249 * \text{Cs} * \text{R0}^{0.75})^{(3/2)}) \dots \\
& + (6 * (2 + \text{L}/6) * (2 - \text{L}/2) - \text{L}^2) * \text{k}^2 * \text{A}^2 * \dots \\
& (\text{RagsS})^2 / ((5 * \text{Ks})^4 * (\text{R0} + 0.249 * \text{Cs} * \text{R0}^{0.75})^2) \dots \\
& - (8 * (2 + \text{L}/6) * (1 - \text{L}/6) + 6 * \text{L} * (2 - \text{L}/2)) * \text{k}^3 * \text{A}^3 * \dots \\
& (\text{RagsS})^{(5/2)} / ((5 * \text{Ks})^5 * \dots \\
& (\text{R0} + 0.249 * \text{Cs} * \text{R0}^{0.75})^{(5/2)}) \dots \\
& + (8 * \text{L} * (1 - \text{L}/6) - 9 * (2 - \text{L}/2)^2) * \text{k}^4 * \text{A}^4 * \dots \\
& (\text{RagsS})^3 / ((5 * \text{Ks})^6 * (\text{R0} + 0.249 * \text{Cs} * \text{R0}^{0.75})^3) \dots \\
& + 24 * (2 - \text{L}/2) * (1 - \text{L}/6) * \text{k}^5 * \text{A}^5 * \dots \\
& (\text{RagsS})^{(7/2)} / ((5 * \text{Ks})^7 * \dots \\
& (\text{R0} + 0.249 * \text{Cs} * \text{R0}^{0.75})^{(7/2)}) \dots \\
& - 16 * (1 - \text{L}/6)^2 * \text{k}^6 * \text{A}^6 * (\text{RagsS})^4 / ((5 * \text{Ks})^8 * \dots \\
& (\text{R0} + 0.249 * \text{Cs} * \text{R0}^{0.75})^4); \\
\text{dw}_{50} = & (1 / (7 * \text{k} * \text{A}))^2 * (7 / 72)^{(2/7)} * ((\text{RagsEp}) / \dots \\
& (0.386 * \text{Cs} * \text{R0}^{0.75}))^{(8/35)} \dots \\
& - ((2 + \text{L}/6)^2 * (\text{RagsS})) / ((5 * \text{Ks})^2 * \dots \\
& (\text{R0} + 0.386 * \text{Cs} * \text{R0}^{0.75})) \dots \\
& + (2 * \text{L} * (2 + \text{L}/6) * \text{k} * \text{A} * (\text{RagsS})^{(3/2)}) / ((5 * \text{Ks})^3 * \dots \\
& (\text{R0} + 0.386 * \text{Cs} * \text{R0}^{0.75})^{(3/2)}) \dots \\
& + (6 * (2 + \text{L}/6) * (2 - \text{L}/2) - \text{L}^2) * \text{k}^2 * \text{A}^2 * (\text{RagsS})^2 / \dots \\
& ((5 * \text{Ks})^4 * (\text{R0} + 0.386 * \text{Cs} * \text{R0}^{0.75})^2) \dots \\
& - (8 * (2 + \text{L}/6) * (1 - \text{L}/6) + 6 * \text{L} * (2 - \text{L}/2)) * \text{k}^3 * \text{A}^3 * \dots \\
& (\text{RagsS})^{(5/2)} / ((5 * \text{Ks})^5 * \dots \\
& (\text{R0} + 0.386 * \text{Cs} * \text{R0}^{0.75})^{(5/2)}) \dots \\
& + (8 * \text{L} * (1 - \text{L}/6) - 9 * (2 - \text{L}/2)^2) * \text{k}^4 * \text{A}^4 * \dots \\
& (\text{RagsS})^3 / ((5 * \text{Ks})^6 * (\text{R0} + 0.386 * \text{Cs} * \text{R0}^{0.75})^3) \dots \\
& + 24 * (2 - \text{L}/2) * (1 - \text{L}/6) * \text{k}^5 * \text{A}^5 * (\text{RagsS})^{(7/2)} / \dots
\end{aligned}$$

$$\begin{aligned}
 & ((5*Ks)^{7*(R0+0.386*Cs*R0^{0.75})^{(7/2)}}) \dots \\
 & - 16*(1-L/6)^{2*k^6*A^6*(RagsS)^4/((5*Ks)^{8*...} \\
 & (R0+0.386*Cs*R0^{0.75})^4); \\
 dw_{75} = & (1/(7*k*A))^{2*(7/72)^{(2/7)}*((RagsEp)/... \\
 & (0.546*Cs*R0^{0.75})^{(8/35)}) \dots \\
 & - ((2+L/6)^{2*(RagsS)})/((5*Ks)^{2*...} \\
 & (R0+0.546*Cs*R0^{0.75}) \dots \\
 & + (2*L*(2+L/6)*k*A*(RagsS)^{(3/2)})/((5*Ks)^{3*...} \\
 & (R0+0.546*Cs*R0^{0.75})^{(3/2)}) \dots \\
 & + (6*(2+L/6)*(2-L/2)-L^2)*k^2*A^2*... \\
 & (RagsS)^2/((5*Ks)^{4*(R0+0.546*Cs*R0^{0.75})^2}) \dots \\
 & - (8*(2+L/6)*(1-L/6)+6*L*(2-L/2))*k^3*A^3*... \\
 & (RagsS)^{(5/2)}/((5*Ks)^{5*...} \\
 & (R0+0.546*Cs*R0^{0.75})^{(5/2)}) \dots \\
 & + (8*L*(1-L/6)-9*(2-L/2)^2)*k^4*A^4*(RagsS)^3/... \\
 & ((5*Ks)^{6*(R0+0.546*Cs*R0^{0.75})^3}) \dots \\
 & + 24*(2-L/2)*(1-L/6)*k^5*A^5*(RagsS)^{(7/2)}/... \\
 & ((5*Ks)^{7*(R0+0.546*Cs*R0^{0.75})^{(7/2)}}) \dots \\
 & - 16*(1-L/6)^{2*k^6*A^6*(RagsS)^4/((5*Ks)^{8*...} \\
 & (R0+0.546*Cs*R0^{0.75})^4); \\
 ddw_{50} = & (1/(7*k*A))^{2*(7/72)^{(2/7)}*(-8/35)*... \\
 & ((RagsEp)^{(8/35)}/(0.386*Cs*R0^{0.75})^{(43/35)}) \dots \\
 & + ((2+L/6)^{2*(RagsS)})/((5*Ks)^{2*...} \\
 & (R0+0.386*Cs*R0^{0.75})^2) \dots \\
 & - (3/2)*(2*L*(2+L/6))*k*A*(RagsS)^{(3/2)}/... \\
 & ((5*Ks)^{3*(R0+0.386*Cs*R0^{0.75})^{(5/2)}}) \dots \\
 & - 2*(6*(2+L/6)*(2-L/2)-L^2)*k^2*A^2*(RagsS)^2/... \\
 & ((5*Ks)^{4*(R0+0.386*Cs*R0^{0.75})^3}) \dots \\
 & + (5/2)*(8*(2+L/6)*(1-L/6)+6*L*(2-L/2))*k^3*A^3*... \\
 & (RagsS)^{(5/2)}/((5*Ks)^{5*(R0+0.386*... \\
 & Cs*R0^{0.75})^{(7/2)}}) \dots \\
 & - 3*(8*L*(1-L/6)-9*(2-L/2)^2)*k^4*A^4*... \\
 & (RagsS)^3/((5*Ks)^{6*(R0+0.386*Cs*R0^{0.75})^4}) \dots
 \end{aligned}$$

$$\begin{aligned}
& - (7/2)*24*(2-L/2)*(1-L/6)*k^5*A^5*... \\
& (RagsS)^{(7/2)} / ((5*Ks)^{7*(R0+0.386*... \\
& Cs*R0^{0.75})^{(9/2)})... \\
& + 4*16*(1-L/6)^2*k^6*A^6*(RagsS)^4 / ... \\
& ((5*Ks)^{8*(R0+0.386*Cs*R0^{0.75})^5});
\end{aligned}$$

$$\begin{aligned}
eqn5 = & (1/(7*k*A))*(7/72)^{(1/7)}*... \\
& ((RagsEp/Rex)/(R-RB))^{(4/35)} \dots \\
& + ((2+L/6)*(RagsS/Rex)^{0.5}) / (5*Ks*R^{0.5})... \\
& - (L*k*A*(RagsS/Rex)) / ((5*Ks)^{2*R}) \dots \\
& - (3*(2-L/2)*k^2*A^2*(RagsS/Rex)^{1.5}) / ... \\
& ((5*Ks)^{3*R^{1.5}})... \\
& + (4*(1-L/6)*k^3*A^3*... \\
& (RagsS/Rex)^2) / ((5*Ks)^{4*R^2})*... \\
& (C1/2+C2/3+C3/4+C4/5) \dots \\
& - (7/72)^{(1/7)}*A*((RagsEp/Rex) / ... \\
& (R-RB))^{(4/35)} \dots \\
& *((1/(RagsS/Rex))*(R-1)*Rethetax)^{(-1)};
\end{aligned}$$

elseif yvalue == 2

$$\begin{aligned}
dw_f = & (1/(7*A))^{2*(7/(72*k))^{(2/7)}*... \\
& ((RagsEp/Rex)/(R-RB))^{(8/35)}... \\
& - ((2+L/6)^2*(RagsS/Rex)) / ((5*Ks)^{2*R})... \\
& + (2*L*(2+L/6)*A*(RagsS/Rex)^{(3/2)}) / ... \\
& ((5*Ks)^{3*(R)^{(3/2)}}) \dots \\
& + (6*(2+L/6)*(2-L/2)-L^2)*A^2*(RagsS/Rex)^2 / ... \\
& ((5*Ks)^{4*(R)^2})... \\
& - (8*(2+L/6)*(1-L/6)+6*L*(2-L/2))*A^3*... \\
& (RagsS/Rex)^{(5/2)} / ((5*Ks)^{5*(R)^{(5/2)}})... \\
& + (8*L*(1-L/6)-9*(2-L/2)^2)*A^4*(RagsS/Rex)^3 / ... \\
& ((5*Ks)^{6*(R)^3})... \\
& + 24*(2-L/2)*(1-L/6)*A^5*(RagsS/Rex)^{(7/2)} / ... \\
& ((5*Ks)^{7*(R)^{(7/2)}})... \\
& - 16*(1-L/6)^2*A^6*(RagsS/Rex)^4 / ((5*Ks)^{8*(R)^4});
\end{aligned}$$

$$\begin{aligned}
 dw_{25} = & (1/(7*A))^2*(7/(72*k))^(2/7)*... \\
 & ((RagsEp)/(0.249*Cs*R0^0.75))^(8/35)... \\
 - & ((2+L/6)^2*(RagsS))/((5*Ks)^2*... \\
 & (R0+0.249*Cs*R0^0.75))... \\
 + & (2*L*(2+L/6)*A*(RagsS)^(3/2))/((5*Ks)^3*... \\
 & (R0+0.249*Cs*R0^0.75)^(3/2))... \\
 + & (6*(2+L/6)*(2-L/2)-L^2)*A^2*(RagsS)^2/... \\
 & ((5*Ks)^4*(R0+0.249*Cs*R0^0.75)^2)... \\
 - & (8*(2+L/6)*(1-L/6)+6*L*(2-L/2))*A^3*... \\
 & (RagsS)^(5/2)/((5*Ks)^5*(R0+0.249*Cs*... \\
 & R0^0.75)^(5/2))... \\
 + & (8*L*(1-L/6)-9*(2-L/2)^2)*A^4*(RagsS)^3/... \\
 & ((5*Ks)^6*(R0+0.249*Cs*R0^0.75)^3)... \\
 + & 24*(2-L/2)*(1-L/6)*A^5*(RagsS)^(7/2)/... \\
 & ((5*Ks)^7*(R0+0.249*Cs*R0^0.75)^(7/2))... \\
 - & 16*(1-L/6)^2*A^6*(RagsS)^4/((5*Ks)^8*... \\
 & (R0+0.249*Cs*R0^0.75)^4); \\
 dw_{50} = & (1/(7*A))^2*(7/(72*k))^(2/7)*((RagsEp)/... \\
 & (0.386*Cs*R0^0.75))^(8/35)... \\
 - & ((2+L/6)^2*(RagsS))/((5*Ks)^2*... \\
 & (R0+0.386*Cs*R0^0.75))... \\
 + & (2*L*(2+L/6)*A*(RagsS)^(3/2))/((5*Ks)^3*... \\
 & (R0+0.386*Cs*R0^0.75)^(3/2))... \\
 + & (6*(2+L/6)*(2-L/2)-L^2)*A^2*... \\
 & (RagsS)^2/((5*Ks)^4*(R0+0.386*Cs*R0^0.75)^2)... \\
 - & (8*(2+L/6)*(1-L/6)+6*L*(2-L/2))*A^3*... \\
 & (RagsS)^(5/2)/((5*Ks)^5*(R0+0.386*Cs*... \\
 & R0^0.75)^(5/2))... \\
 + & (8*L*(1-L/6)-9*(2-L/2)^2)*A^4*... \\
 & (RagsS)^3/((5*Ks)^6*(R0+0.386*Cs*R0^0.75)^3)... \\
 + & 24*(2-L/2)*(1-L/6)*A^5*(RagsS)^(7/2)/... \\
 & ((5*Ks)^7*(R0+0.386*Cs*R0^0.75)^(7/2))... \\
 - & 16*(1-L/6)^2*A^6*(RagsS)^4/((5*Ks)^8*...
 \end{aligned}$$

$$\begin{aligned}
& (R0+0.386*Cs*R0^{0.75})^4); \\
dw_{75} = & (1/(7*A))^{2*(7/(72*k))^{(2/7)}}*((RagsEp)/\dots \\
& (0.546*Cs*R0^{0.75})^{(8/35)}\dots \\
& - ((2+L/6)^{2*(RagsS)})/((5*Ks)^{2*(R0+0.546*Cs*R0^{0.75})})\dots \\
& + (2*L*(2+L/6)*A*(RagsS)^{(3/2)})/((5*Ks)^{3*\dots \\
& (R0+0.546*Cs*R0^{0.75})^{(3/2)}}) \dots \\
& + (6*(2+L/6)*(2-L/2)-L^2)*A^{2*(RagsS)^{2/\dots \\
& ((5*Ks)^{4*(R0+0.546*Cs*R0^{0.75})^2})}\dots \\
& - (8*(2+L/6)*(1-L/6)+6*L*(2-L/2))*A^{3*\dots \\
& (RagsS)^{(5/2)}/((5*Ks)^{5*(R0+0.546*Cs*\dots \\
& R0^{0.75})^{(5/2)}})\dots \\
& + (8*L*(1-L/6)-9*(2-L/2)^2)*A^{4*(RagsS)^{3/\dots \\
& ((5*Ks)^{6*(R0+0.546*Cs*R0^{0.75})^3})}\dots \\
& + 24*(2-L/2)*(1-L/6)*A^{5*(RagsS)^{(7/2)}/\dots \\
& ((5*Ks)^{7*(R0+0.546*Cs*R0^{0.75})^{(7/2)}})\dots \\
& - 16*(1-L/6)^2*A^{6*(RagsS)^{4/((5*Ks)^{8*\dots \\
& (R0+0.546*Cs*R0^{0.75})^4})}; \\
ddw_{50} = & (1/(7*A))^{2*(7/(72*k))^{(2/7)}}*(-8/35)*\dots \\
& ((RagsEp)^{(8/35)}/(0.386*Cs*R0^{0.75})^{(43/35)})\dots \\
& + ((2+L/6)^{2*(RagsS)})/((5*Ks)^{2*(R0+0.386*Cs*R0^{0.75})^2})\dots \\
& - (3/2)*(2*L*(2+L/6))*A*(RagsS)^{(3/2)}/\dots \\
& ((5*Ks)^{3*(R0+0.386*Cs*R0^{0.75})^{(5/2)}}) \dots \\
& - 2*(6*(2+L/6)*(2-L/2)-L^2)*A^{2*(RagsS)^{2/\dots \\
& ((5*Ks)^{4*(R0+0.386*Cs*R0^{0.75})^3})}\dots \\
& + (5/2)*(8*(2+L/6)*(1-L/6)+6*L*(2-L/2))*A^{3*\dots \\
& (RagsS)^{(5/2)}/((5*Ks)^{5*(R0+0.386*Cs*\dots \\
& R0^{0.75})^{(7/2)}})\dots \\
& - 3*(8*L*(1-L/6)-9*(2-L/2)^2)*A^{4*(RagsS)^{3/\dots \\
& ((5*Ks)^{6*(R0+0.386*Cs*R0^{0.75})^4})}\dots \\
& - (7/2)*24*(2-L/2)*(1-L/6)*A^{5*(RagsS)^{(7/2)}/\dots \\
& ((5*Ks)^{7*(R0+0.386*Cs*R0^{0.75})^{(9/2)}})\dots
\end{aligned}$$

```

+ 4*16*(1-L/6)^2*A^6*(RagsS)^4/((5*Ks)^8*...
(R0+0.386*Cs*R0^0.75)^5);

eqn5 = 1/(7*A)*(7/(72*k))^(1/7)*((RagsEp/Rex)/...
(R-RB))^(4/35) ...
+((2+L/6)*(RagsS/Rex)^0.5)/(5*Ks*R^0.5)...
-(L*A*(RagsS/Rex))/((5*Ks)^2*R) ...
- (3*(2-L/2)*A^2*(RagsS/Rex)^1.5)/...
((5*Ks)^3*R^1.5)...
+ (4*(1-L/6)*A^3*(RagsS/Rex)^2)/((5*Ks)^4*R^2) ...
- (7/(72*k))^(1/7)*A*...
((RagsEp/Rex)/(R-RB))^(4/35) ...
*((1/(RagsS/Rex))*(R-1)*Retheta*...
(C1/2+C2/3+C3/4+C4/5))^( -1);

end

end

eqn1 = C1+C2+C3+C4-1;
eqn2 = C1*((R0+0.546*Cs*R0^0.75-Rex)/(Rex*(R-1)))...
+ C2*((R0+0.546*Cs*R0^0.75-Rex)/(Rex*(R-1)))^2 ...
+ C3*((R0+0.546*Cs*R0^0.75-Rex)/(Rex*(R-1)))^3 ...
+ C4*((R0+0.546*Cs*R0^0.75-Rex)/(Rex*(R-1)))^4 ...
-0.75*(dw_75/dw_f);
eqn3 = C1*((R0+0.249*Cs*R0^0.75-Rex)/(Rex*(R-1))) ...
+ C2*((R0+0.249*Cs*R0^0.75-Rex)/(Rex*(R-1)))^2 ...
+ C3*((R0+0.249*Cs*R0^0.75-Rex)/(Rex*(R-1)))^3 ...
+ C4*((R0+0.249*Cs*R0^0.75-Rex)/(Rex*(R-1)))^4 ...
-0.25*(dw_25/dw_f);
eqn6 = C1*((R0+0.386*Cs*R0^0.75-Rex)/(Rex*(R-1))) ...
+ C2*((R0+0.386*Cs*R0^0.75-Rex)/(Rex*(R-1)))^2 ...
+ C3*((R0+0.386*Cs*R0^0.75-Rex)/(Rex*(R-1)))^3 ...
+ C4*((R0+0.386*Cs*R0^0.75-Rex)/(Rex*(R-1)))^4 ...
-0.5*(dw_50/dw_f);
eqn7 = C1/((R-1)*Rex) + ...

```

```

(2*C2*(R0+0.386*Cs*R0^0.75-Rex))/(Rex^2*(R-1)^2) ...
+ (3*C3*(R0+0.386*Cs*R0^0.75-Rex)^2)/(Rex^3*(R-1)^3) ...
+ (4*C4*(R0+0.386*Cs*R0^0.75-Rex)^3)/(Rex^4*(R-1)^4) ...
- (2*(0.412*(3.36)^2)*(0.386)/(Cs*R0^0.75))*...
exp(-0.412*3.36^2*0.386^2)*dw_50/dw_f...
+ (1-exp(-0.412*3.36^2*0.386^2))*ddw_50/dw_f);
F=[eqn1;
    eqn2;
    eqn5;
    eqn3;
    eqn7];
    end
end
end

```

References

- [1] R. E. Mayle, “The role of laminar-turbulent transition in gas turbine engines,” *ASME Journal of Turbomachinery*, vol. 113, no. 509-537, 1991.
- [2] G. B. Schubauer and P. S. Klebanoff, “Contributions on the mechanics of boundary layer transition,” tech. rep., NASA TM 3489, 1955.
- [3] R. Narasimha, “The laminar-turbulent transition zone in the boundary layer,” *Progress in Aerospace Science*, vol. 22, pp. 29–80, 1985.
- [4] M. Gaster, “The structure and behaviour of laminar separation bubbles,” *AGARD CP*, vol. 4, pp. 813–854, 1966.
- [5] R. Narasimha and J. Dey, “Transition-zone models for 2-dimensional boundary layers: A review,” *Sadhana*, vol. 14, no. 2, pp. 93–120, 1989.
- [6] J. O. Hinze, *Turbulence: an introduction to its mechanism and theory*. McGraw-Hill: New York, 1959.

REFERENCES

- [7] M. H. Buschmann and M. G. el Hak, “Turbulent boundary layers: reality and myth - part 1,” *International Journal of Computing Science and Mathematics*, vol. 1, no. 2, pp. 159–176, 2007.
- [8] J. A. Schetz, *Boundary layer analysis*. Prentice-Hall, Inc, 1993.
- [9] C. D. Donaldson, “A computer study of an analytical model of boundary-layer transition,” *AIAA Journal*, vol. 7, pp. 271–278, 1969.
- [10] M. Schneider, “Stroke busters in turbulent blood,” tech. rep., Pittsburgh Supercomputing Center, 2002.
- [11] D. W. Zingg and P. Godin, “A perspective on turbulence models for aerodynamic flows,” *International journal of computational fluid dynamics*, vol. 23, pp. 327–335, Apr 2009.
- [12] F. H. Abernathy, “Fundamentals of boundary layers,” *Harvard University*, pp. 1–7, Nov 1969.
- [13] J. W. Elder, “An experimental investigation of turbulent spots and breakdown to turbulence,” *Journal of Fluid Mechanics*, vol. 9, no. 02, pp. 235–246, 1960.
- [14] H. Schlichting, *Boundary layer theory*. New York, N.Y.: McGraw-Hill, Inc., seventh ed., 1979.
- [15] L. Kleiser and T. A. Zang, “Numerical simulation of transition in wall-bounded shear flows,” *Annual review of fluid mechanics*, vol. 23, no. 1, pp. 495–537, 1991.
- [16] A. Wray and M. Y. Hussaini, “Numerical experiments in boundary-layer stability,” *Proceedings of the Royal Society of London. A. Mathematical and Physical Sciences*, vol. 392, no. 1803, p. 373, 1984.
- [17] D. Arnal and G. Casalis, “Laminar-turbulent transition prediction in three-dimensional flows,” *Progress in Aerospace Sciences*, vol. 36, no. 2, pp. 173–191, 2000.

REFERENCES

- [18] C. Kuan and T. Wang, “Investigation of the intermittent behavior of transitional boundary layer using a conditional averaging technique,” *Experimental Thermal and Fluid Science*, vol. 3, no. 2, pp. 157–173, 1990.
- [19] C. Lee, “Possible universal transitional scenario in a flat plate boundary layer: Measurement and visualization,” *Physical Review E*, vol. 62, no. 3, pp. 3659–3670, 2000.
- [20] M. F. Blair, “Boundary-layer transition in accelerating flow with intense freestream turbulence. i - disturbances upstream of transition onset. ii - the zone of intermittent turbulence,” *ASME, Transactions, Journal of Fluids Engineering*, vol. 114, no. 3, pp. 313–332, 1992.
- [21] M. Omeara and T. Mueller, “Laminar separation bubble characteristics on an airfoil at low reynolds numbers,” *AIAA journal*, vol. 25, no. 8, pp. 1033–1041, 1987.
- [22] M. Jahanmiri, “Laminar separation bubble: Its structure, dynamics and control,” tech. rep., Division of Fluid Dynamics, Department of Applied Mechanics, Chalmers University of Technology, 2011.
- [23] R. Langtry, F. Menter, S. Likki, Y. Suzen, P. Huang, and S. Völker, “A correlation-based transition model using local variables—part ii: Test cases and industrial applications,” *Journal of Turbomachinery*, vol. 128, p. 423, 2006.
- [24] N. A. Jaffe, T. T. Okamura, and A. M. O. Smith, “Determination of spatial amplification factors and their application to prediction transition,” *AIAA Journal*, vol. 8, pp. 301–308, 1970.
- [25] B. J. Abu-Ghannam and R. Shaw, “Natural transition of boundary layers - the effects of turbulence, pressure gradient and flow history,” *Journal Mechanical Engineering Science*, vol. 22, no. 5, pp. 213–228, 1980.
- [26] H. W. Emmons, “The laminar turbulent transition in a boundary layer - part 1,” *Journal of Aeronautical Sciences*, vol. 18, pp. 490–498, 1951.

REFERENCES

- [27] R. Narasimha, “On the distribution of intermittency in the transition region of a boundary layer,” *Journal of Aeronautical Sciences - Readers’ Forum*, pp. 711 – 712, Aug 1957.
- [28] G. Scheuerer, “Numerical prediction of boundary layers and transitional flows,” in *Boundary layers in turbomachines*, Rhode-Saint Genese, Belgium: Von Karman Inst. for Fluid Dynamics, Lecture Series 1991-06, Sept. 1991.
- [29] D. Arnal, “Description and prediction of transition in two-dimensional incompressible flow,” tech. rep., AGARD Rept. 709, June 1984.
- [30] S. Dhawan and R. Narasimha, “Some properties of boundary layer flow during transition from laminar to turbulent motion,” *J. Fluid Mech.*, vol. 3, pp. 418–436, 1958.
- [31] R. L. Panton, “Potential/complex-lamellar velocity decomposition and its relevance to turbulence,” *Journal of Fluid Mechanics*, vol. 88, pp. 97–114, 1978.
- [32] J. W. Yokota, “A kinematic velocity decomposition of stratified flow,” *International journal of computational fluid dynamics*, vol. 9, no. 2, pp. 121–135, 1998.
- [33] J. Finnigan, “A streamline coordinate system for distorted two-dimensional shear flows,” *J. Fluid Mech*, vol. 130, pp. 241–258, 1983.
- [34] J. Hunt and D. Carruthers, “Rapid distortion theory and the ‘problems’ of turbulence,” *Journal of Fluid Mechanics*, vol. 212, no. 1, pp. 497–532, 1990.
- [35] P. Durbin and J. Hunt, “On surface pressure fluctuations beneath turbulent flow round bluff bodies,” *J. Fluid Mech*, vol. 100, no. 1, pp. 161–184, 1980.
- [36] J. W. Yokota, “Potential/complex-lamellar descriptions of incompressible viscous flow,” *Physics of Fluids*, vol. 9, no. 8, pp. 2264–2272, 1997.
- [37] C. Truesdell, *The kinematics of vorticity*. Indiana University Press, Bloomington, IN., 1954.

REFERENCES

- [38] R. Aris, *Vectors, Tensors, and the Basic Equations of Fluid Mechanics*. Dover, New York, 1962.
- [39] R. L. Panton, *Incompressible flow*. John Wiley and Sons, Inc., Hoboken, New Jersey, 2005.
- [40] M. J. Lighthill, “Drift,” *J. Fluid Mech.*, vol. 88, p. 97, 1956.
- [41] C. G. Darwin, “Note on hydrodynamics,” *Proc. Cambridge Philos. Soc.*, vol. 49, p. 342, 1953.
- [42] W. R. Hawthorne, “On the theory of shear flows,” tech. rep., MIT Gas Turbine Laboratory Report No. 88, 1966.
- [43] T. Craig, “On certain possible cases of steady motion in a viscous fluid,” *American Journal of Mathematics*, vol. 3, no. 3, pp. 269–288, 1880.
- [44] A. V. Arena and T. J. Mueller, “Laminar separation, transition, and turbulent reattachment near the leading edge of airfoils,” *AIAA journal*, vol. 18, pp. 747–753, 1980.
- [45] C. P. Häggmark, A. A. Bakchinov, and P. H. Alfredsson, “Experiments on a two-dimensional laminar separation bubble,” *Philosophical Transactions of the Royal Society of London. Series A: Mathematical, Physical and Engineering Sciences*, vol. 358, pp. 3193–3205, 2000.
- [46] K. Pohlhausen, “On the approximate integration of the differential equations of laminar shear layers,” *ZAMM*, vol. 1, pp. 252–268, 1921.
- [47] G. B. Schubauer and H. K. Skramstad, “Laminar boundary layer oscillations and transition on a flat plate,” tech. rep., NACA Report 909, 1948.
- [48] F. K. Owen, “Transition experiments on a flat plate at subsonic and supersonic speeds,” *AIAA Journal*, vol. 8, pp. 518–523, 1970.

REFERENCES

- [49] J. Dey and R. Narasimha, “Transition zone length in incompressible boundary layers,” Tech. Rep. Report 84 FM 9, Dept. Aero. Eng., Ind. Inst. Sci., 1984a.
- [50] W. J. Bellows, *An experimental study in leading edge separating-reattaching boundary layer flows*. PhD thesis, Rensselaer Polytechnic Institute, Troy, NY, 1985.
- [51] J. Clark and T. Praisner, “Predicting transition in turbomachinery. part 1. a review and new model development,” in *Proceedings of ASME Turbo Expo 2004, Power for Land, Sea, and Air, June 14-17, 2004, Vienna, Austria*, 2005.
- [52] W. B. Roberts, “Calculation of laminar separation bubbles and their effect on airfoil performance,” *AIAA journal*, vol. 18, pp. 25–31, 1980.